공학박사학위논문

Development of multiscale 2D/3D fabrication methods for tissue engineering

조직공학응용을 위한 멀티스케일 2 차원/3 차원 제작 기법 개발

2015 년 2 월

서울대학교 대학원

기계항공공학부

김 민 성

Abstract

In this thesis, we suggested multiscale 2D and 3D fabrication methods for tissue engineering applications. In detail, we utilized precisely fabricated nanopatterns through capillary force lithography (CFL) as a screening platform for determining effects of nanotopography on cellular behavior. In addition, to overcome the limitations of present electrospinning methods for adopting tissue engineering field, we have developed new methods based on rolling and stacking process of cell-seeded nanofibers for formation of cell-dense 3D engineered tissues *in vitro*.

Extracellular matrix (ECM) is the nanofibrous environment surrounding cells which serve both mechanical and biochemical stimuli and the cells regulate their functions such as adhesion, proliferation, migration and differentiation by interaction with ECM. Multiscale fabrication methods for mimicking ECM environment in 2D/3D scaffold, therefore, have to be established first. For this aim, we developed nanopatterned 2D platform by using UV-assisted capillary force lithography for investigating adipogenic differentiation affected by geometrical variables. We observed that the cell

crawling into nanogrooves contributed substantially to an enhanced level of differentiation with higher contact guidance, suggesting that cell-to-surface interactions would play a role for the adipocyte differentiation.

To form 3D cell-dense engineered tissue *in vitro*, further, electrospun nanofibers fabricated inclined gap method was used because fabricated nanofibers could be easily transferred to other substrates so that they could be adoptable for 3D fabrication processes such as rolling and stacking with the cells. First, we reported new 3D fabrication method based on rolling of cell-seeded scaffold. It was demonstrated that this hybrid fabrication could produce uniaxially aligned nanofiber scaffolds supported by a thin film, allowing for stable manipulation with aligned cellular morphology. In addition, we successfully formed a cylindrical 3D engineered tissue by rolling up the cell seeded film type scaffold around a melt extruded microfiber. As another approach for 3D engineered tissue formation, we suggested a simple and versatile method for formation of various cell sheets and their layer-by-layer stacking based on electrospun nanofibers. By the performance of nanofibers as a role of structural support, the cell sheets on nanofibrous membrane could sustain their entire geometry even after detached from culture substrate.

In addition, 3D muscle and vascularized skin tissue was achieved by differentiating multilayered myocyte sheets or sandwiching endothelial cell sheet between fibroblast sheets respectively. Taken together, the experimental results indicated that this method provides universal and effective tools for not only stable formation and manipulation of the cell sheet structure but also formation of functional 3D engineered tissue.

Key Words : Extracellular matrix, Micro/nanopatterning, Capillary force lithography, Electrospinning, Rolling-up process, Cell sheet engineering, Layer-by-layer stacking, Adipogenesis, Myogenesis, Vascular network, 3D engineered tissue

Student Number: 2010-20657

Contents

List of Figures

Nomenclature

ECM	Extracellular matrix
CFL	Capillary force lithography
PUA	Polyurethane acrylate
PDMS	Polydimethylsiloxane
PNIPAAm	Poly-N-isopropylacrylamide
HMDS	Hexamethyldisilazane
DMF	Dimethylformamide
DMEM	Dulbecco's Modified Eagle's Medium
EBM	Endothelial basal medium
GM	Growth medium
EGM	Endothelial growth medium
DM	Differentiation medium
FBS	Fetal bovine serum
PS	Penicillin-streptomycin
PDL	Poly-D-lysine
SEM	Scanning electron microscope
AFM	Atomic force microscope
qRT-PCR	Quantitative real-time polymerase chain reaction
TR #n	Number of transfers (n times)
One-way ANOVA	One-way analysis of variance
LBL	Layer-by-layer

Chapter 1. Introduction

Extracellular matrix (ECM) is collection of extracellular molecules such as collagen/elastin nanofibers and proteoglycans. Collagen/elastin nanofibers serve adhesion sites for the cells and mechanical stimuli through cell-nanofiber interactions. Proteoglycans play a role in storage of biochemicals inside ECM by hydration due to their highly negative charged nature. Taken together, the cells receive not only mechanical stumuli but also biochemical stimuli as a result of cell-ECM interaction and regulate their functions such as proliferation, migration and differentiation [1]. Among them, mechanical properties of ECM such as nanotopographical features and matrix stiffness have considered as crucial stimuli which allow regulation of cellular functions through integrin-mediated mechanotransduction [2, 3]. For this reason, fabrication of three-dimensional (3D) scaffolds mimicking nanotopographical features of ECM have been considered as a major challenge in field of tissue engineering whose major aim is to

repair cellular functions of damaged tissues/organs or to replace them to engineered tissues/organs.

Recent development of nano/micropatterning methods accelerates the researches on effect of mechanical stimuli exerted on the cells by nanotopographical features. Especially, polymeric material based nanopatterning methods such as electron beam lithography, colloidal lithography, nanoimprint lithography and capillary force lithography have attracted great attentions because those fabrication methods have strengths of tunability of their mechanical properties and high transparency required for biological assays. Thus, many researchers have used nanopatterns as a tool for investigating effect of nanotopography on cellular functions of diverse cell types such as neural cells [4, 5], muscular cells [6, 7], fibroblasts [8] and stem cells [9, 10]. Fabrication of 3D structures, however, is still remaining limitation of patterning methods for application as a scaffold. Nonetheless, nanopatterns are worthwhile as a platform for determining geometrical characteristics of desired scaffold because their strength in fabricating nanostructures in a precise manner.

In conjunction with nano/micropatterning methods, electrospinning is an another representative method in tissue engineering field due to its strengths such as fibrous morphology similar with ECM, ease in controlling mechanical and chemical properties of nanofibers and capacity for fabricating 3D scaffold composed of random or aligned nanofibers. Unlike randomly oriented nanofibrous mesh, however, aligned nanofibers cannot sustain 3D structure due to their geometrical constraint so that application of electrospinning methods for tissues having uniaxially aligned ECM structures is limited. To address this problem, many fabrication methods such as air/insulator gap methods, pin/blade based methods, ring based methods, rotating disc/drum based methods and their hybrid methods. Among them, air gap methods and hybrid methods have attracted many attentions in tissue engineering field because nanofibers fabricated by air gap methods can be easily transferred to other substrate and resulting thickness and pore size can be controlled by differing number of transfer and fiber density of single transfer.

In addition, nanofibrous meshes have a critical limitation of cellular infiltration which results in different cellular populations according to depth of scaffolds due to their small pore size. To address this problem, many researchers suggested various methods for

increasing pore size such as sequential electrospinning of micro and nanofibers [11, 12] and selective dissolution of water soluble nanofibers from co-electrospun nanofibrous meshes [13], but cellular infiltration problem still remaining unsolved. Other approaches focusing on making 3D engineered tissues with evenly distributed cell populations have also been suggested by repetitive cell seeding and electrospinning on the cultured cell layer [14], but entire cellular populations through the engineered tissue are reduced due to thickness of the nanofibrous mesh.

In this thesis, we suggested various multiscale 2D and 3D fabrication methods to overcome described limitations of previous methods (Figure 1-1). We utilized precisely fabricated nanopatterns through capillary force lithography (CFL) as a tool for investigating cellular behaviors affected by nanotopography. Further, to overcome the limitations of present electrospinning methods, we have developed new methods based on rolling and stacking process of cell-seeded nanofibers for formation of cell-dense 3D engineered tissues *in vitro*.

In chapter 2, we present the effect of nanotopographically defined surfaces on adipocyte differentiation using various nanogroove patterns. Parallel nanogroove arrays with equal inter-groove distance (400 nm, 550 nm, 800 nm width) and varying distances (550 nm width with three different spaces of 550, 1100, and 2750 nm) were fabricated by UV-assisted capillary force lithography (CFL) on 18 mm diameter glass coverslips using biocompatible polyurethane (PU)-based material. After coating with fibronectin and subsequent culture of 3T3-L1 preadipocytes, the degree of adipocyte differentiation was determined by Oil Red O staining and adipogenic gene expression. We observed that adipocyte differentiation was slightly but substantially affected by culture on various nanogrooved surfaces. In particular, the cell crawling into nanogrooves contributed substantially to an enhanced level of differentiation with higher contact guidance, suggesting that cell-to-surface interactions would play a role for the adipocyte differentiation.

In chapter 3, we have successfully fabricated nanofiber-based scaffold complexes of rod and sheet type by combining the three microfabrication techniques of electrospinning, spin-coating, and polymer melt deposition. It was demonstrated that this

hybrid fabrication could produce uniaxially aligned nanofiber scaffolds supported by a thin film, allowing for a mechanically enforced substrate for cell culture as well as facile scaffold manipulation. The results of cell analysis indicated that nanofibers on spin-coated films could provide contact guidance effects on cells and retain them even after manipulation. As an application of the cell-laden nanofiber film, we built a rod type structure by rolling up the film around a mechanically supporting core microfiber which was incorporated by polymer melt deposition. A biocompatible and biodegradable polymer, polycaprolactone (PCL), was used throughout the processes and thus could be used as a directly implantable substitute in tissue regeneration.

Finally in chapter 4, we suggested a simple and versatile method for cell sheet manipulation and 3D engineered tissue formation *in vitro*. The technical result was achieved by integrating an array of electrospun nanofibers into a polydimethylsiloxane (PDMS) assembly containing an opened culture well so that the cultured cells could be peeled off with the nanofibers. By the performance of nanofibers as a role of structural support, the cell sheet-nanofiber complex could sustain its entire geometry even after detached from culture substrate. The nanofibers also allowed the cultured cells to be

oriented in the desired direction and this cell orientation was not impaired by the detachment regardless of cell types when the quantity of integrated nanofibers was offered by the line density of 173 fibers/mm. Compared with conventional methods based on poly-N-isopropylacrylamide (PNIPAAm) which is the most widely used thermoresponsive polymer, cell sheets generated by suggested method based on nanofibers showed almost identical properties and could be used as a building blocks to form 3D tissue constructs *in vitro* by stacking detached cell sheets layer-by-layer. Inspired from these results, we performed experiments for forming 3D engineered muscle tissue and vascularized skin tissue. As results, longitudinally well-developed myotubes were observed through entire muscle tissue and well-organized vascular network was formed inside skin tissue by differentiating multilayered myoblast sheets and co-culturing endothelial cell sheet between fibroblast sheets for 7 days.

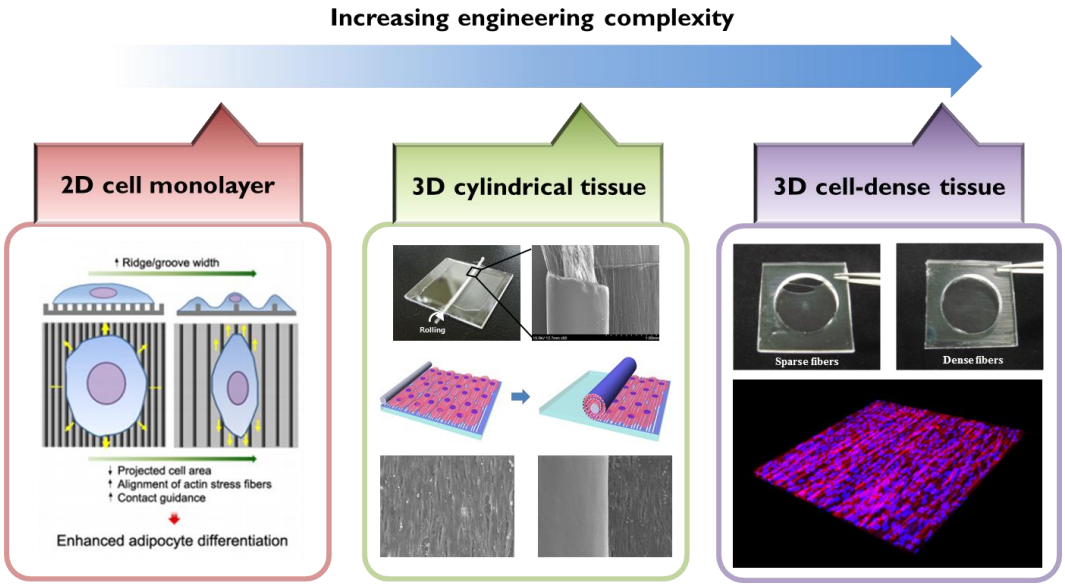

Figure 1-1. An illustration of the goal of this thesis. Multiscale 2D and 3D fabrication methods were suggested.

Chapter 2. Effect of nanogroove geometry on adipogenic differentiation

2.1. Introduction

Cellular response is exquisitely sensitive to the surrounding extracellular matrix (ECM) with nanoscale topographical features [15-18]. Also, cells contain nanoscale physical structures whose size is compatible with embedded ECM, including the intracellular organelles such as cytoskeletal elements (e.g., actin filaments and microtubules) and adhesive structures (e.g., focal adhesions). It is therefore quite reasonable to expect that functioning of many cell types can be regulated *in vitro* by the nanoscale features of the surrounding ECM.

Most of the previous *in vitro* studies have examined cells cultured on two-dimensional flat and rigid surfaces (e.g., Petri dish) despite that most cells *in vivo* are exposed to three-dimensional microenvironments with complex topographical features. In order to address some of the limitations, microfabrication and surface-chemistry-based approaches have provided a versatile set of tools to control the spatial organization and

temporal presentation of cellular cues on a microscale [19, 20]. To better understand the mechanism involved in cellular behavior and function in a microenvironment, nanoscale topographical features have been incorporated into the *in vitro* experimental platform to mimic various *in vivo* three-dimensional ECM environments with structural and mechanical similarity [16]. Previous experiments with various nanotopographic features such as grooves, ridges, pore, wells, and pillar, have shown that nanotopography can strongly influence cell morphology, adhesion, proliferation, and gene regulation [17, 21-24], but the underlying mechanism mediating this cell response still remains unclear.

Recently, we have shown that nanopatterned surfaces of UV-curable polyurethane acrylate (PUA) or polyethylene glycol (PEG) material can be used as a structured biomaterials interface to control various cell functions such in neuronal differentiation [4, 5], osteogenic differentiation [25], directed cell migration [26, 27], and cardiac tissue engineering [6]. The cell culture platform was fabricated by combining UV-assisted capillary force lithography (CFL) and self-replication as schematically illustrated in Figure 2-1. There are a number of advantages with the fabrication method. First, the UV-curable PUA and PEG materials provide excellent biocompatibility for many cell

types, allowing for a long-term cell culture without modification of cell function. Second, the patterned surface can be prepared on a large area, typically larger than 1×1 cm^2, with good uniformity, which is beneficial for various biochemical assays (e.g., Western blotting, RT-PCR, etc.). Third, the self-replication characteristic (i.e., replication from PUA to PUA material) allows a facile duplication of the PUA replica from positive to negative sense (or vice versa), indicating that dot and hole patterns can be prepared from the same silicon master [28, 29].

By taking advantage of the above benefits, we present here the role of nanoscale groove patterns on the adipocyte differentiation. Adipogenesis is referred to as differentiation into adipogenic lineage from preadipocytes. Adipocytes play crucial role in synthesis and storage of energy source in the form of neutral lipid metabolites. Regulation of adipogenesis has been implicated in obesity-related metabolic diseases such as hyperlipidemia, hypertension, and type 2 diabetes. Obese animals often exhibit increase in fat cell size and/or fat cell numbers. Several anti-obesity and/or anti-diabetic drugs such as berberine and thiazolidinediones show beneficial effects through regulating adipogenesis [30, 31]. Recently, *ex vivo* adipocyte differentiation has been intensively

studied for self-fat grafting in the part of cosmetic treatment. In this aspect, some core technologies to control the process of adipocyte differentiation are needed to be established.

Adipocyte differentiation is a complex process regulated by many transcriptional cascades and hormonal stimuli. For example, a certain hormonal change stimulates adipogenesis in concert with adipogenic transcription factors including peroxisome proliferator-activated receptor γ (PPARγ) and CCAAT/enhancer-binding proteins [32-36]. Moreover, it has been reported that ECM proteins or cytoskeleton proteins are also involved in adipocyte differentiation [37, 38]. Therefore, it is likely that the ECM nanoscale topography would affect adipogenesis in an *in vitro* culture platform. Our results demonstrate that the adipogenic differentiation can be up-regulated to a certain extent by changing the nanogroove geometry. In particular, the pattern spacing is more influential than the pattern width such that the largest spacing pattern (width:spacing = 1:5, width = 550 nm) showed the highest differentiation level. In this case, the cells penetrated into the grooves with the actin cytoskeleton being more aligned along the grooves, suggesting that cell-to-surface interactions as characterized by contact guidance

is closely related to the adipogenesis.

2.2. Materials and methods

2.2.1. Preparation of PUA mold

The silicon masters having various parallel arrays of nanogrooves were prepared by standard photolithography and reactive ion etching. A small amount of UV-curable PUA precursor (0.1 – 0.5 mL) was drop-dispensed on the silicon master and covered with a transparent poly(ethylene terephthalate) (PET) film of 50-μm thickness. To cure the resin, the assembly was exposed to UV light (λ = 200 ~ 400 nm, dose = 100 mJ/cm^2) for 25 s. After UV-curing, the PUA replica was peeled off from the silicon master using a sharp tweezer and further exposed to UV light for 10 h for complete annihilation of reactive acrylate groups. Glass coverslips that were used as substrate were sonicated in acetone for 1 h to remove organic contaminants and then dried with N_2 gas.

2.2.2. Fabrication of nanopatterned surfaces

A similar amount of PUA precursor was drop-dispensed on the 18 mm glass coverslip and a PUA mold with engraved nanogrooves was placed carefully to make a conformal contact, leaving behind a replica of the PUA mold after UV exposure for a few

tens of seconds followed by mold removal. To promote adhesion of the patterned layer, the glass coverslip was treated with an adhesion promoter (phosphoric acrylate or acrylic acid dissolved in propylene glycol monomethyl ether acetate (PGMEA), 10 vol %). The nanopatterned surfaces were treated with oxygen plasma for 1 min to make the surface hydrophilic. Then, the fibronectin (1 μg/mL) was coated to increase cell adhesions by dipping the surface for 1 h. To remove unbound fibronectin, the surface was washed with Dulbecco's phosphate buffered saline (DPBS) for 3 times. Prior to cell culture, the fabricated PUA nanopatterns were sterilized by rinsing with ethyl alcohol and D.I. water.

2.2.3. Cell culture

3T3-L1 preadipocytes were maintained in Dulbecco's Modified Eagle's Medium (DMEM) supplemented with 10% bovine calf serum (BCS). To induce adipocyte differentiation, at 2 days post-conflucence, 3T3-L1 cells were incubated with DMEM containing 10% fetal bovine serum (FBS), 0.5 mM 3-isobutyl-1-methylxanthine (IBMX), 1 M dexamethasone and 1 g/ml insulin for 2 days. Then, the culture medium was replaced with DMEM containing 10% FBS and 1 g/ml insulin and the cells were cultured for

additional 2 days. In this manner, the culture medium was changed every two days with DMEM containing 10% FBS.

2.2.4. Oil Red O staining

3T3-L1 cells were washed with PBS and fixed for 5 min with 3.7% formaldehyde solution. Cells were dehydrated with 100% propylene glycol for 5 min. Oil Red O (0.5% in propylene glycol) was incubated with fixed and dehydrated cells for 1 h at room temperature. Cells were re-hydrated with 85% propylene glycol for 5 min and washed with PBS. The stained fat droplets in the cells were visualized under optical microscopy. For statistical significance, each experiment was repeated at least 5 times.

2.2.5. RNA isolation and quantitative real-time PCR (RT-PCR)

Total RNA was isolated with Iso-RNA lysis reagent (5 PRIME, Hamburg, Germany) and subjected to cDNA synthesis using RevertAid M-MuLV reverse transcriptase (Fermentas, Glen Burnie, MD, USA). Relative amounts of mRNA were measured using the CFX96^{TM} Real-Time System (Bio-Rad Laboratories, Hercules, CA.

USA) and calculated by normalization to the level of cyclophilin mRNA. The primer sequences used for quantitative real-time PCR analysis were as follows: PPARγ2-forward (f), 5'-GCATGGTGCCTTCGCTGA-3'; PPARγ2-reverse (r), 5'-TGGCATCTCTGTGT CAACCATG-3'; adiponectin-f, 5'-GGCAGGAAAGGAGAACCTGG-3'; Adiponectin-r, 5'-AGCCTTGTCCTTCTTGAAGAG-3'; aP2-f, 5'-AAG AAGTGGGAGTGGGCTTT-3'; aP2-r, 5'-GCTCTTCACCTTCCTGTCGT-3'; FASN-f, 5'-GCCTACACCCAGAGCTAC CG-3'; FASN-r, 5'-GCCATGGTACTTGGCCTTG-3'; cyclophilin-f, 5'-CAGACGCCAC TGTCGCTTT-3'; cyclophilin-r, 5'-TGTCTTTGGAACTTTGTCTG-3'. The RT-PCR experiment was repeated three times.

2.2.6. Scanning electron microscopy (SEM)

3T3-L1 cells were gently rinsed with DPBS and fixed by 5% glutaraldehyde solution in DPBS containing 0.1 M sodium cacodylate and 0.1 M sucrose for 30 min at 4 °C. After the fixation process, the cells were washed with DPBS for 3 times and dehydrated by sequentially immersing them in gradient ethanol solutions and hexamethyldisilazane (HMDS). The samples were dried in fume hood for 10 h and

observed with SEM (S-48000, Hitachi, Japan).

2.2.7. Quantification of lipid droplet accumulation and projected cell area

To quantify lipid droplet accumulation and projected cell area, ImageJ software (NIH) was used. The images of 3T3-L1 cells stained by Oil Red O were taken for 15 points for each nanopatterned substrate. With the aid of appropriate image processing, stained lipid droplets in the images were highlighted and then the occupied portion of the lipid droplets was calculated. The projected cell area was calculated in a similar manner from arbitrary selection of the cell boundaries for about 100 cells in each SEM image.

2.2.8. Immunofluorescence staining

3T3-L1 cells were washed with PBS for 2 times and fixed with 3.7% formaldehyde solution for 15 min. Fixed cells were treated with 0.1% Triton X-100 in PBS for 10 min to make cells permeable and then treated with antibody buffer (2% bovine serum albumin (BSA) and 0.1% Triton X-100 in PBS) for 30 min to block unspecific bindings. After washing 3 times with PBS, the cells were incubated for 1 h

with tetramethylrhodamine isothiocyanate (TRITC)-phalloidin solution (1:400 in antibody buffer) to stain actin filaments (F-actin).

2.3. Results and Discussion

2.3.1. Preparation of nanogroove patterns on 18 mm glass coverslip

As described earlier, the PUA material has been extensively used for cell culture due to its several excellent properties such as transparency, tunable surface energy [39] and biocompatibility for various cell types [4, 5, 25]. Figure 2-1 shows a schematic diagram for the fabrication of nanopatterned substrates using UV-assisted CFL. Representative SEM images of the nanopatterns are shown in figure 2-2(A-E). In the experiment, five types of nanogroove patterns were used with different width and inter-groove spacing: (A) 400nm 1:1, (B) 550nm 1:1, (C) 800nm 1:1, (D) 550nm 1:2 and (E) 550nm 1:5 (width:spacing). Therefore, for equally-spaced dense nanogroove pattern, the width varied from 400, 550, to 800 nm. For nanogrooves with varying spaces, the width was fixed at 550 nm, while changing the distance from 550 to 2750 nm. For all patterns, the pattern height was fixed at 600 nm. As shown in Figure 2-2(A-E), the patterns exhibited high structural fidelity over large areas (see Figure 2-2F) showing well-defined nanopatterns on 18 mm glass coverslip). To fabricate uniform patterns, it is important to remove trapped air from PUA precursor during replication steps. This is because PUA

precursor cannot fill the cavity occupied by the air trap. To resolve this problem, the rubber roller was mildly rolled on the PET film support before UV-curing process [40].

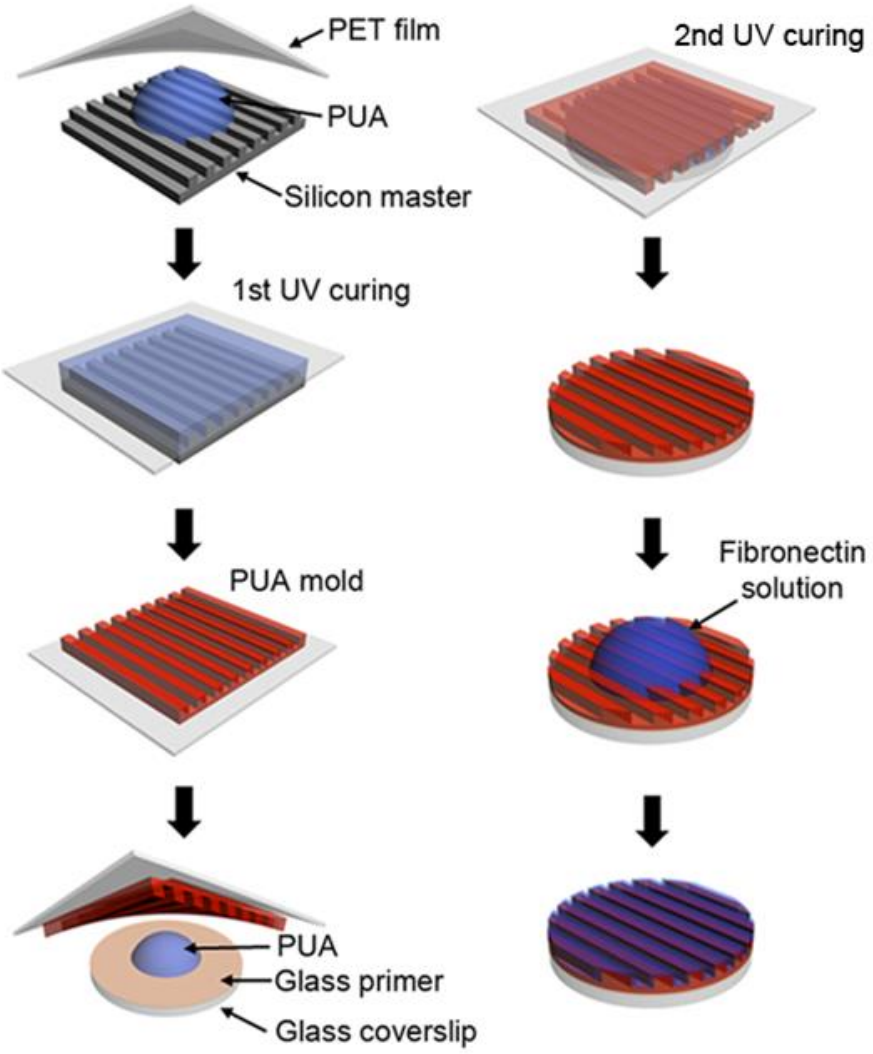

Figure 2-1. A schematic diagram for the fabrication of polyurethane acrylate (PUA) nanogroove patterns using UV-assisted capillary force lithography (CFL).

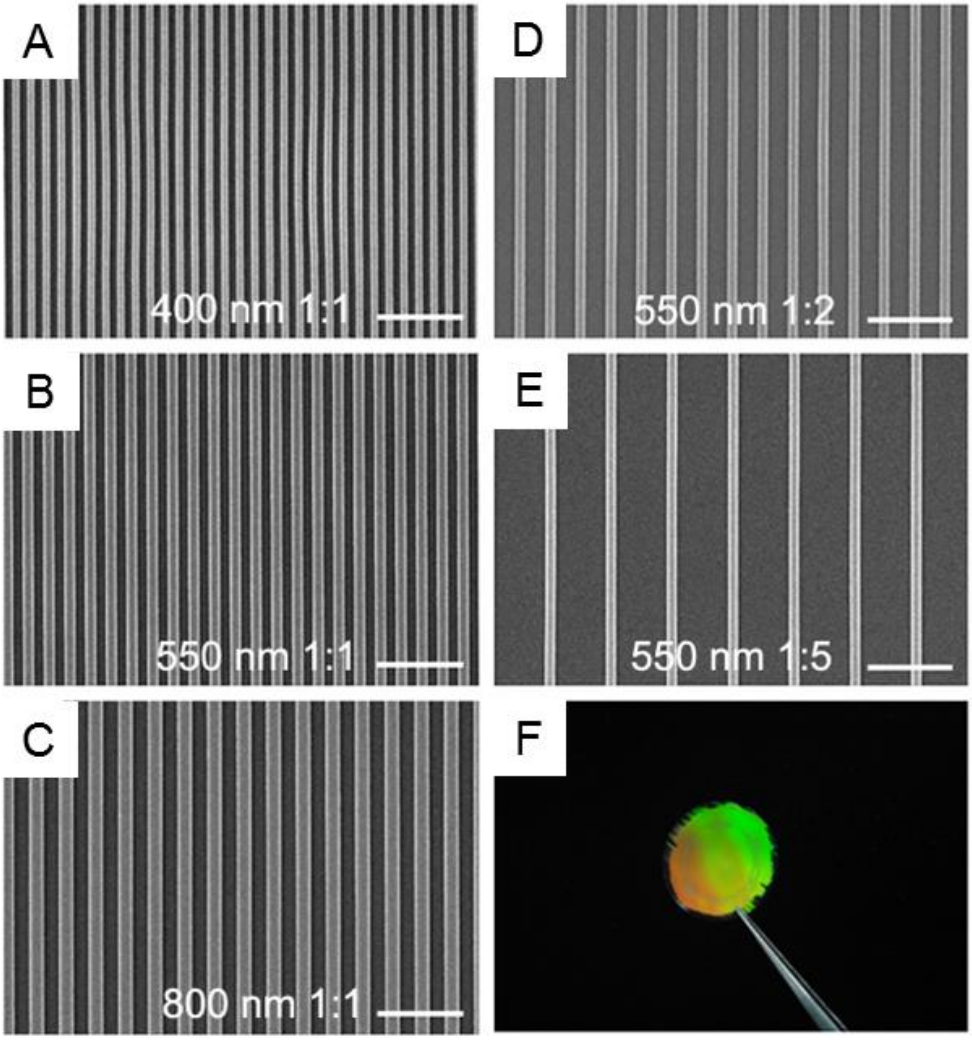

Figure 2-2. Representative SEM images of various PUA nanogrooves: (A) 400 nm 1:1, (B) 550 nm 1:1, (C) 800 nm 1:1, (D) 550 nm 1:2, and (E) 550 nm 1:5 (width : spacing). Scale bars indicate 5 μm. (F) Example of large-area fabrication on 18 mm diameter glass coverslip.

2.3.2. Quantification of adipogenic differentiation on nanogroove patterns

To investigate whether nanotopography would influence adipocyte differentiation, we cultured 3T3-L1 preadipocytes on the various nanogroove surfaces, first for 2 days for confluency and additional 5 days under induction media for adipogenesis. Without the induction media, no appreciable differentiation was observed, suggesting that the effect of media is crucial for the 3T3-L1 preadipocytes. Prior to cell culture, fibronectin was incubated on the surfaces, which turned out to render a uniform coating over the topography without notable difference between ridge and bottom regions [4, 41]. To measure the level of adipocyte differentiation, Oil Red O staining was conducted to stain accumulated intracellular lipid droplets and the results are displayed in Figure 2-3(A-F). For the quantification, two different methods were used: direct calculation of the portion occupied by lipid droplets through image processing (Figure 2-4A and B) and quantitative RT-PCR analysis of the expression of key adipocyte marker genes including PPARγ and its target genes which were up-regulated during adipogenesis (Figure 2-5).

We first examined the effect of groove width on the differentiation. As can be

seen from the Oil Red O stained images shown in Figure 2-3(A-D) and relative amount of lipid accumulation (Figure 2-4A), the differentiation was slightly suppressed compared with control (bare PUA surface, Figure 2-3A) when the cells were cultured on the dense 400 nm and 500 nm 1:1 pattern. In contrast, the differentiation was somewhat enhanced on the largest 800 nm 1:1 pattern, but the level of differentiation was marginal. Next, we examined the effect of groove spacing (Figure 2-3(D-F)). Additionally, we revealed that the level of differentiation was slightly increased with the increase of inter-groove spacing from 550 nm 1:1 to 550 nm 1:5 nanogrooves as evidence by the relative amount of lipid accumulation (Figure 2-4B). In conjunction with the staining results, a similar trend was observed from the quantitative RT-PCR even though the change of marker gene expression was not dramatic (Figure 2-5). Here, relative mRNA levels of several adipogenic marker genes such as PPARγ, adiponectin, aP2, and FASN were measured with respect to that on the control surface.

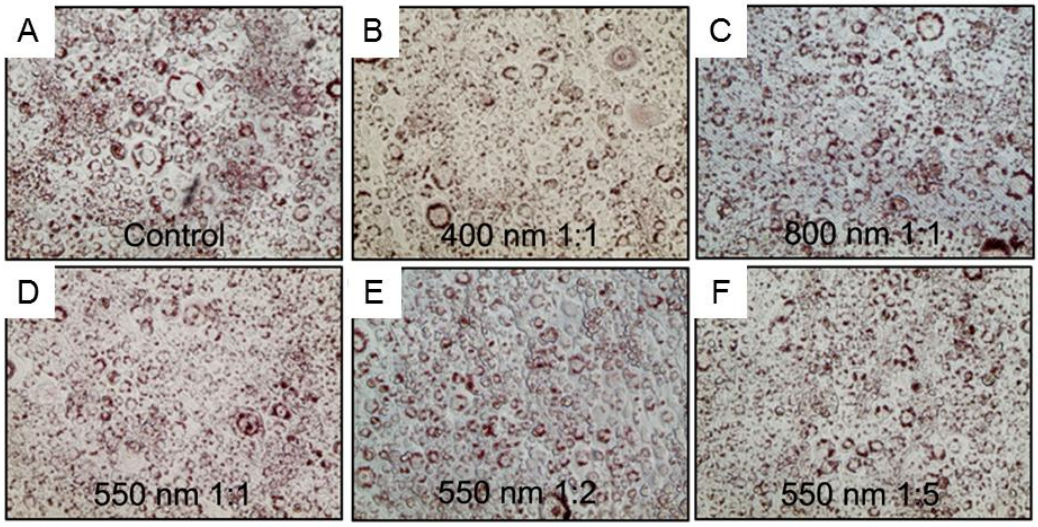

Figure 2-3. Microscopic view of Oil Red O stained 3T3-L1 adipocytes on various nanogroove patterns after culture of 5 days.

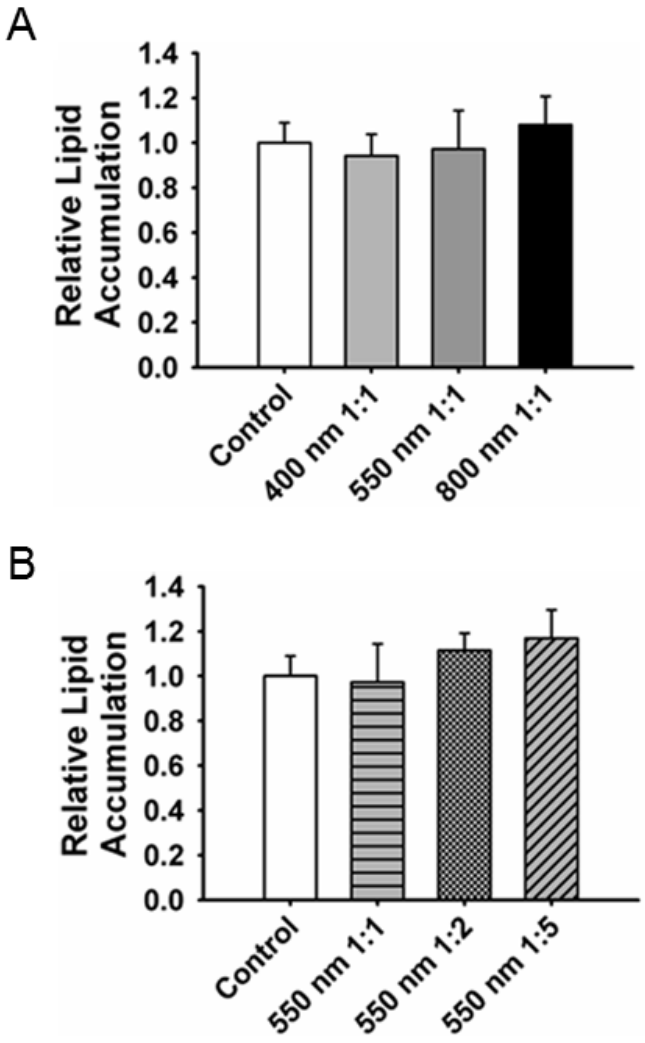

Figure 2-4. Quantitative analysis of relative lipid accumulation obtained by image processing for varying groove width with the same spacing (A) and varying groove spacing with the same width (B).

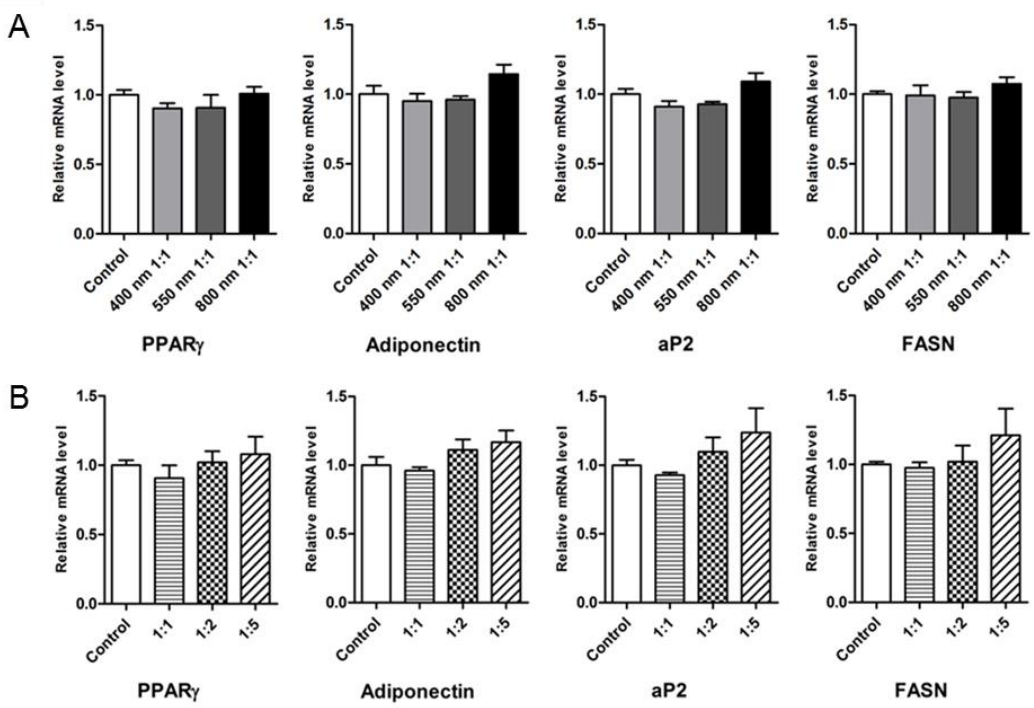

Figure 2-5. Relative mRNA levels of several adipogenic marker genes by quantitative real-time RT-PCR for the dense nanogroove patterns (A) and the nanogrooves of varying spaces (B). The amounts were normalized with respect to that on the control sample.

2.3.3. Effect of cellular morphology on adipogenic differentiation

Based on the observations thus far, it appears that the adipogenesis is associated with the width and spacing of nanogrooves or the geometry of the underlying nanoscale features. To link the geometrical change of nanotopography to cell shape, we measured apparent cell projected area and detailed cell morphology onto nanogrooves by SEM. Representative planar SEM images of the cells cultured for 2 days after plating (i.e., just before the induction of adipogenesis) are shown in Figure 2-6(A-F). According to the SEM images, the cells were less spread with the increase of groove width for the equally-spaced nanogrooves, and with the increase of inter-groove spacing with the same groove width (Figure 2-7(A-B)). For the equally-spaced patterns (Figure 2-6(B-D)), the topographical guidance along the groove direction was less pronounced except for the 800 nm 1:1 pattern, in which a certain degree of cell alignment is apparent. For the various inter-spacing patterns, a dramatic change of cellular morphology was observed (Figure 2-6(D-F)). As the inter-spacing was increased, the projected cell size became smaller with enhanced contact guidance along the groove direction.

For the quantification, the orientation of cell morphology with respect to the

nanogroove direction was plotted in an angular mapping diagram as shown in Figure 2-8. It is seen that the orientation slightly became narrower and directional as the pattern size was increased from 400 to 800 nm. For the nanogrooves with varying spaces, the contact guidance was distinctively enhanced with the increase of the inter-groove spacing from 1:1 to 1:5. Such enhanced contact guidance resulted in relatively reduced cell spreading areas (Figure 2-7(A-B)), which were calculated based on the cell boundaries from the images.

To elaborate on the contact guidance of nanogrooves, the cross-sectional images of the cells were obtained as shown in Figure 2-9. For this experiment, the nanopatterned glass coverslips with dehydrated cells were slightly frozen in a refrigerator (-80℃) for 15 min. A distinct and notable finding from the figure is that the cells only penetrated into the nanogrooves for the largest spacing of 550 nm pattern, in accordance with the enhanced contact guidance shown in Figure 2-6F. This suggests that the cell crawling into the nanogrooves apparently assists in contact guidance. For the less penetrating dense patterns, a careful examination reveals that the cell penetration was slightly increased for the 800 nm 1:1 pattern as compared to the other smaller patterns. Therefore, it is hypothesized that the contact guidance plays a critical role in regulating the adipocyte

differentiation presented in this study.

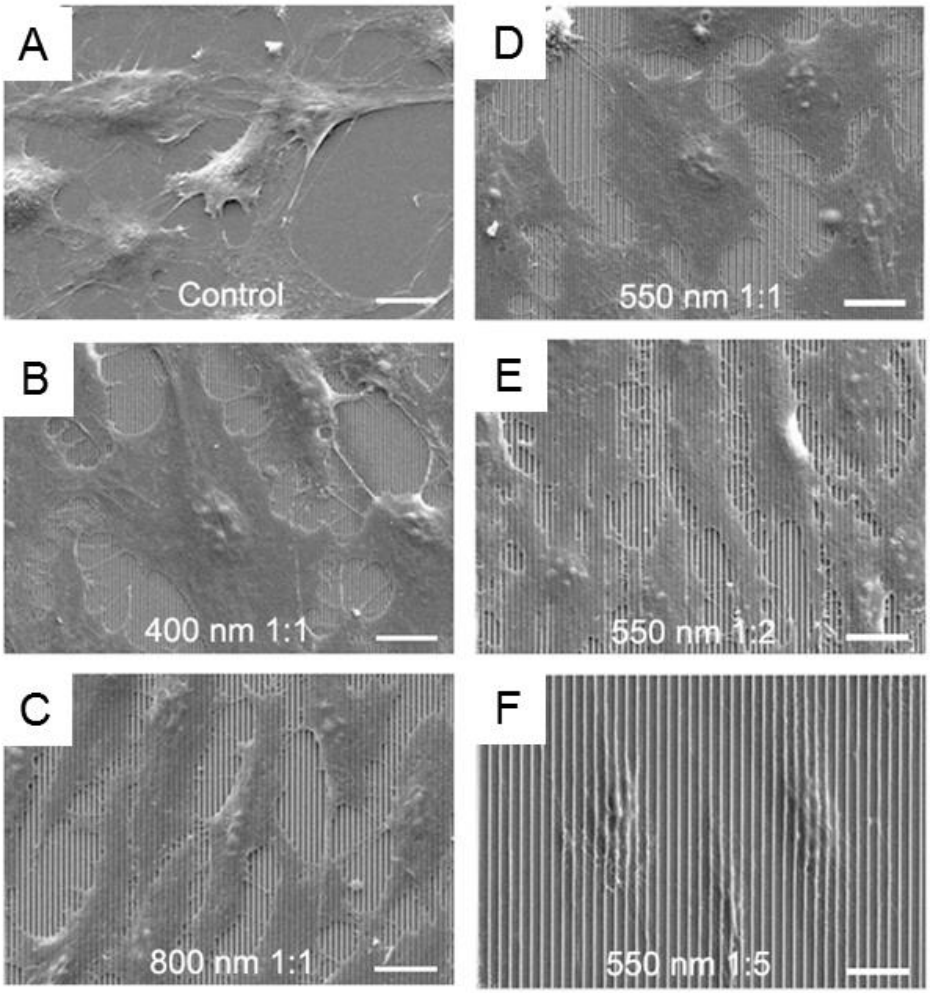

Figure 2-6. Representative SEM images of the 3T3-L1 cells cultured on various nanogroove patterns. The cells were observed after culture for 2 days (before induction of adipogenesis). Scale bar indicates 20 μm.

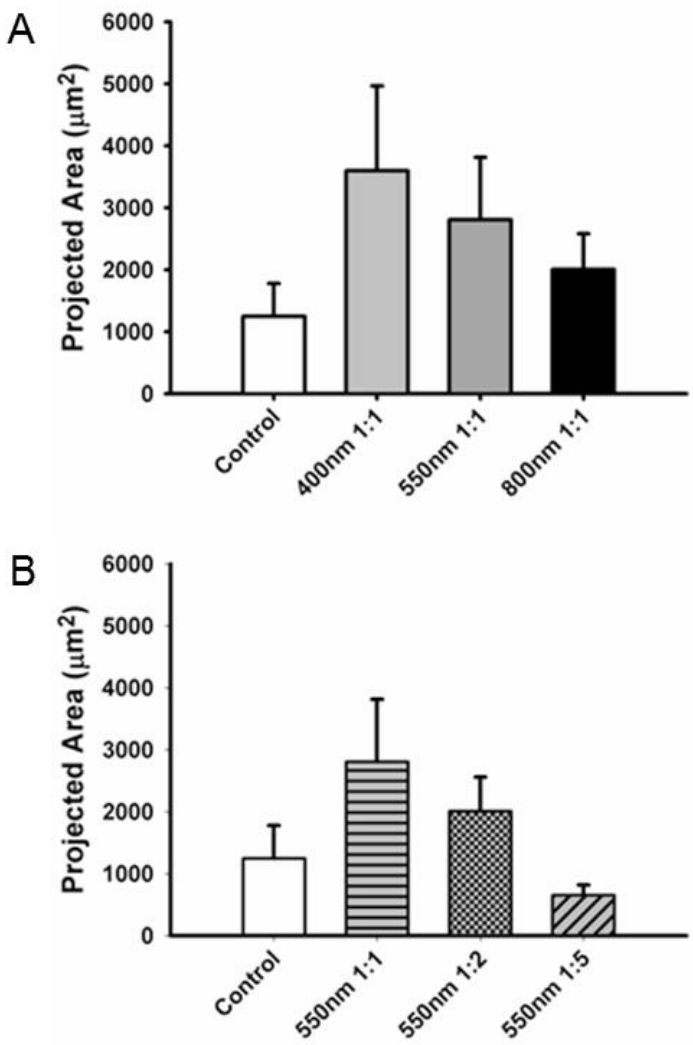

Figure 2-7. Projected cell spreading areas calculated from the SEM images for the dense nanogroove patterns (A) and the nanogrooves of varying spaces (B).

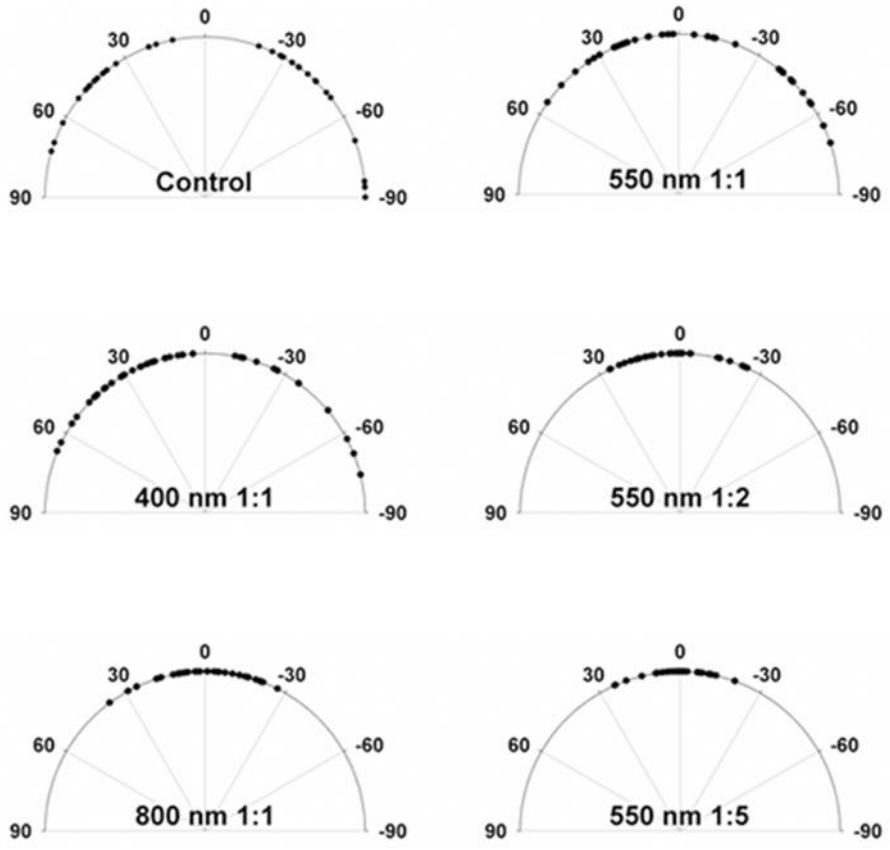

Figure 2-8. Quantification of cellular orientation in angular mapping diagrams for control and various nanogroove patterns. (n = 40).

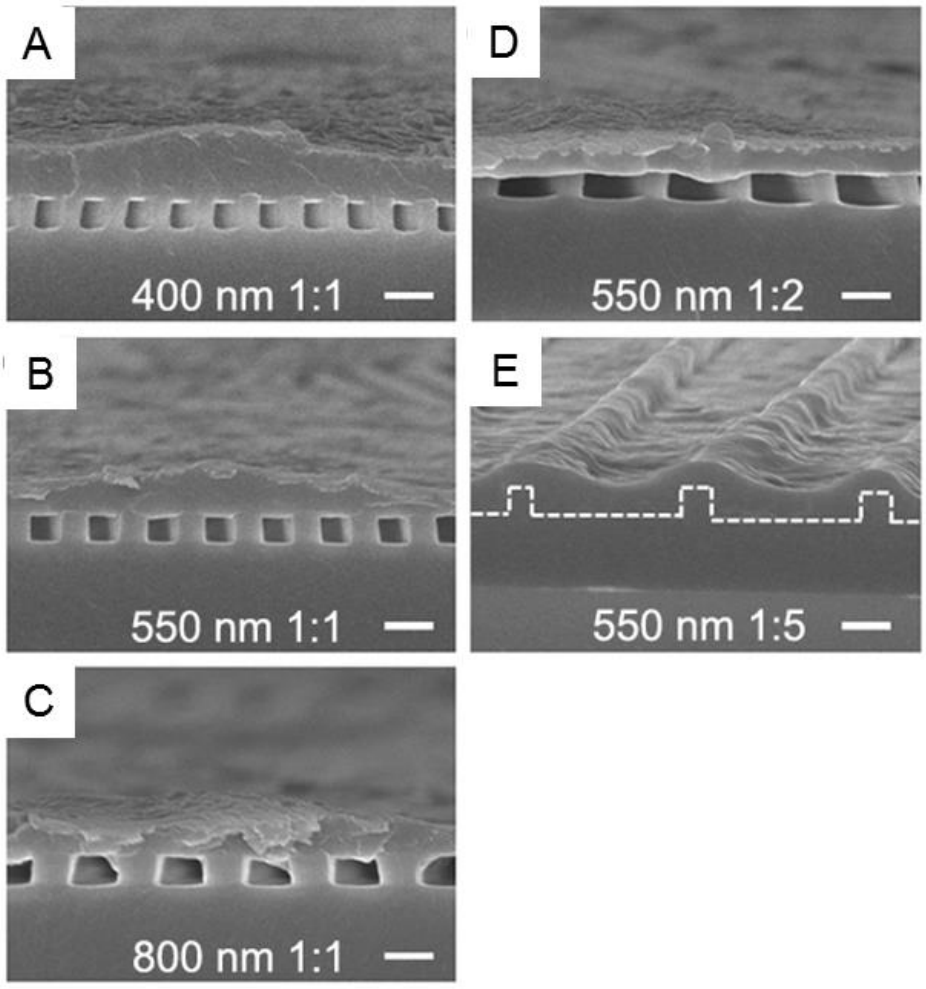

Figure 2-9. Cross-sectional SEM images of the 3T3-L1 cells cultured on various nanogroove patterns. Depending on the width and space of nanogrooves, the cells were spreading only on the ridge regions or penetrated into the grooves. In the case of the 550 nm 1:5 pattern, the cells crawled into the spaces and formed tighter cell adhesions and contact guidance along the groove direction. Scale bar indicates 1μm.

2.3.4. On the role of contact guidance in adipogenic differentiation

The pioneering work by Chen and coworkers revealed that the cell shape can dictate the differentiation of mesenchymal stem cells by modulating cytoskeletal tension and contractility [20, 42]. They reported that as the degree of cell spreading was increased by culturing on large ECM islands, the degree of cytoskeletal tension and contractility was enhanced, which resulted in reduced adipogenesis. In this respect, the degree of actin stress fiber formation can be used as an index for the cytoskeletal tension and contractility [24]. Following the observation by Chen and coworkers, it is expected that the formation of actin filaments would be reduced for the larger width or inter-spacing nanogroove patterns.

To evaluate the degree of cytoskeletal organization, we conducted immunofluorescent staining for actin filaments as shown in Figure 2-10(A-D). While some alignment was seen for the 800 nm pattern, well-organized and aligned actin fibers were mainly observed on the 550 nm 1:5 pattern in contrast with the other dense nanogrooves and PUA control. This suggests that a simple nanogroove pattern has ability to down- or up-regulate adipocyte differentiation by modulating cell shape and cytoskeletal organization. Further, the contact guidance can be used as an indicator to determine the

degree of adipocyte differentiation.

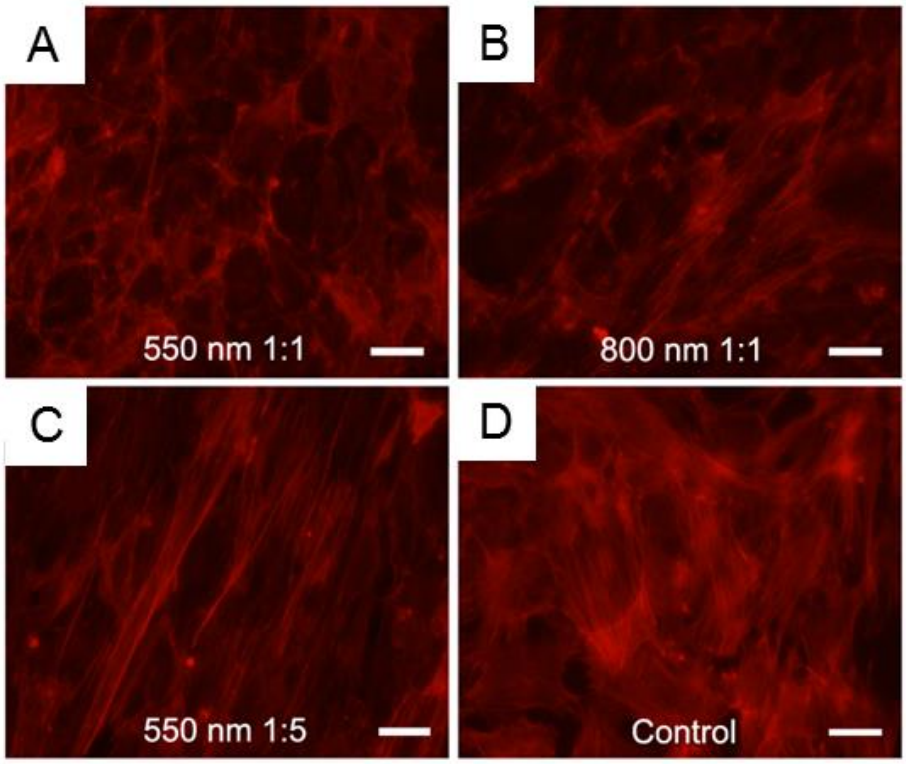

Figure 2-10. Fluorescence images of the 3T3-L1 cells immunostained for F-actin. Well-organized actin stress fibers were observed for the largest spacing of the 550 nm pattern. Scale bar indicates 100 μm.

2.4. Summary

We have presented the role of ECM nanotopographical features in the form of parallel nanogroove arrays on the adipocyte differentiation of 3T3-L1 preadipocytes. Data from Oil Red O staining, relative amount of lipid accumulation, and adipogenic marker gene expression have implied that the adipogenesis could be modulated by culture on various nanogroove patterns with different widths and spaces. In particular, the differentiation level was potentially enhanced on the 550 nm 1:5 pattern by 20 % as compared to the control without nanopatterns. Such small enhancement might be attributed to the dominant effect of the induction media that is needed for the differentiation. The SEM measurement has shown that the cell morphology was distinctly different on different nanogroove patterns. Surprisingly, the cells penetrated into the grooves with better contact guidance only for the 550 nm 1:5 pattern, in good correlation with the differentiation level. A cartoon in Figure 2-11 depicts the role of nanogroove geometry on adipogenic differentiation observed in this study. Although a detailed study elucidating biological mechanisms is required, the present study shows that contact guidance, which is closely related to integrin-mediated adhesions, plays a critical role in

regulating adipocyte differentiation. Therefore, a simple index for contact guidance might be useful to predict the level of differentiation.

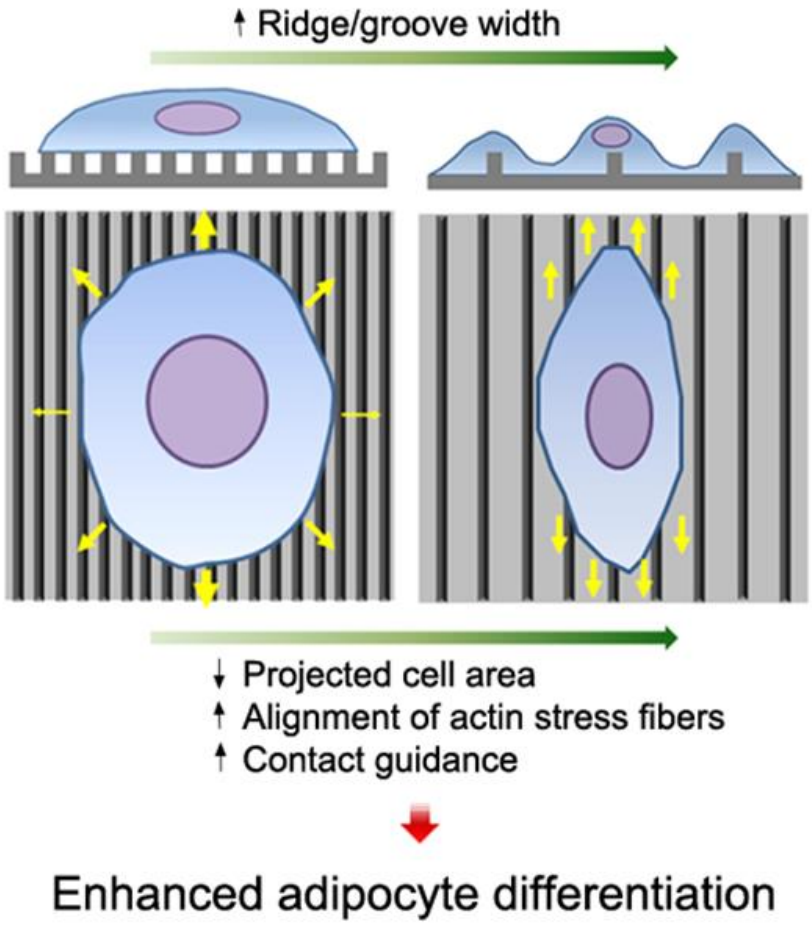

Figure 2-11. A cartoon depicting the role of nanogroove geometry on the adipocyte differentiation.

Chapter 3. Hybrid microfabrication of nanofiber-based sheets and rods for tissue engineering applications

3.1. Introduction

One of the important issues in the tissue engineering field is to provide cultured cells with a biocompatible template, or scaffold, which mimics the natural extracellular matrix (ECM), to regulate cell functions, such as adhesion, migration, proliferation, and differentiation [43-45]. Through the scaffold-based strategies, a wide range of research has been conducted to understand the cellular processes controlled by the surrounding microstructure as well as to develop scaffolds for practical applications in clinical settings [16, 46, 47]. Among many micro- and nano- processing tools for the scaffold fabrication, the electrospinning process has offered unique advantages due to its ability to produce nanofiber networks that closely simulate the ECM structure, which is a complex network with various nanoscale fibrils such as collagen, elastin, fibronectin and laminin [48-51]. The ECM mimicry is beneficial for cell activation and characterized by high productivity,

simplicity, and material universality in manufacturing the nanofibers.

Because the electrospinning process is driven by strong electrostatic force from high voltage, the as-spun fibers usually form a randomly configured nonwoven matrix. Recently, the nanofiber patterning technique has been diversified by modulating its configuration from simple random networks to uniaxially aligned form, which in turn can generate desired cell morphogenesis. The feasibility of aligned nanofiber scaffolds has been demonstrated using various cells such as fibroblasts, myoblasts, neuron cells, and mesenchymal stem cells [52-58]. Especially in the case of myoblasts, their native tissue, skeletal muscle, has a highly organized anatomical structure that consists of many parallel bundles formed by fusion of the myoblasts. It naturally follows a necessity of highly oriented nanofiber scaffold that resembles the native muscle architecture. In order to achieve the ordered fiber configuration, a variety of methods have been proposed by developing specific collecting mechanisms such as rotating cylinder, sharp-edged disk, wire-framed drum, near-field working distance, and parallel electrodes [59-63].

We previously reported a novel processing technique to acquire the ordered nanofiber array scaffold not only with better alignment but also with quantitatively

controlled fiber density [64]. The multiple transfers of nanofibers, by which the nanotopographic spacing could be modulated, were a favorable feature to demonstrate the contact guidance effect of nanofiber pattern. In particular, the well-aligned nanofiber pattern with the controlled configuration showed improved biological functions in cellular adhesion and morphogenesis [65]. However, the previous nanofiber manufacturing methods need to be assisted by some post-processing procedures, allowing for facile manipulation of the produced nanofibers. While the random mesh has a number of overlapping junctions on the constituent nanofibers, the structural interconnections in the aligned mesh are not abundant so that it cannot be handled as an individual entity. The sparse connectivity between aligned nanofibers implies that a supportive structure should be incorporated to prevent a possible distraction of nanofibers.

Here, we introduce an effective hybrid fabrication method to build a new kind of rod- or sheet-type composite scaffold that consists of a spin-coated polymer film and an array of electrospun nanofibers. A series of polycaprolactone (PCL) solutions with diluted concentrations were used for fabricating thin films with varying thicknesses from 1.5 to 35 μm. The polymer films over 20 μm thickness turned out to exhibit favorable stiffness

that allowed manipulation with tweezers. By using a relatively thick film as an underlying substrate, the mechanically stable scaffold was achieved in combination with the transferred electrospun nanofibers. C2C12 myoblasts were cultured to confirm the cellular morphogenesis such as cell alignment and elongation, which may be guided by the nanofiber configuration. In addition to the sheet-type scaffold, the films with thickness less than 10 μm were transformed into a rod-type scaffold by rolling up with the cell-fiber complex sheet. To facilitate the rolling manipulation with thin structures, a cylindrical core of microscale diameter was thermally extruded through a micro needle and deposited at one edge of the nanofiber film. Taken together, some potential obstacles associated with handling fragile nano-sized scaffold materials were alleviated by employing the microfabricated supportive structures with controllable size. For additional manipulations including folding and laminating, the current hybrid scaffolds are fully composed of biodegradable polymers, which could potentially meet the needs of tailored scaffolds for tissue engineering applications.

3.2. Materials and methods

3.2.1. Spin coating process

For spin coating solutions, polycaprolactone (PCL, Mw = 80,000 g/mol, Aldrich) was dissolved in chloroform (Sigma) at three different concentrations of 5, 10, and 20 wt%. As shown in Figure 3-1A, a certain quantity of PCL solution drop was deposited on the glass substrate on the spin-coating machine (JD tech) before spin coating at different speeds in the range from 1000 to 4000 rpm. The spinning time had no significant effect on the film thickness; thus it was fixed at 30 sec. Most of the solvent was evaporated while spinning, because chloroform is a highly volatile solvent. To remove the possible residue of the solvent in the film, the specimens were kept in a fume hood for one hour. The films coated on the glass substrate were incised using a sharp blade for thickness measurement. The film thickness was measured by an Alpha step surface profiler (Nanospec AFT/200, KLA TENCOR), which was determined by the height difference between the top of the coated film and the glass substrate.

3.2.2. Electrospinning process and nanofiber transfer

The PCL was also dissolved in the mixture of chloroform (Sigma) and dimethylformamide (Junsei) at a volume ratio of 75/25. Here, dielectric properties generated from the dimethylformamide enhanced electrospinning capability. The solution concentration was chosen to be ~20 wt%, which had been confirmed as a proper condition in the previous work [64, 65]. The PCL solution was stored in a syringe equipped with a 23-gauge metal needle which was connected to a high voltage DC power supply. The syringe module was loaded on a syringe pump and infused at a rate of 1.5 mL/h. The DC voltage of 15 kV was applied to the solution drop formed at the needle tip. The collector for crop of aligned nanofiber was designed as shown in Figure 3-1B. Two separate aluminum strips were perpendicularly arranged, and the ejected nanofibers were suspended across the air gap between the strips. Due to the repulsive interaction between the adjacent nanofibers hanging on the strips, well-aligned nanofibers could be obtained. More detailed information about the collecting mechanisms and conditions are described in our previous work [64]. The nanofibers were transferred onto the as-prepared PCL film via spin-coating. To vary the scaffold line density, which is determined by the number of

nanofibers along a unit distance perpendicular to the direction of nanofiber alignment, the overlapping transfer was carried out in a repetitive manner. The electrospinning time for each transfer was fixed at 1 min, and 3 and 12 transfers were performed respectively for low and high density. The resultant nanofiber scaffolds were measured using scanning electron microscope (SEM, S-48000, Hitachi). From the SEM images, the fiber alignment was analyzed by measuring the angles between the longitudinal and vertical directions of the fibers.

3.2.3. Thermal extrusion of core structure for rolled-up scaffold

The PCL has good formability for thermal processing due to its low melting temperature at 60℃. We previously developed a polymer melt deposition system for fabricating a three dimensional woodpile shape scaffold that was comprised of a number of thermally extruded microfibers [65]. In this approach, the microfiber-shaped structure was used not only as a core template to provide a tool for rolling manipulation but also as a mechanical support of the overall hybrid architecture. Figure 3-1C illustrates the thermal extrusion procedure following the prior processes for nanofiber-patterned film

fabrication. The system consists of a thermally conductive metal syringe equipped with a micro precision needle, a coil heater surrounding the syringe module, a pneumatic dispenser delivering compressed air, and a micro-positioning system driven by step motors. When the air pressure was applied to the polymer melts stored in the syringe, the microfiber-shaped polymer melts were extruded out through the micro needle. The initially molten state microfiber was then deposited onto the pre-processed nanofiber film surface, and fused with the film as solidified at ambient conditions. The inner diameter of the micro needle was 400 μm and the processing temperature of the coil heater was set up at 150℃. The applied pressure and the moving velocity of the micro needle were controlled in the range of 550~750 kPa and 0.5~2 mm/sec, respectively. Subsequently, the nanofiber film structure, even with cultured cells on its surface, could be easily rolled up along the fabricated microfiber core structure.

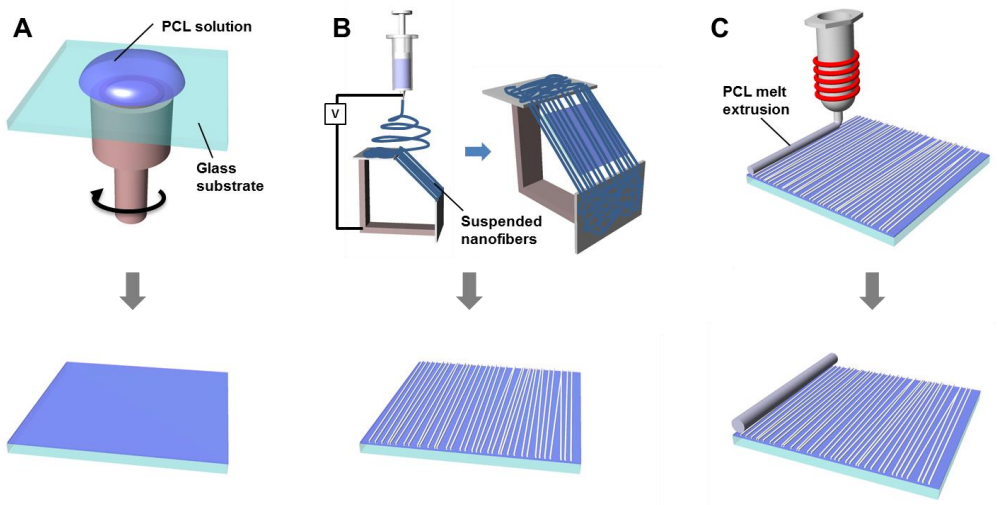

Figure 3-1. Fabrication process of hybrid nanofiber scaffold: (A) spin coating process to fabricate a PCL thin film, (B) electrospinning process to secure aligned nanofibers and transfer onto the film, and (C) polymer melt deposition process to place a microfiber core structure for subsequent rolling process.

3.2.4. Cell culture

All reagents used in the experiments related to cell culture were purchased from Sigma Aldrich, unless otherwise specified. C2C12 mouse myoblasts were purchased from ATCC and maintained in Dulbecco's Modified Eagle's Medium (DMEM, GIBCO) supplemented with 20 % fetal bovine serum (FBS, GIBCO) and 1 % penicillin-streptomycin (PS, GIBCO). Prior to cell seeding, all scaffolds were sterilized for one hour under ultraviolet irradiation, treated with oxygen plasma for 1 min, and coated with fibronectin of 10 mg/mL for one hour at room temperature. The cells were seeded onto the prepared scaffold at the density of 2×10^5 cells/cm^2 and cultured for two days until the cells formed a confluent monolayer.

3.2.5. Immunostaining

C2C12 cells on the scaffolds were gently washed with PBS and fixed with 3.7 % formaldehyde solution for 10 min. Fixed cells were washed with PBS three times and immersed in antibody buffer (0.1 % Triton X-100 and 2 % bovine serum albumin (BSA) in PBS) for 15 min to make the cells permeable and prevent unspecific binding of

antibodies. After washing three times with PBS, the cells were then sequentially stained with 4′,6-diamidino-2-phenylindole dihydrochloride (DAPI) solution (1:1000) for nucleus and phalloidin-TRITC solution (1:400) for actin cytoskeleton for 40 min each. To prevent photobleaching, the cells were embedded with a small amount of ProLong Gold antifade reagent (Invitrogen) and observed with fluorescence microscopy (Eclipse Ti, Nikon).

3.2.6. Scanning electron microscopy (SEM) measurement

The nanofiber film scaffolds with C2C12 cells were rinsed with PBS and rolled up using the developed method. The samples were fixed with 5 % glutaraldehyde solution supplemented with 0.1 M sodium cacodylate and 0.1 M sucrose for 30 min. For further fixation, the samples were treated with 1 % osmium tetroxide solution containing 0.1 M sodium cacodylate and 0.1 M sucrose for 1 h. After washing three times with PBS, the samples were slowly dehydrated by immersing them in ethanol solutions of increasing concentration and hexamethyldisilazane (HMDS, J.T.Baker) to prevent collapse of cell morphology. The samples were completely dried in a fume hood overnight and were observed using SEM (S-48000, Hitachi).

3.2.7. Quantitative analysis

The images of the C2C12 cells stained with DAPI were taken 5 times for each sample and used for analysis. Cell orientation was determined by the angle of long axis of nuclei against nanofiber alignment direction. Nucleus elongation was calculated by dividing the short axis length over the long axis length. In a similar manner, SEM images of nanofibers were taken 10 times for each sample and used for calculating nanofiber orientation.

3.3. Results and discussion

3.3.1. Spin-coating of PCL films

Figure 3-1 illustrates the process for fabricating a hybrid scaffold consisting of electrospun nanofibers supported on a thin film. The overall scaffolds were made of a well-known biodegradable and biocompatible polymer, PCL, which is widely used for various biomedical applications. Since it has a low glass transition temperature of -60℃ and exists in a rubbery state at room temperature, the PCL based structure has better mechanical compliance than other biodegradable polymers. This property makes it ideal for use as a flexible scaffold material. In this research, we exploited the shape-deformable characteristic of PCL by employing and integrating three consecutive microfabrication methods of spin-coating, electrospinning and deposition of polymer melt.

At first, we fabricated a thin PCL film using the spin coating method with variables such as angular speed of spinning and polymer solution concentration. It was observed that the increase of spinning duration time beyond 30 sec had no significant effect on the film thickness (data not shown) because the solution almost solidified from the fast evaporation of chloroform that was used as the solvent. Figure 3-2 shows the

correlation between film thickness and spinning speed at three different solution concentrations of 5, 10, and 20 wt%. As seen from the figure, the relatively thin films made from 5 and 10 wt% solutions displayed less dependency on the spinning speed. The variations of film thickness between 1000 and 4000 rpm appeared to be approximately 15% and 18% in the cases of 5 and 10 wt% solutions, respectively. As the solvent evaporation occurred in a very short period of time during the spinning, the film thicknesses at lower concentrations were less sensitive to the change of spinning speed and thus their standard deviations were very small below 0.3 μm. As with the typical spin coating process, thicker films were obtained as the solution concentration became higher. In the case of 20 wt% concentration, the thickness of all specimens exceeded 15 m from 1000 to 4000 rpm, and the thickness at 1000 rpm was two times higher than that at 4000 rpm, suggesting a significant dependency on the spinning speed. Figure 3-3A shows an example of the coated film peeled off from the glass substrate. We found that the film thicker than 20 μm was sufficiently rigid to manipulate by any tweezers, which was used as a basement substrate for a free standing nanofiber-transferred scaffold. As observed in other works [66-68], a certain degree of crystallization was found on the surface of PCL

film after spin coating as shown in Figure 3-3B and C. Here, the spherulitic crystals that were formed regularly on the entire films are believed to yield good mechanical stability and formability. When a thick film was spun from 20 wt% solution, however, some defects such as trapped or burst bubbles were frequently observed. To remove such defective bubbles, the films were heated on a hot plate above the PCL melting temperature (100℃) and held undisturbed for 10 min. After cooling back to room temperature, a uniform membrane was obtained without bubble defects as shown in Figure 3-3D.

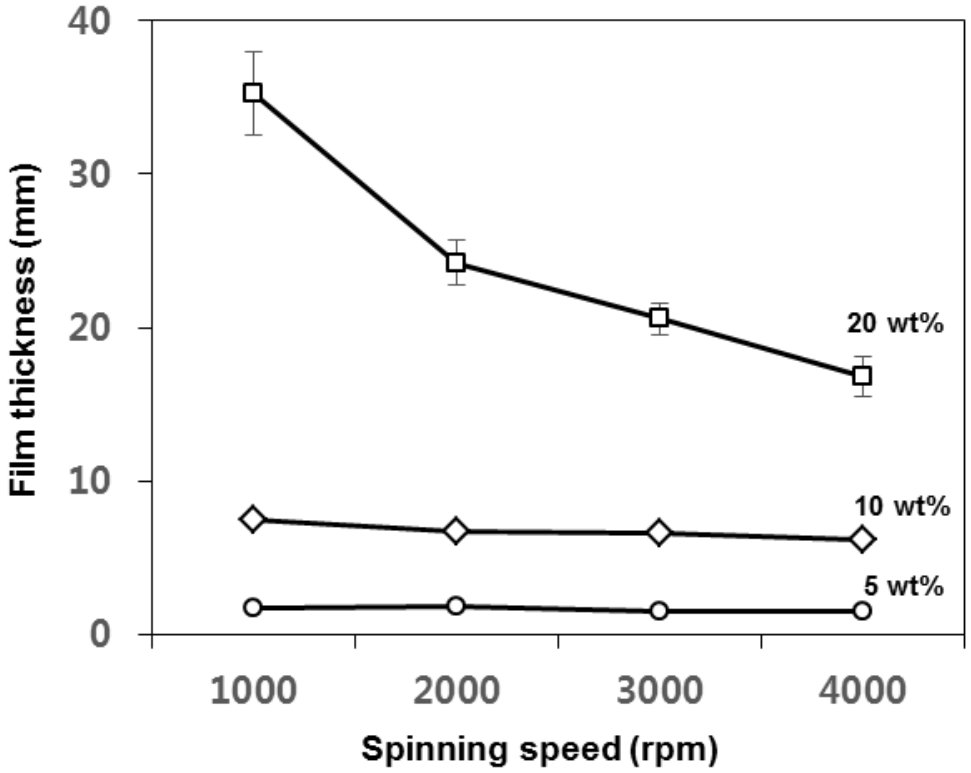

Figure 3-2. Relationship between film thickness and spinning speed at three different PCL solution concentrations of 5, 10 and 20 wt%.

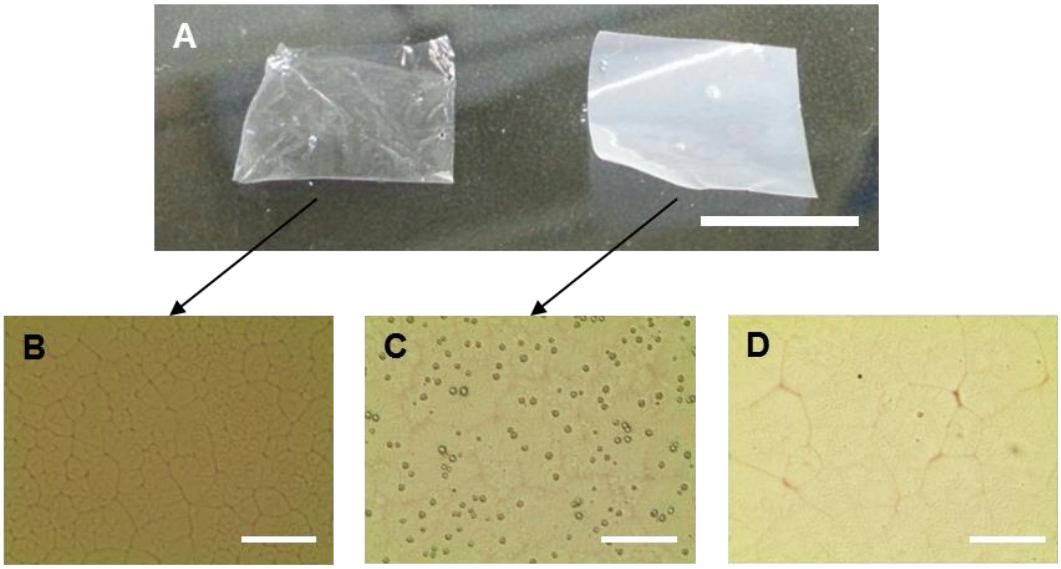

Figure 3-3. (**A**) Thin (left) and thick (right) films were respectively made from 5 and 20 wt% solutions at a speed of 3000 rpm. The scale bar is 5 mm. Optical microscope images of the PCL film surfaces made from (B) 5 and (C) 20 wt% solutions. (D) The thick film surface (case D) after removing bubble defects by heat treatment. The scale bar in B is 50 μm with the same magnification in C and D.

3.3.2. Electrospinning of PCL nanofibers for sheet-type scaffold

Next, nanofiber-microfilm hybrid constructs were generated by multiple transfers of nanofibers hanging on the void gap collector (Fig. 3-1B). In this way the density of collected nanofibers could be controlled in a quantitative fashion. Figure 3-4A and B show the resulting fibers of average densities of 108 and 384 fibers/mm with 3 and 12 transfers, respectively. Such different densities are expected to yield different contact guidance cues in the cell seeding experiments. As for nanofiber orientation in this scaffold, the fibers placed on PCL film were quantified by measuring the inclined angles with respect to the reference direction. As shown in Figure 3-4C and D, all of the transferred fibers were distributed within a narrow range of ±25° and more than 90% of the fibers were oriented within ±10° to the reference direction. The fiber alignment was nearly reproducible for every single-step electrospinning process, indicating that the nanofiber transfer repetition in both cases of 3 and 12 transfers did not significantly impair the fiber alignment.

Recently, a number of studies on contact guidance have been conducted via template-assisted techniques such as electrochemical deposition, soft lithography, and

nanoimprinting [69]. Although they provide reproducible construction of nanoscaffolds with high precision, the electrospun nanofibers have an advantage in terms of direct transplantation in their initial architecture. In order to demonstrate the feasibility of the developed nanofiber-based scaffold, C2C12 myoblasts were cultured for two days and morphological changes were analyzed from immunofluorescent imaging. We employed three types of scaffolds: i) flat film without nanofiber, ii) nanofiber scaffold of low density (3 transfers) and iii) that of high density (12 transfers). As shown in Figure 3-5, the nuclei and cytoskeletons of cells appeared to align along the unidirectionally oriented nanofibers. Also, the nuclei stained with DAPI showed that the nanofibers on film gave rise to elongated morphology in the direction along the fiber alignment. In contrast, neither the cell alignment nor elongated morphology was shown for the cells cultured on a flat PCL film surface without fibers.

For quantification, the distribution of aligned cell morphology was analyzed using angular mapping plots as shown in Figure 3-6 (A-B). On the scaffolds without nanofibers, it is seen that the cell alignment and elongation were hardly observed (Figure 3-6A and D). On the other hand, the cells grown on nanofiber scaffolds with 3 and 12

transfers showed distinct alignment and elongation guided by the nanofibers as shown in Figure 3-6 (B-D). As the nanofiber density increased from 108 (3 transfers) to 384 nanofibers/mm (12 transfers), both morphological changes of alignment and elongation became more pronounced. The correlations between fiber density and cell morphology were identified in accordance with the previous work [70]. It is noteworthy that a nanofiber set of relatively low density also provided the desired morphological changes similar to a high-density fiber set, while recognizing that a considerable amount of cells were still not affected by the fibers due to the larger fiber spacing. When considering the confluent state of cultured cells as shown in Figure 3-5, the cells aligned directly by nanofibers seemed to affect the shape of adjacent cells due to tight cell-cell interactions even in the presence of the low-density fiber network.

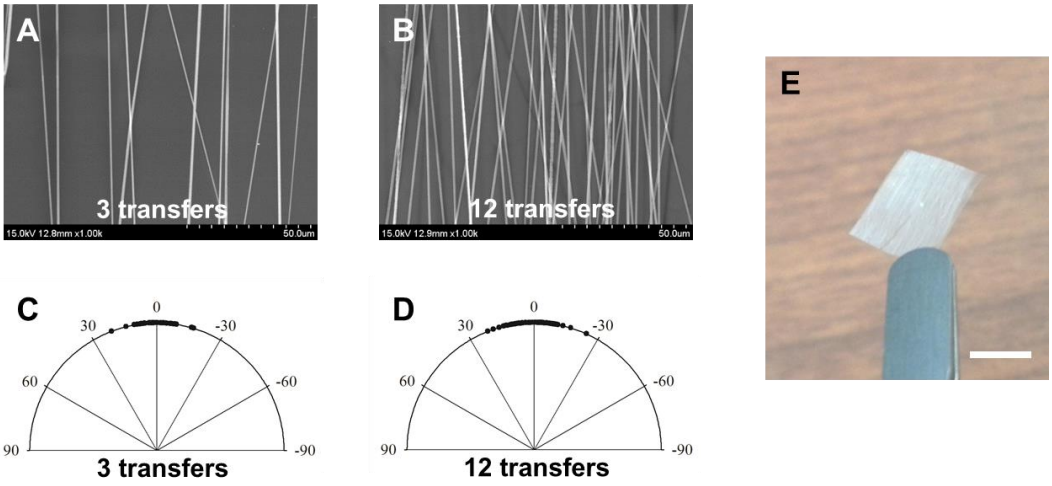

Figure 3-4. SEM images of the repetitively cropped nanofibers on PCL films: (A) 3 transfers and (B) 12 transfers. Angular mapping plots to quantify nanofiber alignment: (C) 3 transfers (n=70) and (D) 12 transfers (n=100). (E) Photograph of sheet-type hybrid scaffold integrated with aligned nanofibers. The scale bar is 5 mm.

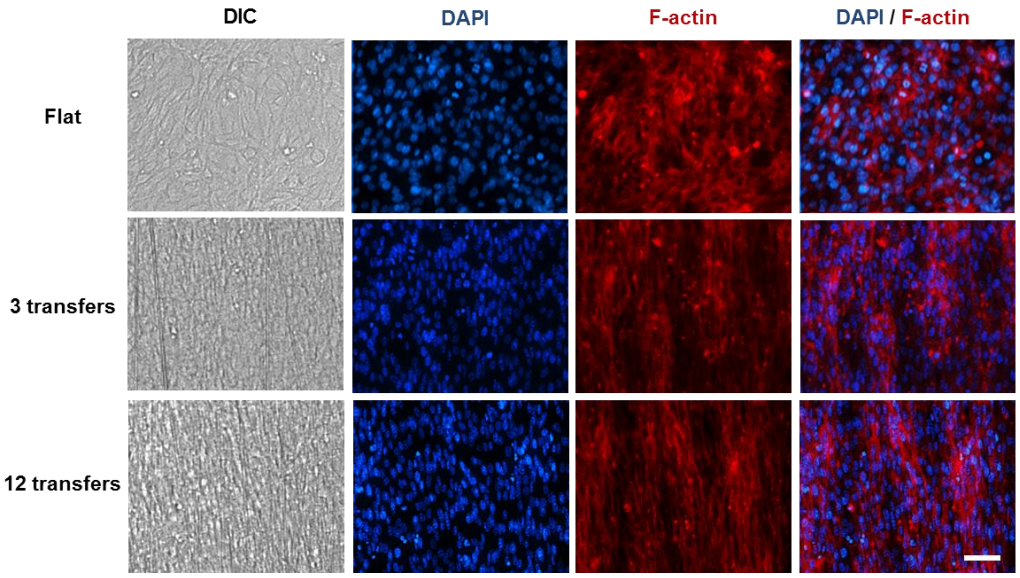

Figure 3-5. Diffraction interference contrast images (first column) and immunofluorescent staining images of cells cultured on flat PCL film (first row), nanofiber-integrated scaffold with 3 transfers (second row) and 12 transfers (third row). DAPI, F-actin and their merged stack are arranged in the second, third, and fourth column, respectively. The scale bar in A is 25 μm, and the other images are at the same magnification.

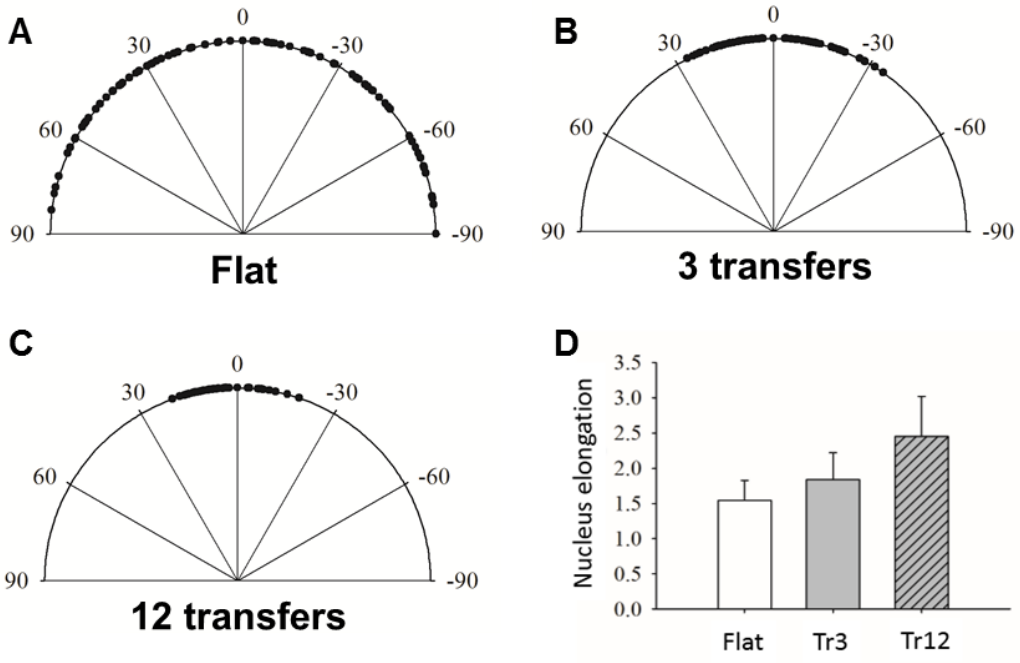

Figure 3-6. Angular mapping plots to quantify cell alignments of (A) flat PCL film and (B) nanofiber-integrated scaffold with (B) 3 transfers and (C) 12 transfers. (D) Degree of nucleus elongation of each scaffold. Data shown as mean ± standard deviation (n=100 in each scaffold).

3.3.3. Rolling of PCL nanofibers for rod-type scaffold

One of the crucial factors for an ideal scaffold is to offer a three-dimensional (3D) mechanical support for tissue growth. Since electrospun nanofiber structures are too subtle to provide the mechanical support for scaffolds, a number of studies have been made towards a stiff microstructure so as to overcome the inherent delicacy and two-dimensional limitation of nanofibers [64, 71-73]. To this end, 3D roll-type nanofiber scaffolds are demonstrated here by incorporating a core microfiber structure by polymer melt extrusion. Figure 3-7A shows the relation of the extruded microfiber radius versus the velocity of needle movement at two different applied air pressures. These results imply that the dimension of core structure could be adjusted as shown in Figure 3-7B and C, allowing for a simple route to controlling the final size of rolled scaffold. The dimensional variation could be further tailored by adopting different sizes of micro needles. As mentioned earlier, the microfiber structure was aimed to facilitate the rolling-up process; it was used to pack the planar nanofiber film around the core microfiber as shown in Figure 3-8A and B. For the basement substrate, a thin film made from 10 wt% solution yielding a thickness less than 10 μm was used for its enough flexibility to be

rolled up.

The rolling-based manipulation was even possible after culturing cells on the nanofiber film. As the region of cell-nanofiber construct on the film could be intact in the course of careful handling of microfiber, the cell structures on the nanofiber scaffold were not damaged during the rolling procedure as shown in Figure 3-9. Also, the nanofiber-induced cell alignments in both cases of 3 and 12 transfer scaffolds were not impaired (Fig. 3-9(C-F)). The mechanical properties of constituent components, such as nanofiber and micro thin film, were fairly compliable and flexible enough to retain their assembly. It is worthwhile nothing that the ability to embed cells in a rolled 3D scaffold would be beneficial when it is needed to retain the final shape of scaffolds after completing cell culture. If the cell culture is carried out on a 3D shape scaffold by simple top-seeding method, one would encounter various problems such as difficulties of cell penetration and nutrient/waste exchange. In future studies, more detailed cell experiments with handling the sheet scaffolds will be performed to determine the potential biofunctional significance based on the aforementioned issues of mass transfer through scaffold.

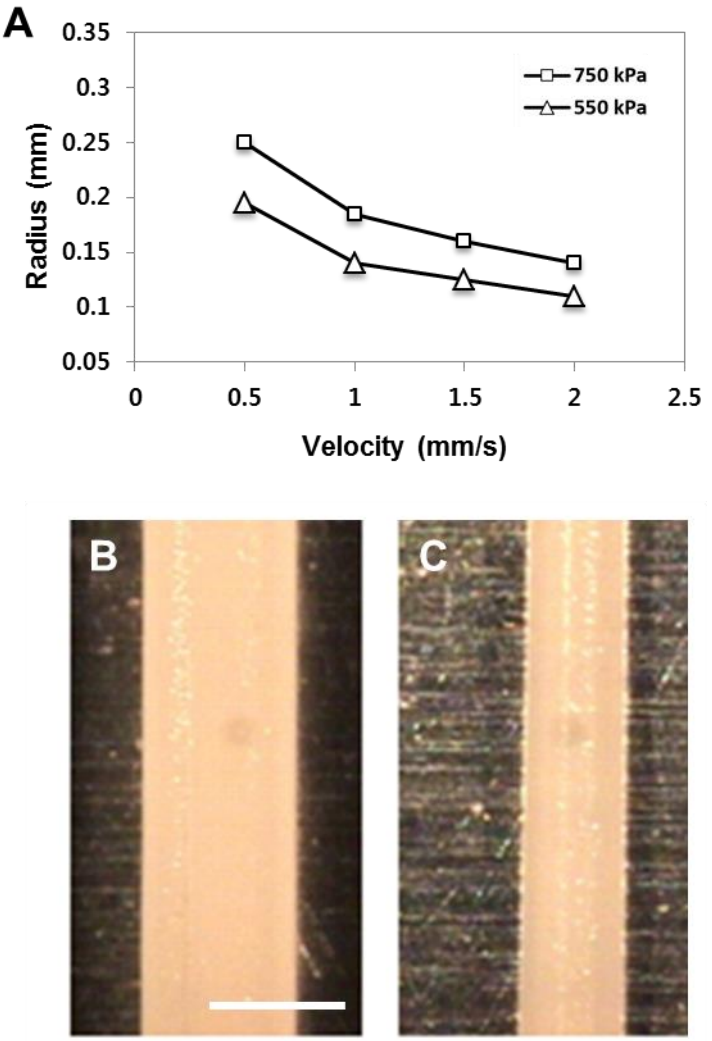

Figure 3-7. Results of thermally extruded microfibers. (A) Plots of microfiber radius vs. needle movement velocity at different applied pressures of 550 and 750 kPa. Optical microscopy images of microfibers fabricated by needle movement of (B) 0.5 and (C) 1.5 mm/sec at an air pressure of 750 kPa. The scale bar indicates 500 μm.

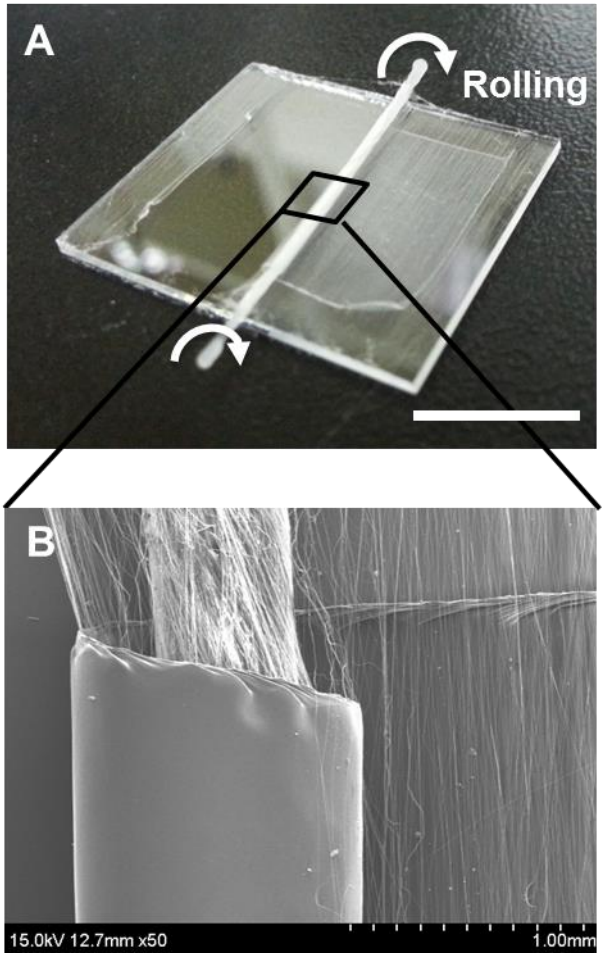

Figure 3-8. Photograph of rolling process and (E) SEM image of the resulting roll scaffold. The scale bar indicates 10 mm.

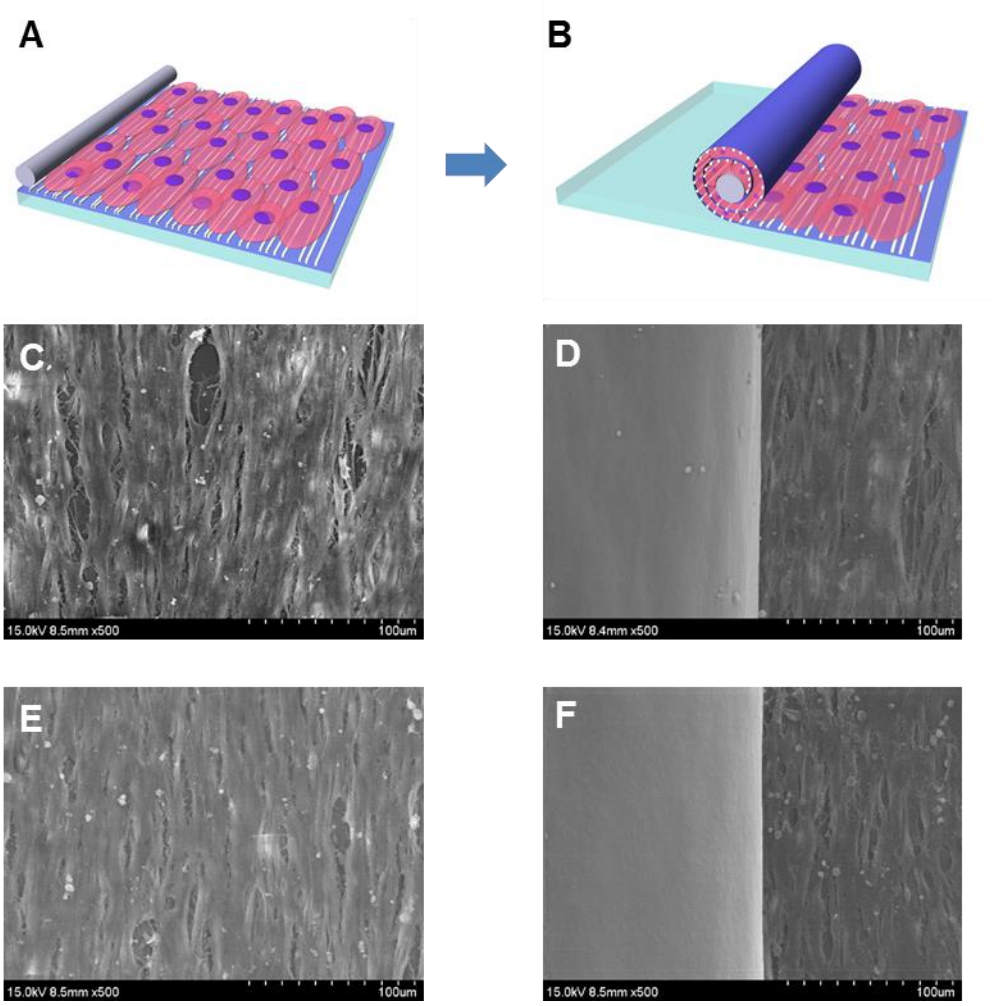

Figure 3-9. (A, B) Schematic diagrams of rolling process with embedding cells on nanofiber film scaffold. SEM images of the cultured cells (C, E) before and (E, F) after the rolling process. (C, D) 3 transfers and (E, F) 12 transfers of nanofibers were respectively performed on the scaffold for cell culture.

3.4. Summary

The present study has introduced our initial effort to utilize nanofiber scaffold in practical ways via some physical manipulation such as nanofiber alignment or scaffold rolling. Spin-coated PCL films with varied thicknesses enabled nanofiber manipulation for the development of sheet-type scaffolds. The film thickness could be modulated by adjusting solution concentration rather than spinning speed because of the highly volatile property of chloroform used as the solvent. Well-aligned nanofibers were transferred onto the film with multiple times ($\leq$ 12), which have proven effective to provide contact guidance cues on cultured cells. As expected, the presence of nanofibers yielded morphological changes of myoblasts into aligned and elongated shapes. In addition to sheet-type scaffolds, we developed rod-shaped roll constructs by exploiting the mechanical support of thermally extruded microfiber and the flexibility of nanofiber-film complex. The rolling process could be carried out without any appreciable damage to cultured cells. These results collectively suggest that the hybrid fabrication method presented here has the potential to overcome various obstacles involved in practical uses of the nanofibrous scaffold in clinical settings or other tissue engineering applications.

Chapter 4. Aligned nanofibrous membrane as a versatile tool for cell sheet manipulation and cell-dense 3D engineered tissue formation

4.1. Introduction

Current tissue engineering technology has matured with two major techniques, namely, the application of premade porous scaffolds seeded with or without cells [74, 75] and the direct transplantation of cells with hydrogels [76]. The former, namely scaffold-based strategy, possesses great advantages for regulation of cellular activity amechanical support by virtue of the scaffold micro- and macro- architecture. Although a number of biomaterials and processing techniques have been successful for a lot of clinical trials, they still have concerns for inflammatory responses caused by physiological and mechanical mismatch of the implanted scaffold material with host diseased area.

As another approach to the cell-based regenerative therapy, cell sheet engineering with no use of scaffold, or at least, has attracted much attention. The cell sheet engineering aims to harvest confluently cultured cells in an intact sheet-like form

without any damage of cell-cell attachment. The thermoresponsive culture surface, representatively poly-N-ispropylacrylamide (PNIPAAm), has been exploited for dissociation of the cell sheet which is a core procedure in the cell sheet engineering [77]. PNIPAAm becomes switchable between hydrophilic and hydrophobic surface at a critical temperature of 32℃, thus the cell attachment and detachment from culture substrate can be modulated by simple temperature changes. In contrast to enzymatic digestion as a usual method for cell dissociation, the cell sheet detachment using thermoresponsive polymer substrate allows to preserve not only the cell-to-cell junction but also the extracellular matrix (ECM) underlying the cell sheet. Taking advantage of this characteristic, PNIPAAm surfaces have been developed in a variety of forms, including silicon, tiissue culture polystyrene (TCPS), and polydimethylsiloxane (PDMS) [78-80]. Although the cell sheet techniques have been successful for various tissue engineering applications, the inherent mechanical instability and delicacy of cell sheets still make it difficult to manipulate them for practical transplantation. Furthermore, the preparation of such thermoresponsive surface could require labor-consuming tasks and cautious optimization of the processing parameters.

Some of native tissues, such as skeletal muscle tissue, have a unidirectional alignment in their anatomic microstructures. As the anisotropic organization of cell or ECM determines the physiological functions of tissues, it is extremely important to realize the biomimetic anisotropy in the cell sheets. Recently, a growing number of patterning techniques based on the thermoresponsive polymer have been introduced to produce the cell alignment in the cell sheets. For instance, Lin et al. presented a PNIPAAm-grafted surface based on microtextured PDMS substrate using traditional soft lithography [80]. Takahashi et al. showed a PNIPAAm stripe micropattern utilizing site-specific grafting method with hydrophilic polymer that has a repellent property for cell adhesion [81]. In those works, they discussed the shrinkage of detached cell sheets. The stresses on the aligned cell sheet caused more shrinkage along the direction of pattern alignment. It naturally follows the need for a mechanical support frame to prevent the uneven shrinkage in the cell sheets.

Here we introduce a simple method to build and manipulate cell sheets utilizing electrospun nanofibrous membrane as a tool. The nanofibers were integrated with a PDMS assembly involving a well for cell culture. After myoblasts were cultured to a

confluent state and formed a sheet-like structure, the cell sheet could be detached without any damage and contraction of the sheet structure by lifting off the nanofiber sieve. We demonstrated the feasibility of this dissociation method by immunofluorescent microscopic visualization of the cell morphology and the live/dead cell assay. Furthermore, it was observed that the nanofiber configuration optimized by control of fiber density could strengthen the structural stability of cell sheet and the nanofiber-guided cell orientation. Finally, we verified that even ordinary PDMS surface provided the same availability for base substrate of cell dissociation as PNIPAAm-grafted surface. These characteristics reported in this article would be appropriate for creating more effective and practical applications to cell sheet based tissue engineering.

4.2. Materials and methods

4.2.1. Fabrication of aligned nanofibrous membrane

Figure 4-1A illustrates the overall procedures to fabricate the device for cell sheet formation and manipulation. The device was comprised of a set of nanofiber array and two PDMS blocks involving a cell culture well in the upper block. The silicon resin and the curing agent (Sylgard 184 PDMS kit, Dow Corning, Midland, MI) were mixed at 10:1 weight ratio. A certain quantity of the PDMS prepolymer mixture was poured over petri dish to obtain approximately 2 mm and 5 mm thick slabs, which were used as base substrate and well barrier respectively. After curing at 70℃ for 1 h, the PDMS slabs were peeled off from the dishes and cut into square-shape blocks with a sharp blade. Hole was punched through the each 5 mm thick block for forming the cell culture well.

Polycaprolactone (PCL, average MW 80000, Sigma) was employed as the electrospun nanofiber material. Base solvent was prepared by mixing chloroform (Sigma) and N,N-dimethyformamide (DMF, Sigma) at a volume ratio of 75/25. The PCL granules were dissolved into the base solvent at a concentration of 20 wt%. The PCL solution was electrospun from the system consisting of a 23-gauge needle, a high-voltage power

supply and a syringe pump. The applied voltage and the infusion rate were 15 kV and 1.5 ml/h respectively. We previously reported on the fabrication process to build a well-aligned nanofiber array [64]. Using two separate metal strips arranged perpendicularly, we could obtain well-oriented nanofibers across the strip gap and transfer the nanofibers onto any kind of substrate. The more detailed information about the collecting mechanisms is described in our previous works [64, 70]. In order to crop the well aligned nanofiber, we used the developed electrospinning method and fixed the spinning time at 1 min. The nanofibers were transferred onto a surface of the punched PDMS block prepared in advance. Prior to the nanofiber transfer, the PDMS block surface was treated with oxygen plasma for 1 min (0 W, PDC-32G, Harrick Scientific) to enhance the charge-induced adhesion with positively charged nanofibers. The nanofiber sieves with quantitatively controlled fiber densities were fabricated by varying the number of transfers from 1, 3 to 6.

4.2.2. Characterization of aligned nanofibrous membrane

To investigate fiber diameter and orientation of fabricated nanofibrous membranes, samples were observed with scanning electron microscope (SEM, S-48000, Hitachi) and analyzed using ImageJ software. For measurement of membrane thickness, images of the samples were obtained using atomic force microscope (AFM, Park systems) and analyzed using XEI software (Park systems).

4.2.3. Cell culture

Murine skeletal muscle cell line (C2C12), mouse embryo fibroblast cell line (NIH-3T3) and human foreskin fibroblast cell line (HS68) were purchased from American Type Culture Collection (ATCC). Human umbilical vein endothelial cells (HUVECs) were purchased from Lonza. The cells except for HUVECs were maintained with Dulbecco's modified eagle medium (DMEM, Gibco) supplemented with 10 % fetal bovine serum (FBS, Hyclone) and 1 % penicillin-streptomycin (PS, Hyclone) (growth medium, GM) and HUVECs were maintained with EBM-2 medium supplemented with EGM-2 bullet kit (endothelial growth medium, EGM, Lonza).

To induce myogenic differentiation, the cultured C2C12 cells were shifted to DMEM supplemented with 2 % donor equine serum (Hyclone) and 1 % PS (differentiation medium, DM) cultured for 7 days with changing DM every other day.

4.2.4. Manipulation and layer-by-layer stacking of detached cell sheets

Nanofibrous membrane and base PDMS substrate assemblies were treated with oxygen plasma for 1 min to enhance surface hydrophilicity and sterilized with UV light for 2 h. Sequentially, the samples were treated with poly-D-lysine solution for enhancing initial cell adhesion and washed with 1X phosphate buffered saline (PBS, Hyclone) for 2 times. After washing steps, cells were seeded at a density of 1×10^5 cells/cm^2 for C2C12 cells and 5×10^5 cells/cm^2 for other cells. After the cells reached confluent state, nanofibrous membrane with cell sheet, upper part of assemblies, was carefully detached from base PDMS substrate using sharp tweezers and transferred to cell culture dish.

Layer by layer stacking procedures were schematically described in figure 4-1B. Because aligned nanofibers maintained their morphology by applied tension, removal of tension by cutting or detaching from structural frame resulted in loss of nanofiber

alignment. In conjunction with nanofibers, detached cell sheets on nanofibrous membranes lost their morphology when detached from structural frame. Thus structural frame was essential for stable manipulation of detached cell sheet during layer-by-layer stacking procedures. Punched PDMS frame, however, was not adaptable for stacking process due to its low mechanical property and difficulty of precise fabrication. Thus, we used three types of laser-cutted acrylic frame instead of punched PDMS frame used in above (i. e. 23 × 23 mm^2 with 20 × 20 mm^2 through hole, 26 × 26 mm^2 with 23 × 23 mm^2 through hole and 29 × 29 mm^2 with 26 × 26 mm^2 through hole). All of other parameters except for frame were identical. Layer-by-layer staking of detached cell sheet was accomplished by assembling smaller frame with cell sheet to bigger one.

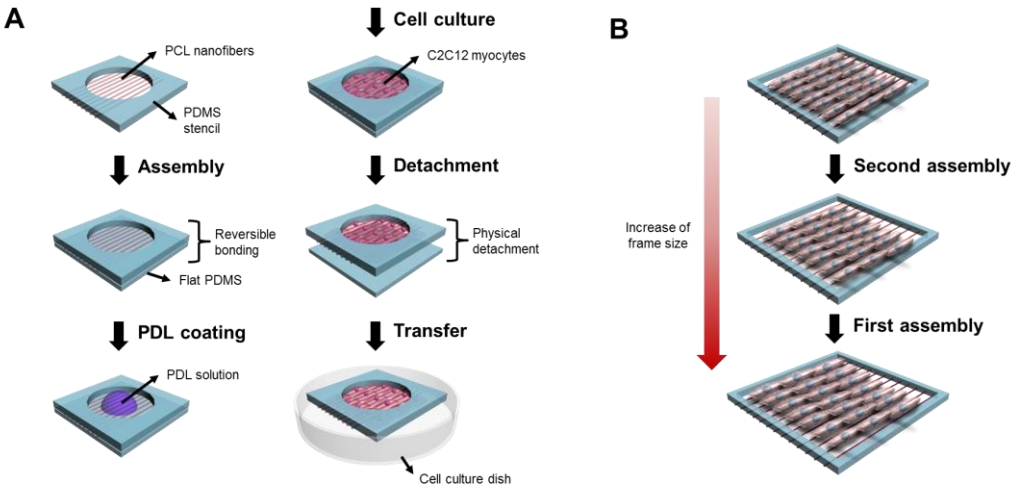

Figure 4-1. Schematic diagrams of (A) cell sheet detachment and manipulation using nanofibrous membranes and (B) layer-by-layer stacking of detached cell sheets to form 3D engineered tissue *in vitro*.

4.2.5. Tube formation assay

Growth factor reduced basement membrane matrix (Matrigel) was purchased from BD Biosciences. A small amount of Matrigel was dropped on prechilled glass coverslip with PDMS reservoir and then carefully covered with detached endothelial cell sheet. Consequently, same amount of Matrigel was dropped on the cell sheet and incubated to induce gelation for 30 min. After gelation, the samples were immersed with EGM and cultured for 5 days.

4.2.6. Immunostaining

For immunostaining, cultured cells at appropriate time point were washed with PBS for 3 times and fixed with chilly 4 % paraformaldehyde solution for 15 min at room temperature. Fixed cells were permeabilized with 0.2 % Triton-X solution (Sigma) for 15 min and blocked with blocking solution containing 3 % bovine serum albumin (BSA, Sigma) in PBS to prevent non-specific binding of antibodies for 1 h. Then, the samples were immersed in antibody solutions and incubated for 1 h. Antibodies used in this study are phalloidin-TRITC (1:500, Sigma) for f-actin, 4',6-diamidino-2-phenylindole (DAPI,

1:1000, Sigma) for nucleus, anti-arcomeric α-actinin produced in mouse (1:500, Sigma) as a primary antibody for myotube, anti-mouse IgG conjugated with Alexa 488 produced in goat (1:500, Invitrogen), anti-mouse IgG conjugated with Cy3 produced in goat (1:500, Molecular Probes) as a secondary antibody for myotube, and Alexa 488 anti-human CD31 antibody conjugated with Alexa 488 (1:200, clone WM59, BioLegend) for platelet endothelial cell adhesion molecule-1 (PECAM-1). Immunofluorescent images were taken using FluoView FV1000 confocal laser scanning unit with the IX81 inverted microscope (Olympus) and EVOS® FL (Life technologies) fluorescent microscope. To get 3D reconstructed images of fabricated engineered tissues, IMARIS software (Bitplane) was used.

4.2.7. Quantitative and statistical analysis of the cells

The quantification analysis presented in this study such as cellular orientation, nucleus elongation, number of myotubes and maturation index were analyzed with ImageJ software. For statistical analysis, Kruskal-Wallis one-way ANOVA on rank test for comparison of more than three groups were performed using Sigmaplot software.

4.3. Results and discussion

4.3.1. Fabrication and analysis of aligned nanofibrous membrane

To mimic extracellular matrix environment surrounding muscle cells, polycaprolactone (PCL), one of biodegradable polymers was selected due to its properties of electrospinning suitability and functional modification [82-84]. To fabricate aligned nanofibers, electrospinning based on inclined gap method which enabled transfer of nanofibers for nanofiber density control was used. In general, the longer spinning time in the electrospinning process, the more increased nanofibers can be collected. However, loss in nanofiber alignment was observed at longer collection time. Thus, we controlled the density of collected nanofibers by repetitive transfer at a fixed spinning time of 1 min.

As shown in figure 4-2A, electrospun nanofibers showed ~ 750 nm in diameter and increased fiber density (number of nanofibers perpendicular to alignment axis) as repeating transfers. A single transfer of nanofibers served the fiber density of 32 fibers/mm in average. The number of transfer times was increased up to 3 and 6, the higher line densities were followed respectively to 79 and 173 fibers/mm in average. In addition, distributions of nanofiber orientation shown in figure 4-2B suggest that all of

nanofibers were within 25 ˚ to the alignment axis regardless of the number of transfer.

To investigate thickness of fabricated nanofibrous membranes with various nanofiber densities (TR #1, #3 and #6), samples were analyzed by atomic force microscope. Through 3D profiles and cross-sectional profiles of the samples shown in figure 4-3, thickness of nanofibrous membrane was ~ 750 nm at single nanofibers and ~ 1.5 μm at points where two nanofibers were overlapped, which is summed value of diameters of two nanofibers. Points which were overlapped more than three nanofibers were barely observed in low magnification optical images.

In addition, porosity and distance between nanofibers of nanofibrous membranes were analyzed due to demonstration of their potentials as a tool which could serve enough spaces for cellular infiltration. Nanofibrous membranes showed very high porosity of 95.250, 88.229 and 76.214 % for TR #1, #3 and #6 respectively (figure 4-4A). Distance between nanofibers distributed in a wide range from 0 μm to several hundreds μm and showed average distance of 26.836, 9.684 and 6.465 μm, which values were smaller than average diameter of the cells except for TR #1 (figure 4-4B). However, cellular infiltration seemed to be possible because there were many points wider than diameter of

the cells overdue to their wide distribution.

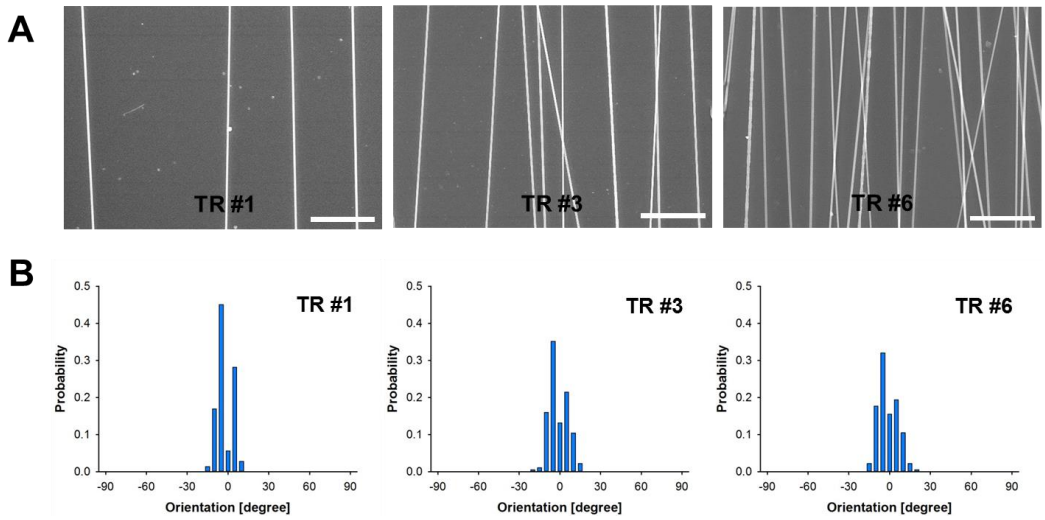

Figure 4-2. (A) Representative SEM images of nanofibrous membranes with various number of transfers (1, 3 and 6 times). (B) Distributions of nanofiber orientation of each nanofibrous membranes (n = 142, 182 and 181 for TR #1, #3 and #6 respectively). The scale bar indicates 25 μm.

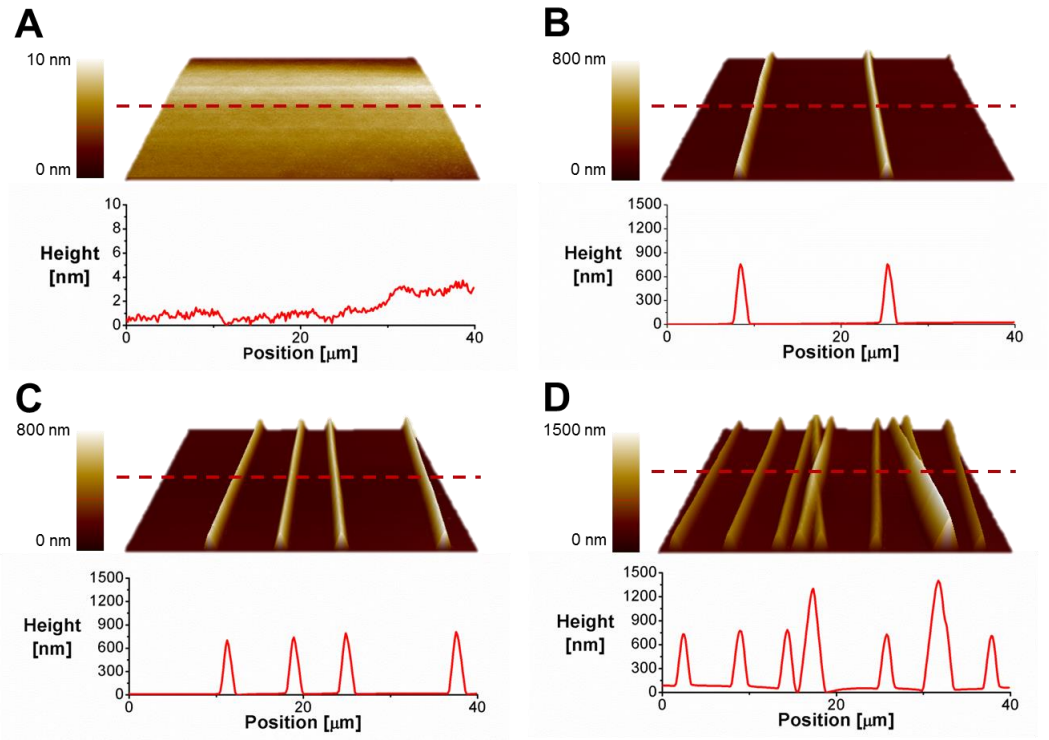

Figure 4-3. Representative atomic force microscope images and cross-sectional profiles of (A) flat, (B) TR #1, (C) TR #3 and (D) TR #6. Thickness of nanofibrous membranes was ~ 750 nm which was identical value of single nanofiber except for overlapped points of 2 nanofibers. Overlapped points of more than 3 nanofibers were barely observed.

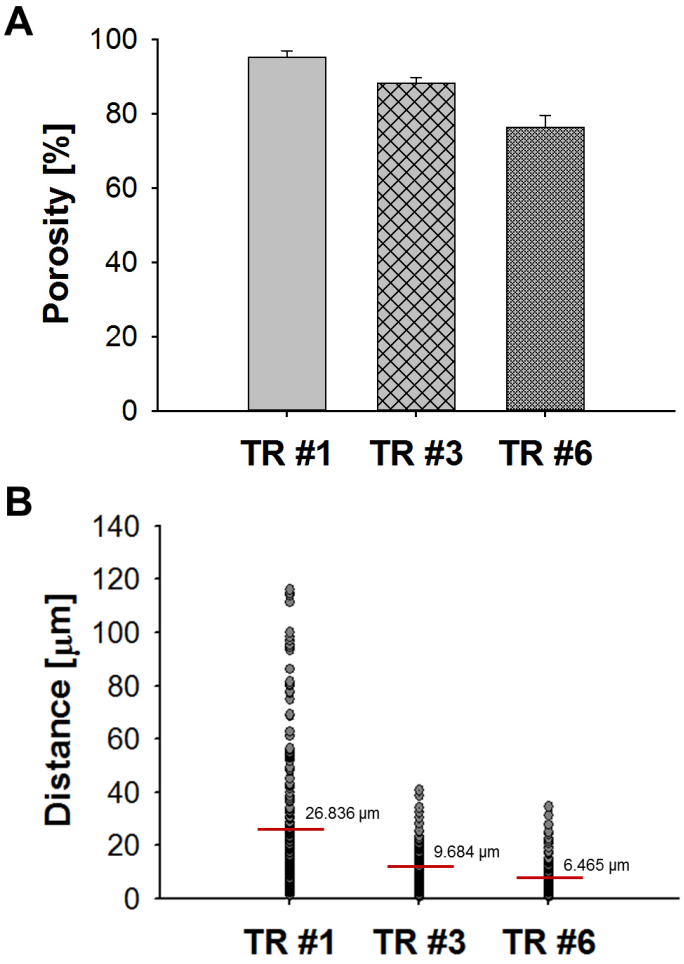

Figure 4-4. (A) Porosity and (B) distribution of distance between nanofibers. 5 samples for each case were analyzed for porosity analysis and total 200 points of 5 samples for each case were measured for distance analysis.

4.3.2. Detachment of various types of cell sheet

Though PDMS has widely used in biological researches due to its biocompatibility, additional chemical/ECM protein treatment is required to compensate its poor cell adhesion property. In accordance with previous researches, we observed that confluent C2C12 cell layer on PDMS substrate was easily delaminated from the surface as a sheet when slight deformation was applied to the substrate (figure 4-5). Inspired from this finding, we hypothesized that there may be minimal nanofiber density which enables stable manipulation of detached cell sheet with maintenance of induced cellular morphology. To verify our hypothesis, we cultured various types of cells including myoblasts, fibroblasts and endothelial cells on nanofibrous membranes with different densities and detached when they formed confluent cell sheet. Entire procedures of cell sheet detachment and manipulation is illustrated in figure 4-1A.

As shown in figure 4-6A, all of cell types cultured on TR #6 were successfully detached as a sheet without notable defects. In addition, fluorescent images of transferred cell sheets except for HUVECs sustained their aligned morphology as before detachment (figure 4-6B). In case of HUVECs, the cells seemed to be aligned along nanofibers just

after cell seeding, however, morphology of the cells was gradually changed to polygonal shape as the cells reached confluent state. Thus transferred endothelial cell sheet also showed polygonal cell shape as before detachment (figure 4-6B).

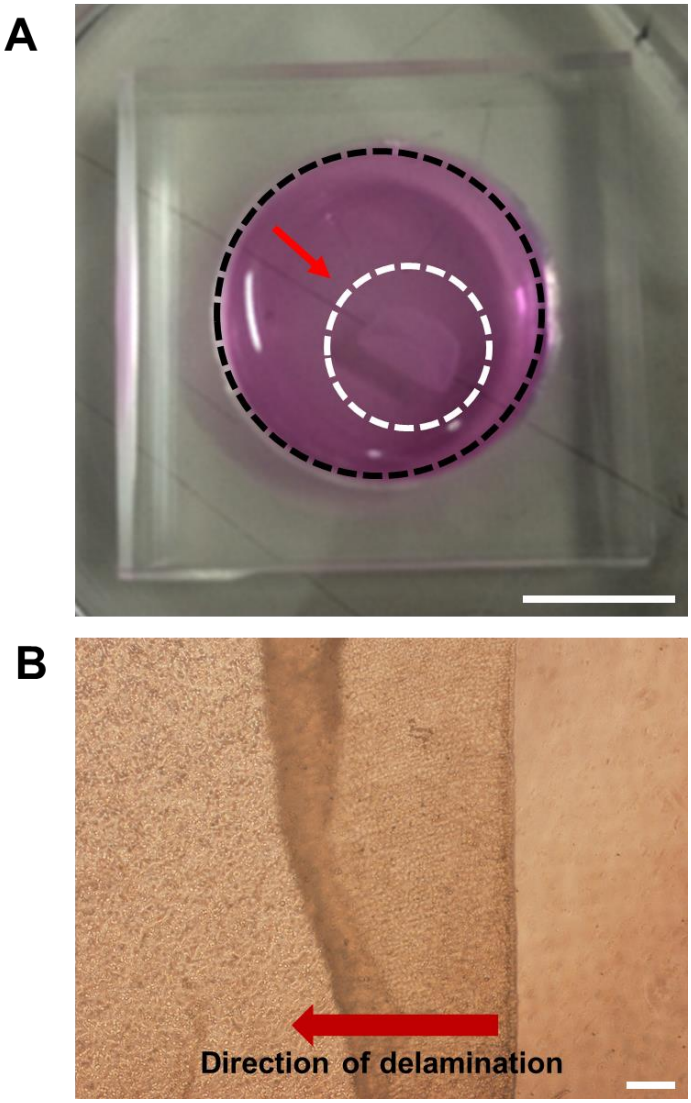

Figure 4-5. (A) Photograph of delaminated C2C12 cell sheet cultured on PDMS substrate. Significantly reduction in size was observed due to loss of cellular morphology after delamination. (B) Microscopic images of cell sheet during delamination.

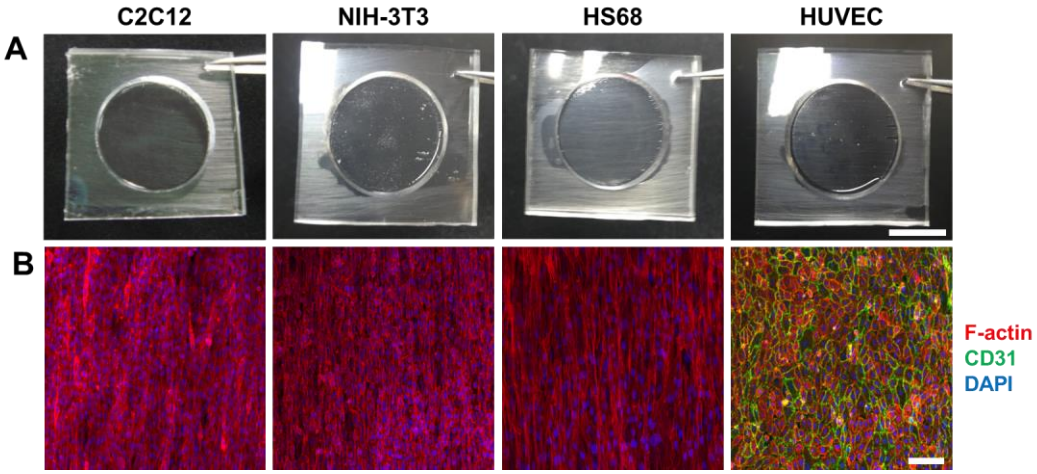

Figure 4-6. (A) Photographs of detached various cell sheets using TR #6 nanofibrous membrane. (B) immunofluorescent images of transferred cell sheets for f-actin cytoskeleton, endothelial cell-specific CD31 and DAPI. Morphologies of the cells were preserved after transfer. The scale bars indicate 1 cm for A and 100 μm for B.

4.3.3. Formation of 3D engineered muscle tissue

4.3.3.1. Effect of nanofiber density on morphological change of C2C12 cells

To investigate effects on cellular orientation and elongation according to various nanofiber densities, we cultured C2C12 myoblasts on various densities of nanofibers and analyzed cellular orientation and nucleus elongation from immunofluorescent images.

Figure 4-7 shows representative fluorescent images for the cells cultured on bare PDMS substrate for control and nanofibrous membrane with various densities. The cells on bare PDMS substrate showed randomly oriented and round morphology. In contrast, the cells on relatively high fiber densities (TR #3 and TR #6) showed highly aligned and elongated morphology with well-developed actin stress fiber along nanofiber direction but the cells on relatively low fiber density (TR #1) showed intermediate state between control and high fiber densities. To verify these findings, we analyzed distributions of cellular orientation for all cases and plotted in figure 4-8A together. As expected, the cells showed increased alignment ratio (number of highly aligned cells within ± 20˚ / total cell number) of 0.361, 0.469, 0.777 and 0.890 for control, TR #1, TR #3 and TR #6 respectively.

Similarly, nuclei of the cells showed more elongated shape and increased average nucleus aspect ratio (length of long axis/length of short axis) of 1.520, 1.533, 1.976 and 2.057 for control, TR #1, TR #3 and TR #6 respectively (figure 4-8B). Notable finding was that there were statistical significances of nucleus elongation between control group and relatively high nanofiber density groups (TR #3 and TR #6), whereas no statistical significance was observed between control group and TR #1 group. These results indicate that there is minimal fiber density for inducing sufficient nucleus elongation for mechanical regulation of cellular functions [85].

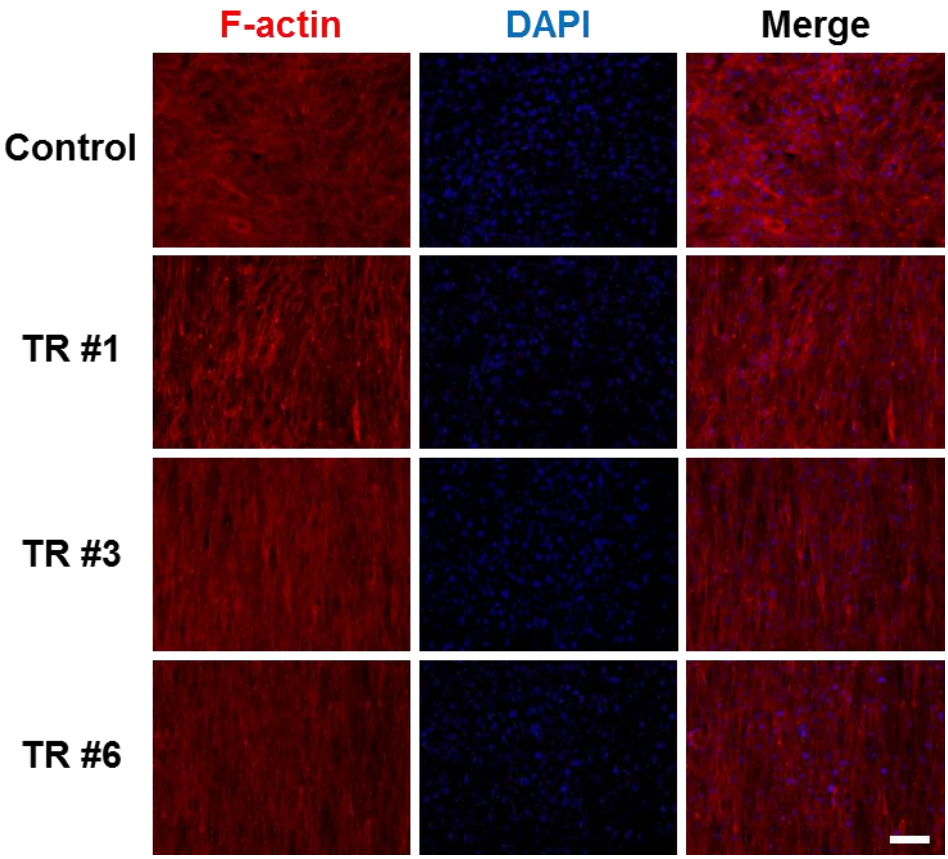

Figure 4-7. Representative immunofluorescent images of f-actin cytoskeleton and nucleus for identification of cellular alignment. As increasing of number of transfers, well-developed actin stress fibers along nanofibers were observed. The scale bar indicates 100 μm.

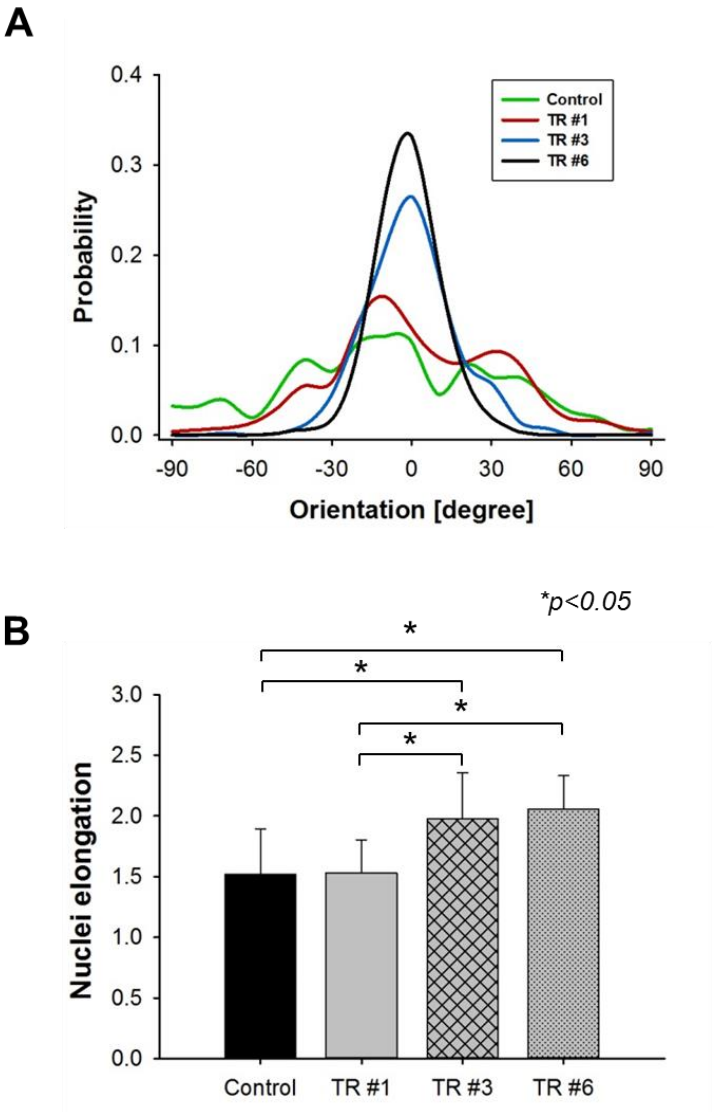

Figure 4-8. Results of (A) cellular orientation and (B) nucleus elongation analysis (n = 200). Enhanced cellular alignment and nucleus elongation were observed as increasing nanofiber density. For comparison of nucleus elongation between groups, Kruskal-Wallis one-way ANOVA on rank test was performed. Asterisk indicates *p < 0.05.

4.3.3.2. Effect of nanofiber density on myogenic differentiation

Structural feature of native skeletal muscle tissue is a densely packed bundle of uniaxially aligned multinucleate myotubes which play a role in generating uniaxial contractile force. Thus, uniaxial alignment and formation of large numbers of myotubes in unit area are key issues in muscle tissue engineering. To investigate effect of nanofibrous membrane with various nanofiber densities on myogenic differentiation, we carried out immunostaining for identifying myotube sturcture, quantification of myotube orientation for determining degree of alignment and quantification of number of myotubes in unit area and maturation index for determining degree of differentiation.

Figure 4-9 shows representative images of myotubes on various densities of nanofibrous membrane. Similar to alignment tendency of myoblasts, increased alignment tendency was observed as increasing nanofiber density. Alignment ratio of the myotubes was 0.199, 0.778, 1 and 1 for control, TR #1, TR #3 and TR #6 respectively (figure 4-10). Namely, all of the myotubes on intermediate and high nanofiber density were within 20 ˚ with respect to axis of nanofiber alignment.

Average number of myotubes per mm^2 was 83.4, 120.6, 115.6 and 104.8 and

average maturation index (number of myotubes with more than 5 nuclei/total number of myotubes) was 0.775, 0.659, 0.818 and 0.810 for control, TR #1, TR #3 and TR #6 respectively (figure 4-11A and B). Taken together, cellular fusion of the cells on control occurred in not only longitudinal but also horizontal direction which resulted in thick but less myotube formation. In contrast, long but relatively thin myotubes along nanofibers were observed on TR #3 and TR #6, which indicated that longitudinal cellular fusion was dominantly occurred.

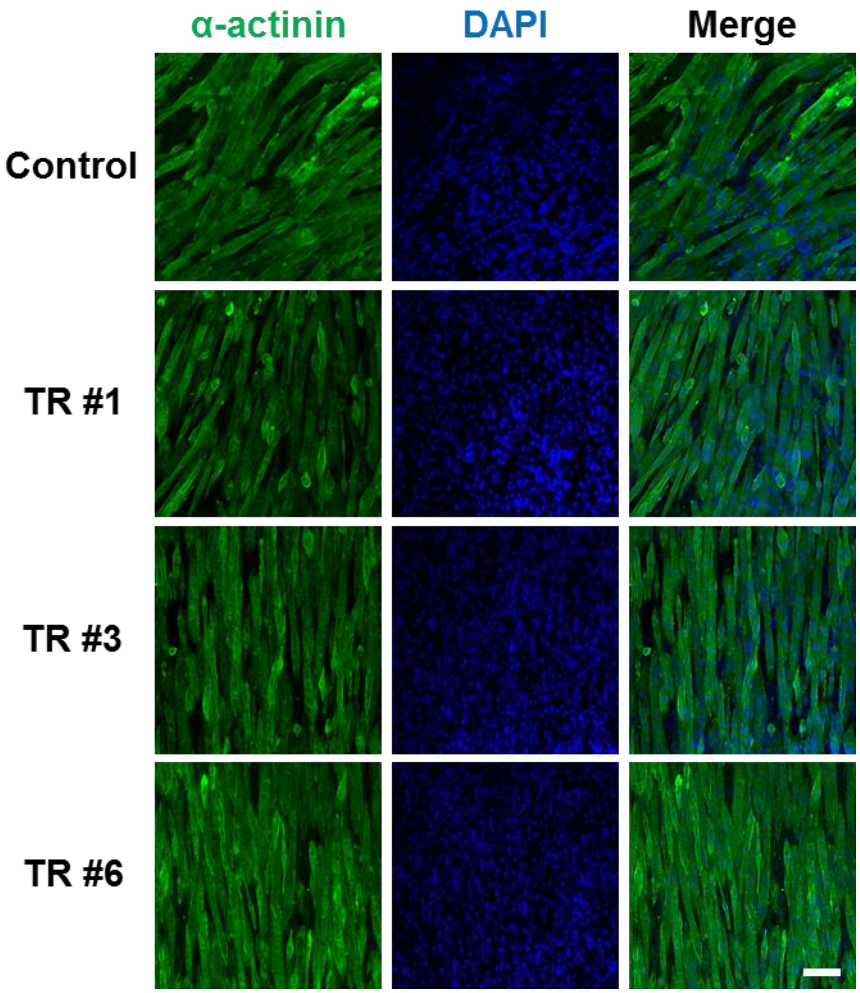

Figure 4-9. Representative immunofluorescent images of differentiated myotubes on nanofibrous membranes with various nanofiber densities. Well-developed multinucleated myotubes along nanofiber direction was observed on TR #3 and #6. The scale bar indicates 100 μm.

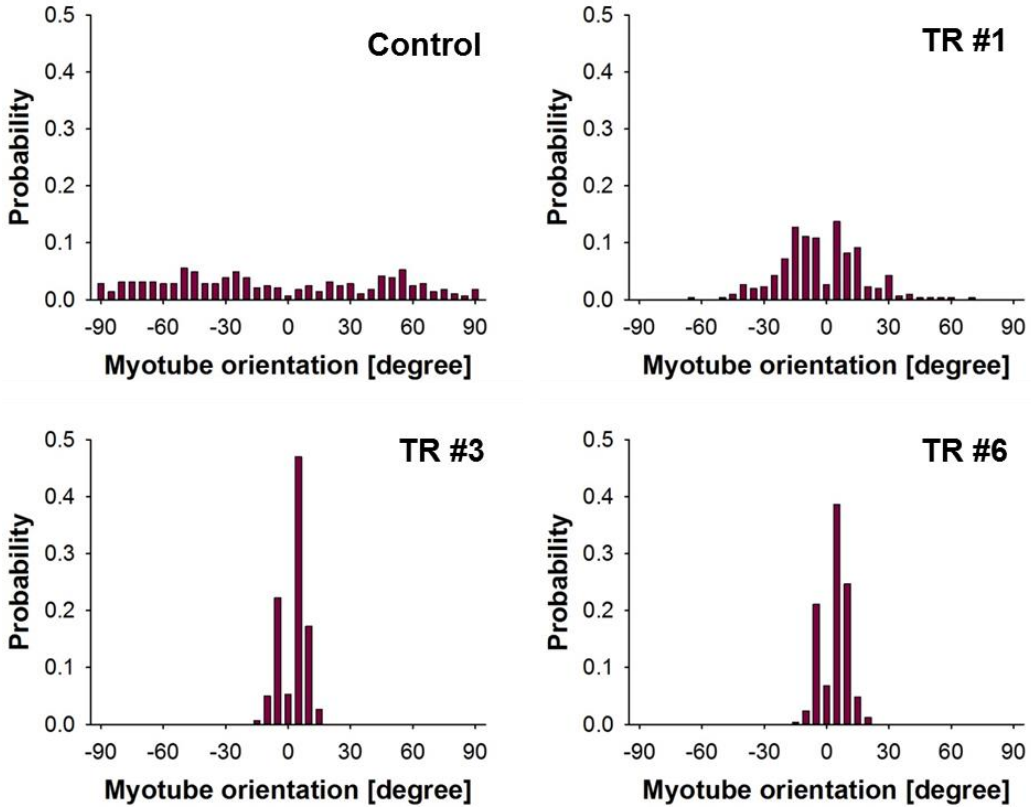

Figure 4-10. Distributions of myotube orientations on nanofibrous membranes with various nanofiber densities.

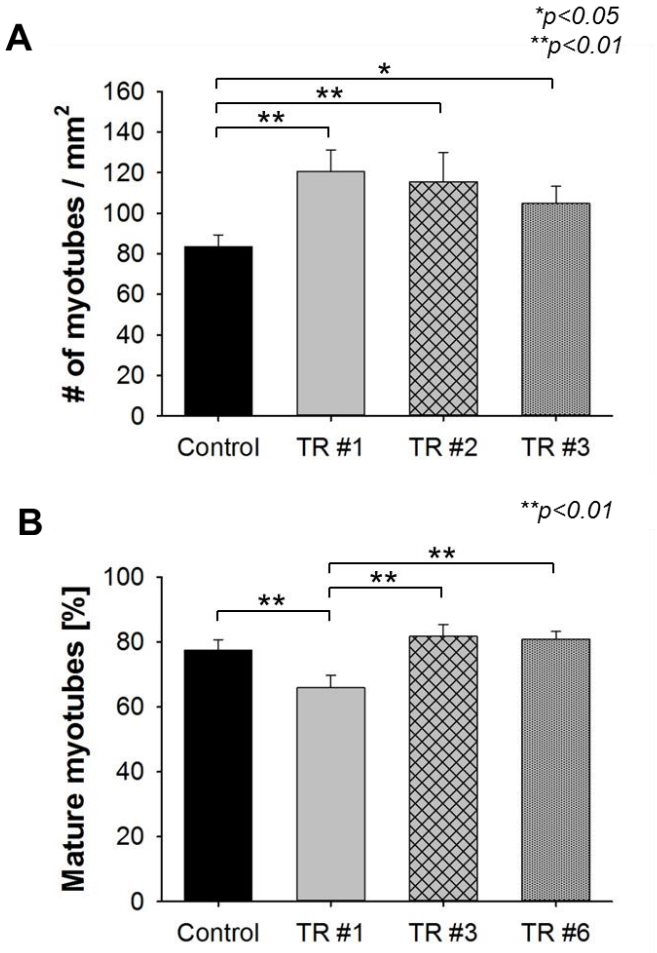

Figure 4-11. Quantitative analysis of (A) number of myotubes in unit area and (B) ratio of mature myotubes with more than 5 nuclei for investigating degree of differentiation. . For comparison of groups, Kruskal-Wallis one-way ANOVA on rank test was performed. Asterisks indicate *p < 0.05 and **p < 0.01.

4.3.3.3. Formation of 3D engineered muscle tissue by LBL stacking

As shown in figure 4-12A, detached cell sheets on the membrane with low and intermediate nanofiber density (TR #1 and TR #3) were fractured during or after detachment. In contrast, detached cell sheets on the membrane with high nanofiber density (TR #6) were stably maintained sheet form with high viability (figure 4-12B). Success rates of cell sheet detachment were 0 %, 15 % and 100 % in 20 trials for TR #1, TR #3 and TR #6 respectively. This result indicated that nanofiber density of TR #6 (173 fibers/mm) was minimal density for stable cell sheet detachment and manipulation.

To investigate whether cellular morphology and nucleus elongation maintained after transfer, detached cell sheets were transferred to cell culture dish and stabilized for 2 h then analyzed. From representative fluorescent images of transferred cell sheets shown in figure 4-12B and C, aligned actin stress fibers and elongated nucleus were clearly observed with high viability. In addition, there was no significant difference between distribution of cell orientation at before and after transfer (figure 4-13A). Nucleus elongation was slightly decreased from 2.057 to 1.909 after transfer. It might be local recovery of nucleus elongation at nanofiber-free area (figure 4-13B). However, decreased

value of nucleus elongation after transfer showed no statistical significance compared with value of nucleus elongation on TR #3. This result indicated that mechanical stimulus exerted on the cells is sustained in similar degree with TR #3.

Using detached cell sheets as building blocks, 3D engineered tissues were successfully fabricated by layer-by-layer stacking. As mentioned above, stacking process was achieved by assembling cell sheet with smaller frame to cell sheet with bigger frame. Three dimensional engineered tissues with two and three layers of cell sheets stacked in parallel and perpendicular manners were shown in figure 4-14 and 4-15. Each cell sheet in engineered tissue shows sustained cellular morphology as before detachment. Resulting thicknesses were ~ 10 um and ~ 15 um for two and three layers respectively.

To fabricate functional engineered muscle tissue, samples with two layers of myocytes were differentiated for 7 days. Similar with the result of myogenic differentiation in 2D, longitudinally well-developed myotubes along nanofibers were observed through entire 3D engineered tissue (figure 4-16 and 4-17).

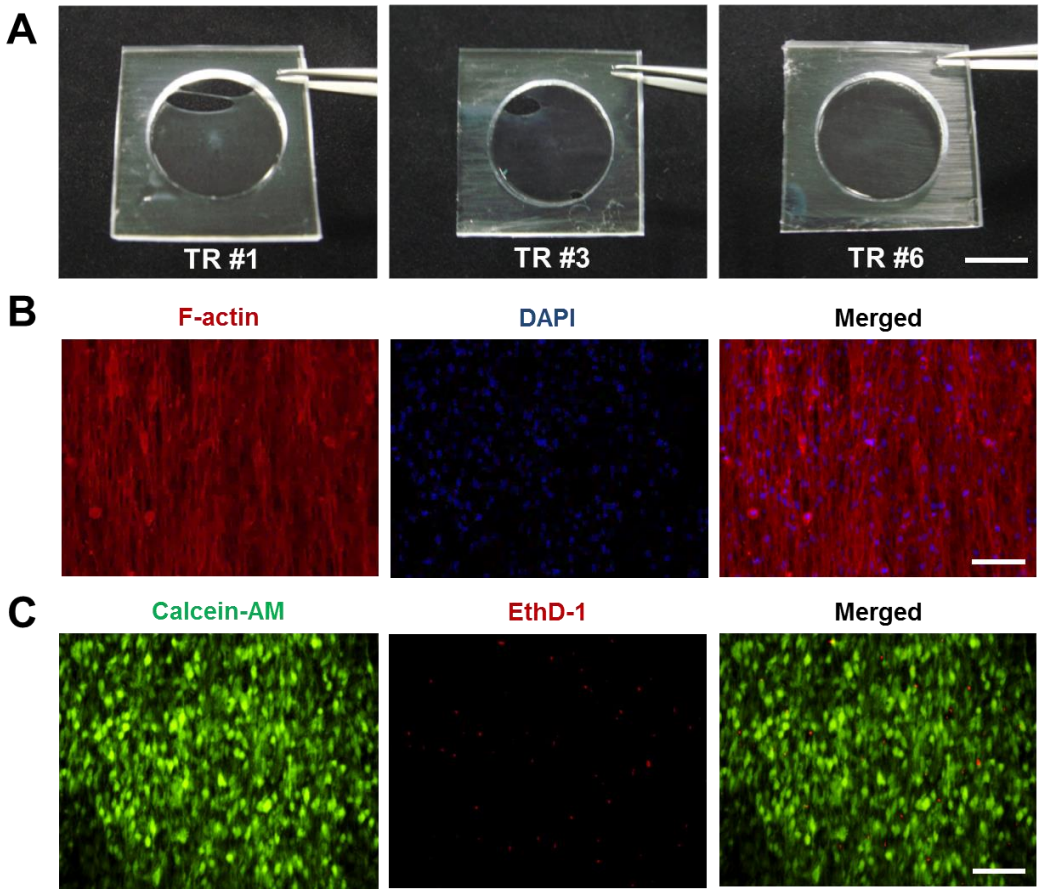

Figure 4-12. (A) Photographs of detached cell sheets using various nanofibrous membranes. Only cell sheet on TR #6 successfully detached from base PDMS substrate. Notable morphological changes and damages were not observed through (B) immunofluorescent images of f-actin cytoskeleton and viability test. The scale bars indicate 1 cm for A and 100 μm for B and C.

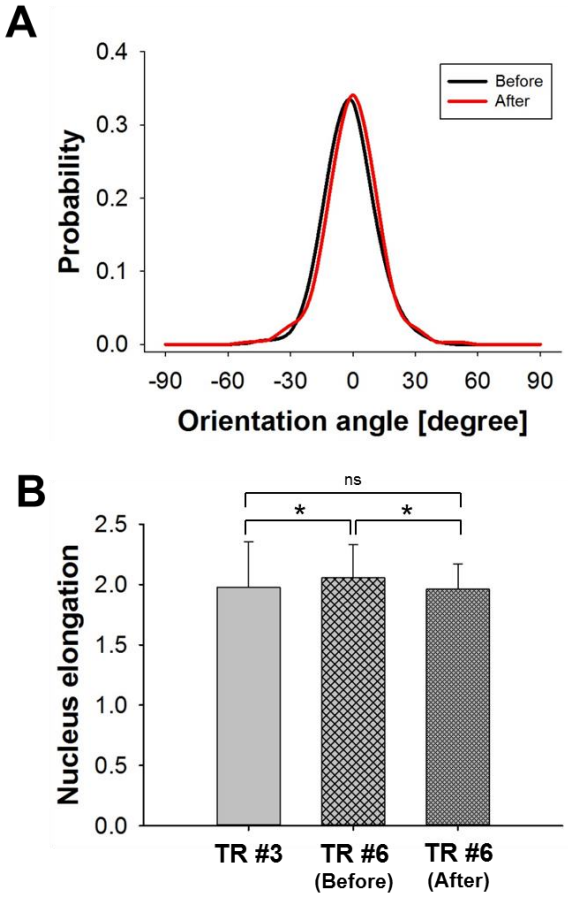

Figure 4-13. (A) Comparison of cellular orientation distributions between before and after detachment. Cellular alignment sustained after detachment. (B) Nucleus elongation was slightly decreased after detachment, but sustained the level similar with the cells on TR #3 before detachment. For comparison of nucleus elongation between groups, Kruskal-Wallis one-way ANOVA on rank test was performed. Asterisk indicates *p < 0.05.

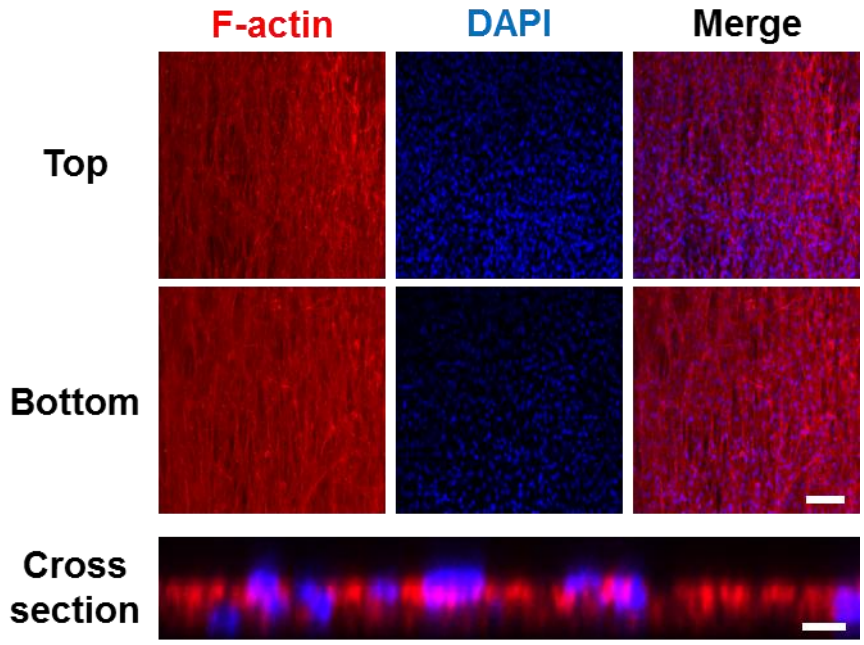

Figure 4-14. Immunofluorescent images of 3D engineered tissue formed by stacking 2 layers of cell sheets in parallel manner. The scale bars indicate 100 μm in planar images and 10 μm in cross-sectional image.

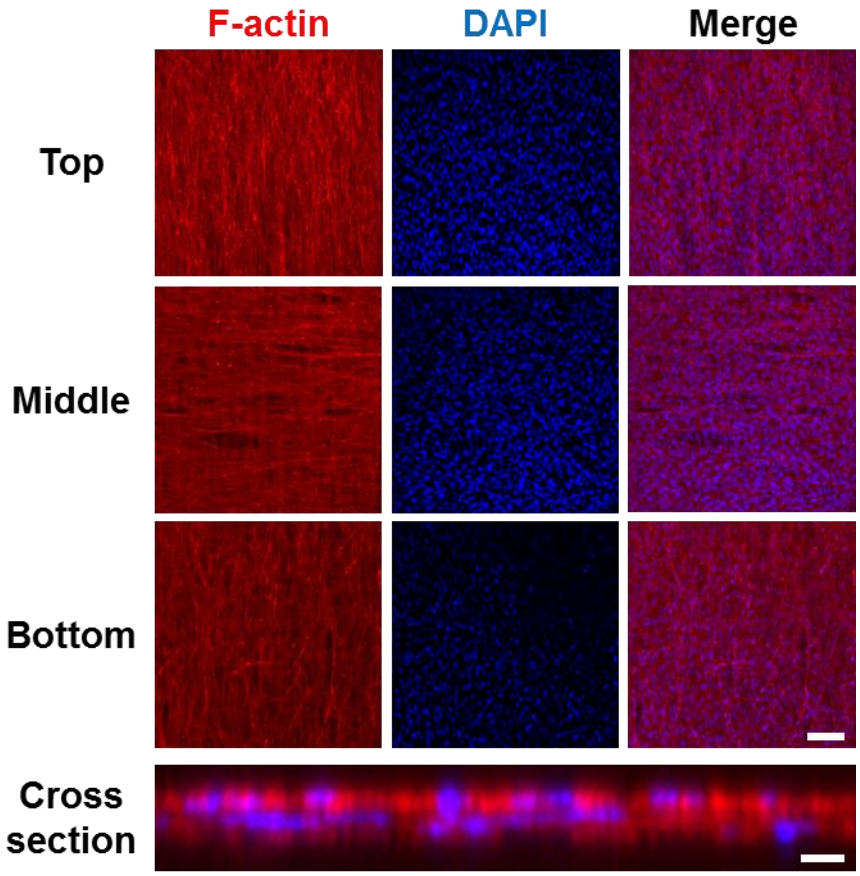

Figure 4-15. Immunofluorescent images of 3D engineered tissue formed by stacking 3 layers of cell sheets in perpendicular manner. The scale bars indicate 100 μm in planar images and 10 μm in cross-sectional image.

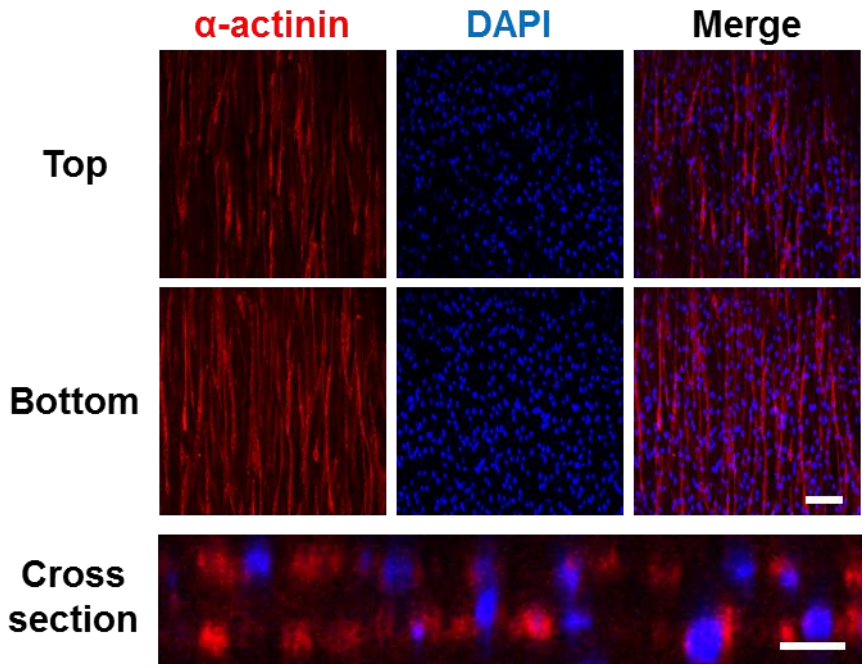

Figure 4-16. Immunofluorescent images of functional 3D engineered tissue formed by induction of myogenic differentiation of 2-layered tissue. The scale bars indicate 100 μm in planar images and 10 μm in cross-sectional image.

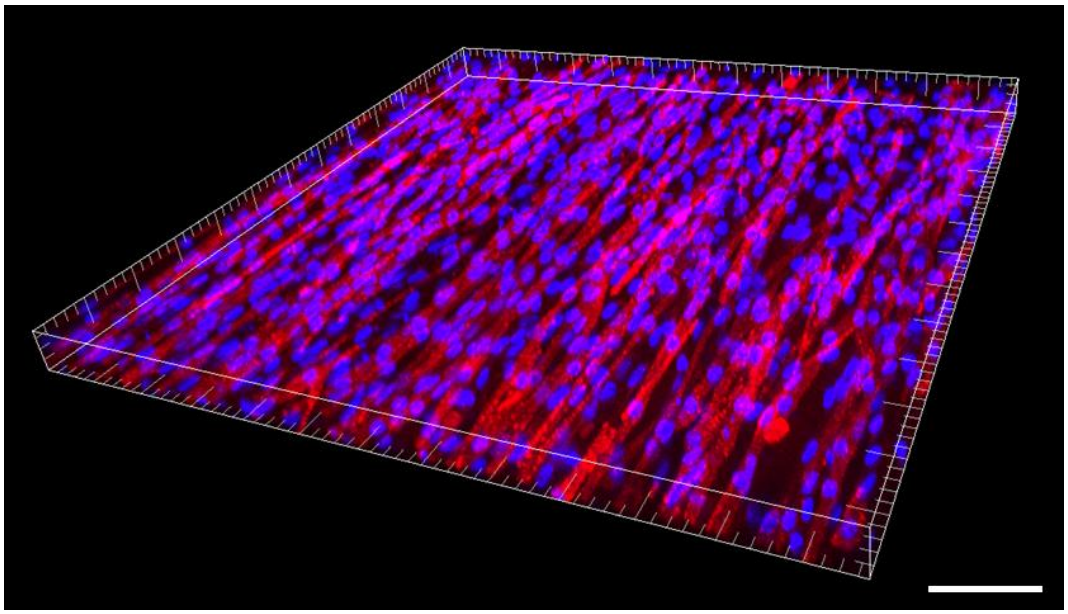

Figure 4-17. 3D reconstructed image of functional 3D engineered tissue. The scale bar indicates 100 μm.

4.3.4. Formation of vascularized 3D engineered skin tissue

4.3.4.1. Tube formation of endothelial cell sheet embedded in Matrigel

In vitro tube formation assay based on Matrigel have been widely used due to not only Matrigel itself has a potential of inducing vasculogenesis but also it is convenient to screen the effect of various factors [86]. Therefore, detached endothelial cell sheet was embedded in Matrigel matrix as shown in figure 4-18A to determine whether the endothelial cells maintained their ability of forming vascular networks or not.

At day 0, embedded endothelial cell sheet maintained their interconnected morphology as before detachment. However, local disconnection of cellular junctions and formation of tube-like structures were observed at day 1 and well-organized tube-like structures were formed over the entire region at day 5 (figure 4-18B). To evaluate 3D structure of formed tube-like structures, immunostaining was performed at day 5 and analyzed using confocal microscope. Similar with optical microscope images, well-organized tube-like structures were observed from the fluorescent images and 3D reconstructed image shown in figure 4-19A and B. These results indicated that detached endothelial cell sheet sustained their ability to form vascular networks. Interestingly,

endothelial cells did not penetrate into the gel layers which resulted in restricted formation of tube-like structures on nanofibrous membrane (figure 4-19A). These results might be related with stiffness of surrounding Matrigel matrix. On soft matrix such as Matrigel and low concentration collagen gel, endothelial cells were known to show suppressed proliferation and invasion which were essential cellular behaviors for angiogenesis and form tube-like structures through vasculogenesis [87-89].

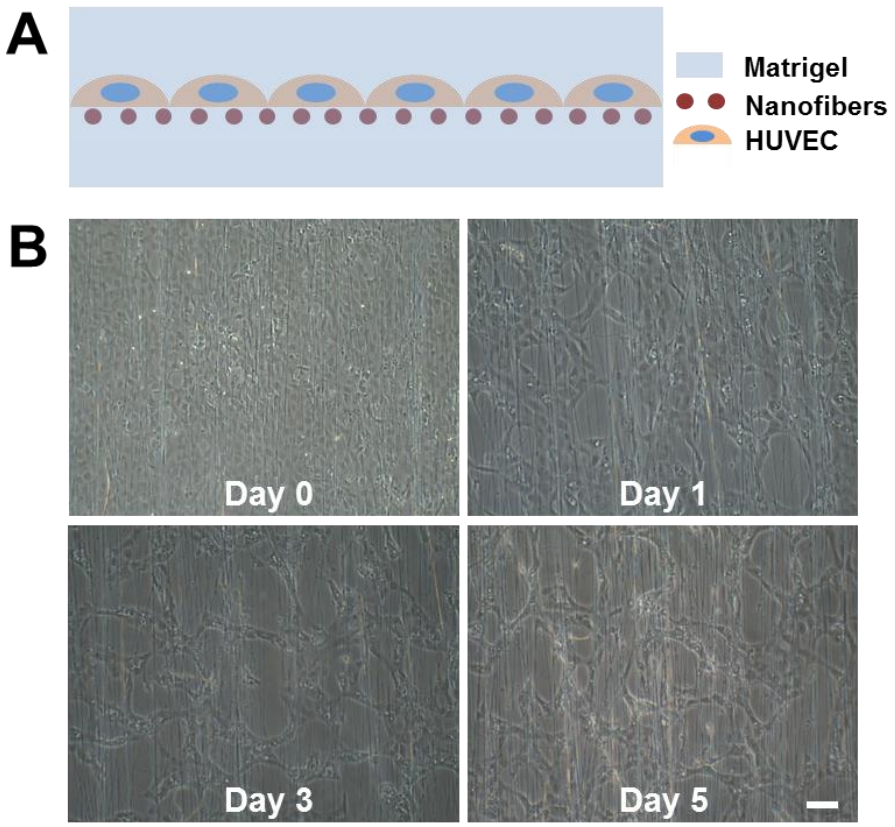

Figure 4-18. (A) Schematic illustration of tube formation assay for endothelial cell sheet embedded in Matrigel. (B) Time-lapse microscope images of transferred endothelial cell sheet. The scale bar indicates 100 μm.

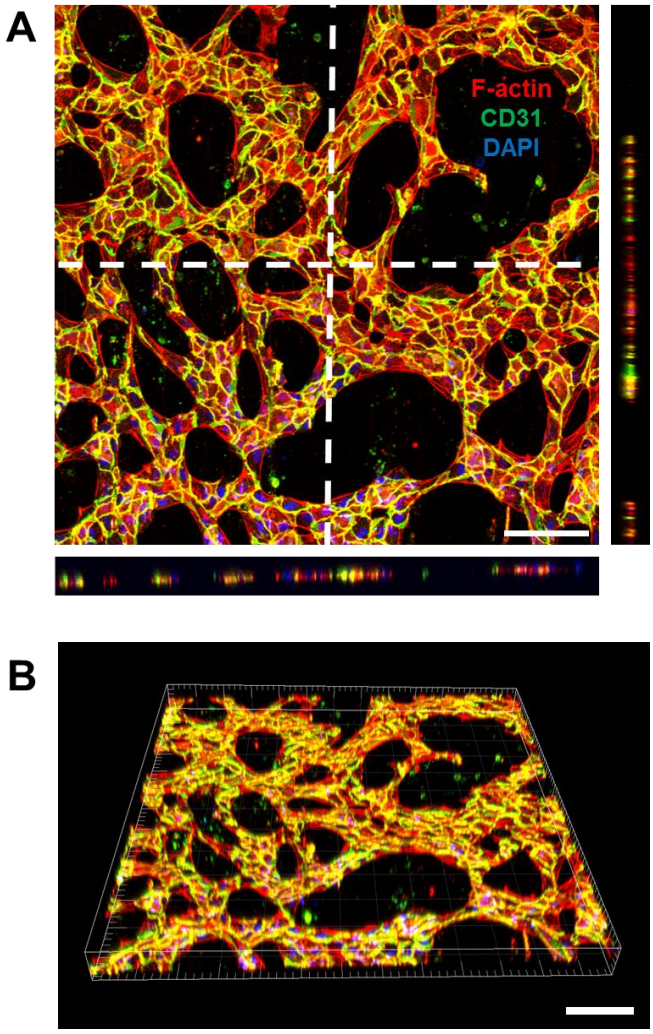

Figure 4-19. (A) Planar and cross-sectional fluorescent images and (B) 3D reconstructed image of tube-like structures at day 5. The scale bars indicate 100 μm.

4.3.4.2. Vascularized 3D engineered skin tissue formation by LBL stacking

In this experiments, mouse embryo fibroblast cell line (NIH-3T3) and human foreskin fibroblast cell line (HS68) was used as a model cells for making 3D skin tissue *in vitro*. To determine feasibility of stacking different cell sheets, detached endothelial cell sheet was stacked on HS68 cell sheet. Fluorescent images shown in figure 4-20 and reconstructed 3D image shown in figure 4-21 which were taken 4 h after stacking confirmed that stacking process was successfully accomplished without any morphological change. To investigate vasculogenic behavior inside 3D engineered skin tissue, furthermore, endothelial cell sheet was stacked between two HS68 sheets and two NIH-3T3 sheets and entire tissue constructs were cultured for additional 5 days. As shown in figure 4-22, sandwiched endothelial cells between HS68 sheets successfully formed lumenized vascular networks. These results were well coincident with previous research which demonstrated that endothelial lumens could be detectable after culturing 5 more days after stacking process [90]. In contrast, endothelial cells between NIH-3T3 sheets formed tube-like structures at day 3 (figure 4-23A), but they cannot sustained their structures and degenerated at day 5 (figure 4-23B). Taken together, formation and

stabilization of lumenized vascular networks might be strongly influenced surrounding cells.

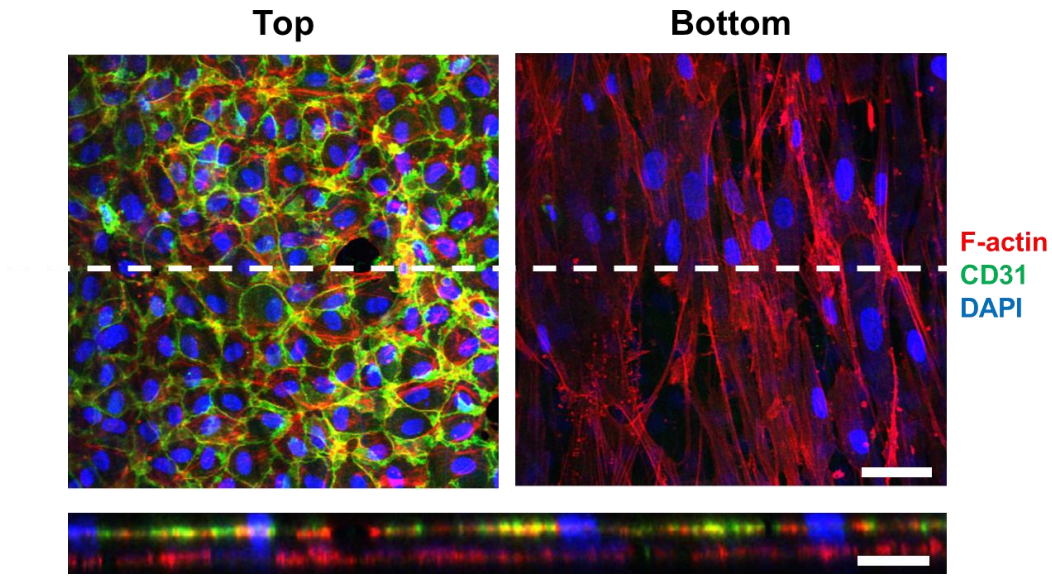

Figure 4-20. Immunofluorescent images of HUVEC sheet stacked on HS68 human fibroblast sheet in parallel manner. The scale bars indicate 50 μm in planar images and 25 μm in cross-sectional image.

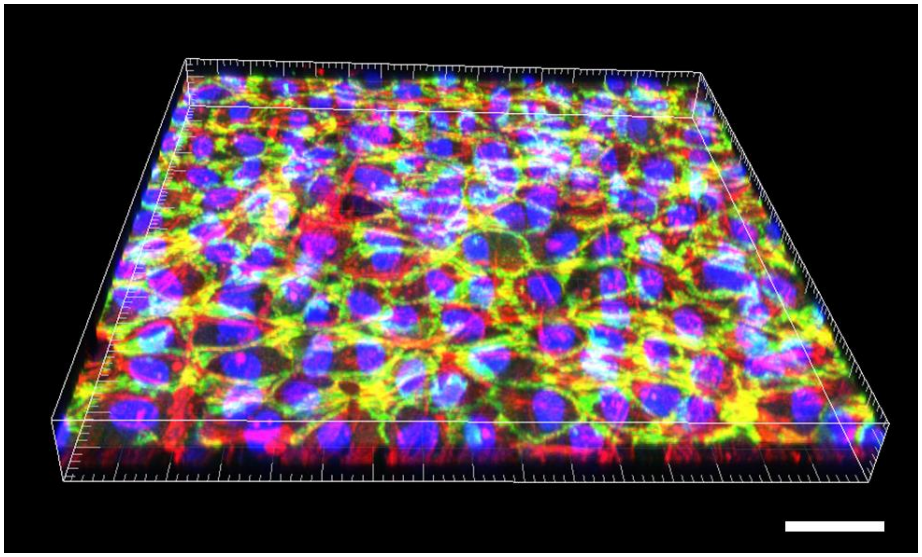

Figure 4-21. 3D reconstructed image of HS68-HUVEC tissue construct. The scale bar indicates 50 μm.

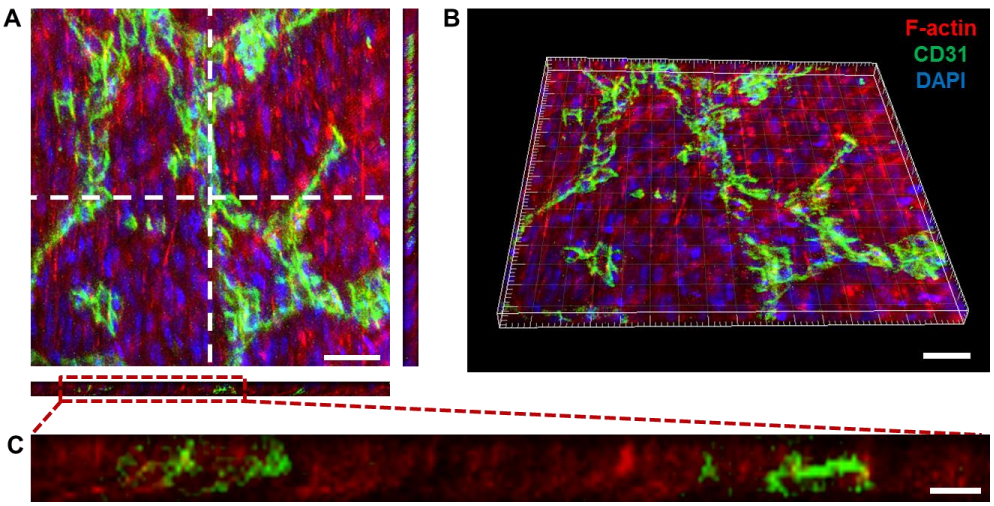

Figure 4-22. Immunofluorescent images of HS68-HUVEC-HS68 tissue construct stacked in parallel manner at day 5. (A) Planar image and (B) 3D reconstructed image of vascularized tissue construct. (C) Cross-sectional image of vascular lumens inside tissue construct. The scale bars indicate 50 μm (A, B) and 10 μm (C).

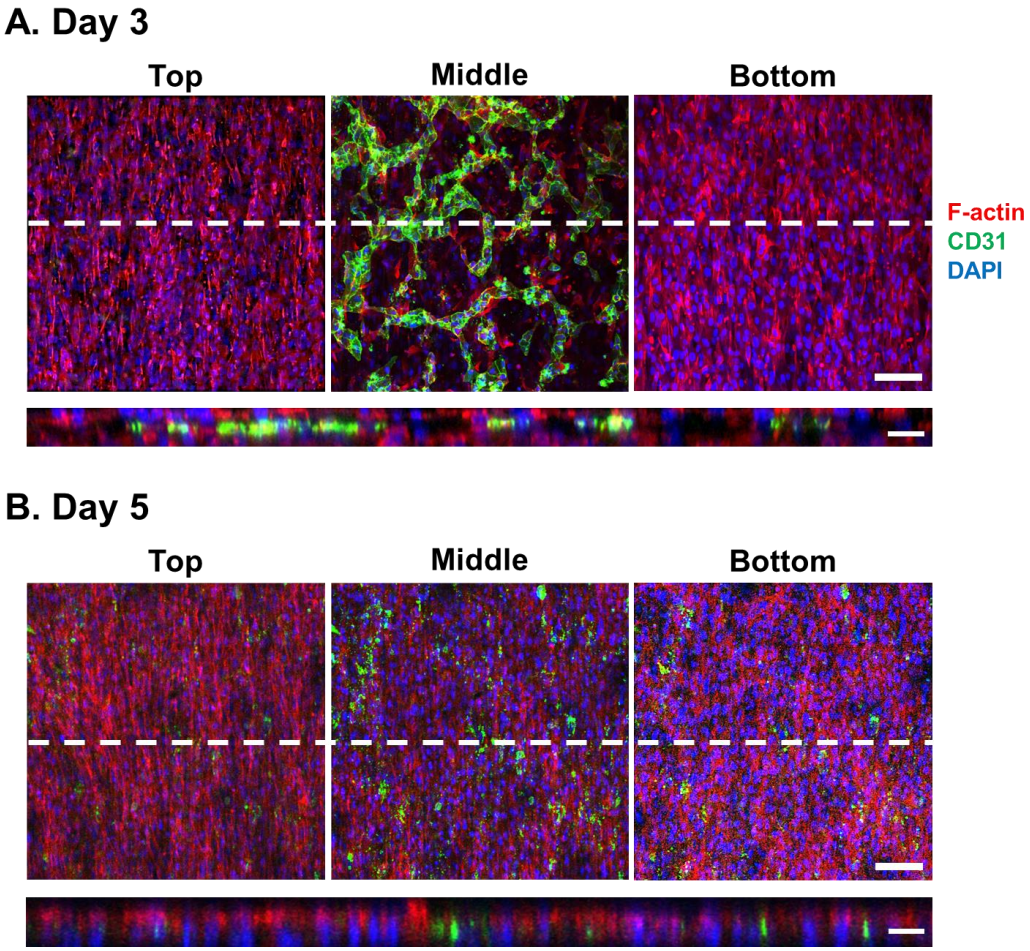

Figure 4-23. Immunofluorescent images of 3T3-HUVEC-3T3 tissue construct stacked in parallel manner at (A) day 3 and (B) day 5. Degeneration of formed tube-like structures was observed at day 5. The scale bars indicate 100 μm in planar images and 25 μm in cross-sectional images.

4.4. Summary

The major aim of this study was to demonstrate that thin, highly porous and aligned nanofibrous membrane could be used as a tool for cell sheet manipulation and formation of various cell-dense 3D engineered tissues *in vitro*.

Since cell sheet engineering based on PNIPAAm which is one of thermoresponsive polymers was suggested by Okano group, cell sheet engineering have attracted great attentions as a reliable method for formation of diverse 3D engineered tissues such as cardiac, skeletal muscle and skin tissue with vascular network for the reasons of simple cell sheet formation by dropping temperature below 20 ˚C, capacity of thick cell-dense 3D engineered tissue formation and easy implantation. Compared with previous researches, our method suggested in this study is noteworthy as another approach which enables cell sheet engineering based on well-known electrospinning method without any morphological changes between before and after transfer. In addition, because electrospinning method has a potential for fabricating functional nanofibers by adopting various growth factors and/or drugs, we expect that enhancement of cellular functions and controlled release of loaded drugs could be achieved.

Undoubtedly, because the current experimental method requires frame for maintaining tension of nanofibers, effective area is reduced as increasing number of stacking. In relation to tensional maintenance, collection problem of 3D engineered tissues without any morphological changes for *in vitro* implantation has to be solved through future researches.

References

[1] Kleinman, H.K., D. Philp, and M.P. Hoffman, *Role of the extracellular matrix in morphogenesis.* Current Opinion in Biotechnology, 2003. **14**(5): p. 526-532.

[2] Jalali, S., M.A. del Pozo, K.D. Chen, H. Miao, Y.S. Li, M.A. Schwartz, J.Y.J. Shyy, and S. Chien, *Integrin-mediated mechanotransduction requires its dynamic interaction with specific extracellular matrix (ECM) ligands (vol 98, pg 1042, 2001).* Proceedings of the National Academy of Sciences of the United States of America, 2001. **98**(9): p. 5369-5369.

[3] Orr, A.W., B.P. Helmke, B.R. Blackman, and M.A. Schwartz, *Mechanisms of mechanotransduction.* Developmental Cell, 2006. **10**(1): p. 11-20.

[4] Jang, K.J., M.S. Kim, D. Feltrin, N.L. Jeon, K.Y. Suh, and O. Pertz, *Two Distinct Filopodia Populations at the Growth Cone Allow to Sense Nanotopographical Extracellular Matrix Cues to Guide Neurite Outgrowth.* Plos One, 2010. **5**(12).

[5] Lee, M.R., K.W. Kwon, H. Jung, H.N. Kim, K.Y. Suh, K. Kim, and K.S. Kim, *Direct differentiation of human embryonic stem cells into selective neurons on nanoscale ridge/groove pattern arrays.* Biomaterials, 2010. **31**(15): p. 4360-4366.

[6] Kim, D.H., E.A. Lipke, P. Kim, R. Cheong, S. Thompson, M. Delannoy, K.Y. Suh, L. Tung, and A. Levchenko, *Nanoscale cues regulate the structure and function of macroscopic cardiac tissue constructs.* Proceedings of the National Academy of Sciences of the United States of America, 2010. **107**(2): p. 565-570.

[7] Yang, H.S., N. Ieronimakis, J.H. Tsui, H.N. Kim, K.Y. Suh, M. Reyes, and D.H. Kim, *Nanopatterned muscle cell patches for enhanced myogenesis and dystrophin expression In a mouse model of muscular dystrophy.* Biomaterials, 2014. **35**(5): p. 1478-1486.

[8] Kim, H.N., Y. Hong, M.S. Kim, S.M. Kim, and K.Y. Suh, *Effect of orientation and density of nanotopography in dermal wound healing.* Biomaterials, 2012. **33**(34): p. 8782-8792.

[9] Il Cho, Y., J.S. Choi, S.Y. Jeong, and H.S. Yoo, *Nerve growth factor (NGF)-conjugated electrospun nanostructures with topographical cues for neuronal*

differentiation of mesenchymal stem cells. Acta Biomaterialia, 2010. **6**(12): p. 4725-4733.

[10] You, M.H., M.K. Kwak, D.H. Kim, K. Kim, A. Levchenko, D.Y. Kim, and K.Y. Suh, *Synergistically Enhanced Osteogenic Differentiation of Human Mesenchymal Stem Cells by Culture on Nanostructured Surfaces with Induction Media.* Biomacromolecules, 2010. **11**(7): p. 1856-1862.

[11] Kim, S.J., D.H. Jang, W.H. Park, and B.M. Min, *Fabrication and characterization of 3-dimensional PLGA nanofiber/microfiber composite scaffolds.* Polymer, 2010. **51**(6): p. 1320-1327.

[12] Pham, Q.P., U. Sharma, and A.G. Mikos, *Electrospun poly(epsilon-caprolactone) microfiber and multilayer nanofiber/microfiber scaffolds: Characterization of scaffolds and measurement of cellular infiltration.* Biomacromolecules, 2006. **7**(10): p. 2796-2805.

[13] Baker, B.M., A.O. Gee, R.B. Metter, A.S. Nathan, R.A. Marklein, J.A. Burdick, and R.L. Mauck, *The potential to improve cell infiltration in composite fiber-aligned electrospun scaffolds by the selective removal of sacrificial fibers.* Biomaterials, 2008. **29**(15): p. 2348-2358.

[14] Yang, X.C., J.D. Shah, and H.J. Wang, *Nanofiber Enabled Layer-by-Layer Approach Toward Three-Dimensional Tissue Formation.* Tissue Engineering Part A, 2009. **15**(4): p. 945-956.

[15] Wheeldon, I., A. Farhadi, A.G. Bick, E. Jabbari, and A. Khademhosseini, *Nanoscale tissue engineering: spatial control over cell-materials interactions.* Nanotechnology, 2011. **22**(21).

[16] Bettinger, C.J., R. Langer, and J.T. Borenstein, *Engineering Substrate Topography at the Micro- and Nanoscale to Control Cell Function.* Angewandte Chemie-International Edition, 2009. **48**(30): p. 5406-5415.

[17] Sniadecki, N., R.A. Desai, S.A. Ruiz, and C.S. Chen, *Nanotechnology for cell-substrate interactions.* Annals of Biomedical Engineering, 2006. **34**(1): p. 59-74.

[18] Kim, D.H., P.K. Wong, J. Park, A. Levchenko, and Y. Sun, *Microengineered Platforms for Cell Mechanobiology.* Annual Review of Biomedical Engineering, 2009. **11**: p. 203-233.

[19] Raghavan, S. and C.S. Chen, *Micropatterned environments in cell biology.* Advanced Materials, 2004. **16**(15): p. 1303-1313.

[20] McBeath, R., D.M. Pirone, C.M. Nelson, K. Bhadriraju, and C.S. Chen, *Cell shape, cytoskeletal tension, and RhoA regulate stem cell lineage commitment.* Developmental Cell, 2004. **6**(4): p. 483-495.

[21] Chung, S.H., S.J. Son, and J. Min, *The nanostructure effect on the adhesion and growth rates of epithelial cells with well-defined nanoporous alumina substrates.* Nanotechnology, 2010. **21**(12).

[22] Hu, W., A.S. Crouch, D. Miller, M. Aryal, and K.J. Luebke, *Inhibited cell spreading on polystyrene nanopillars fabricated by nanoimprinting and in situ elongation.* Nanotechnology, 2010. **21**(38).

[23] Dalby, M.J., A. Hart, and S.J. Yarwood, *The effect of the RACK1 signalling protein on the regulation of cell adhesion and cell contact guidance on nanometric grooves.* Biomaterials, 2008. **29**(3): p. 282-289.

[24] Dalby, M.J., *Topographically induced direct cell mechanotransduction.* Medical Engineering & Physics, 2005. **27**(9): p. 730-742.

[25] You, M.H., M.K. Kwak, D.H. Kim, K. Kim, A. Levchenko, K.Y. Suh, and D.Y. Kim, *Synergistically Enhanced Osteogenic Differentiation of Human Mesenchymal Stem Cells by Culture on Nanostructured Surfaces with Induction Media.* Biomacromolecules, 2010. **11**(7): p. 1856-1862.

[26] Kim, D.H., K. Han, K. Gupta, K.W. Kwon, A. Levchenko, and K.Y. Suh, *Mechanosensitivity of fibroblast cell shape and movement to anisotropic substratum topography gradients.* Biomaterials, 2009. **30**(29): p. 5433-5444.

[27] Kim, D.H., C.H. Seo, K. Han, K.W. Kwon, A. Levchenko, and K.Y. Suh, *Guided Cell Migration on Microtextured Substrates with Variable Local Density and Anisotropy.* Advanced Functional Materials, 2009. **19**(10): p. 1579-1586.

[28] Suh, K.Y., S.J. Choi, S.J. Baek, T.W. Kim, and R. Langer, *Observation of high-aspect-ratio nanostructures using capillary lithography.* Advanced Materials, 2005. **17**(5): p. 560-+.

[29] Suh, K.Y., M.C. Park, and P. Kim, *Capillary Force Lithography: A Versatile Tool for Structured Biomaterials Interface Towards Cell and Tissue Engineering.*

Advanced Functional Materials, 2009. **19**(17): p. 2699-2712.

[30] Kletzien, R.F., S.D. Clarke, and R.G. Ulrich, *Enhancement of adipocyte differentiation by an insulin-sensitizing agent.* Mol Pharmacol, 1992. **41**(2): p. 393-8.

[31] Lee, Y.S., W.S. Kim, K.H. Kim, M.J. Yoon, H.J. Cho, Y. Shen, J.M. Ye, C.H. Lee, W.K. Oh, C.T. Kim, C. Hohnen-Behrens, A. Gosby, E.W. Kraegen, D.E. James, and J.B. Kim, *Berberine, a natural plant product, activates AMP-activated protein kinase with beneficial metabolic effects in diabetic and insulin-resistant states.* Diabetes, 2006. **55**(8): p. 2256-64.

[32] Rosen, E.D., C.H. Hsu, X. Wang, S. Sakai, M.W. Freeman, F.J. Gonzalez, and B.M. Spiegelman, *C/EBPalpha induces adipogenesis through PPARgamma: a unified pathway.* Genes Dev, 2002. **16**(1): p. 22-6.

[33] Rosen, E.D., P. Sarraf, A.E. Troy, G. Bradwin, K. Moore, D.S. Milstone, B.M. Spiegelman, and R.M. Mortensen, *PPAR gamma is required for the differentiation of adipose tissue in vivo and in vitro.* Mol Cell, 1999. **4**(4): p. 611-7.

[34] Tanaka, T., N. Yoshida, T. Kishimoto, and S. Akira, *Defective adipocyte differentiation in mice lacking the C/EBPbeta and/or C/EBPdelta gene.* EMBO J, 1997. **16**(24): p. 7432-43.

[35] Tontonoz, P., E. Hu, and B.M. Spiegelman, *Stimulation of adipogenesis in fibroblasts by PPAR gamma 2, a lipid-activated transcription factor.* Cell, 1994. **79**(7): p. 1147-56.

[36] Wu, Z., E.D. Rosen, R. Brun, S. Hauser, G. Adelmant, A.E. Troy, C. McKeon, G.J. Darlington, and B.M. Spiegelman, *Cross-regulation of C/EBP alpha and PPAR gamma controls the transcriptional pathway of adipogenesis and insulin sensitivity.* Mol Cell, 1999. **3**(2): p. 151-8.

[37] Kilian, K.A., B. Bugarija, B.T. Lahn, and M. Mrksich, *Geometric cues for directing the differentiation of mesenchymal stem cells.* Proc Natl Acad Sci U S A, 2010. **107**(11): p. 4872-7.

[38] Weiner, F.R., A. Shah, P.J. Smith, C.S. Rubin, and M.A. Zern, *Regulation of collagen gene expression in 3T3-L1 cells. Effects of adipocyte differentiation and*

tumor necrosis factor alpha. Biochemistry, 1989. **28**(9): p. 4094-9.

[39] Choi, S.J., P.J. Yoo, S.J. Baek, T.W. Kim, and H.H. Lee, *An ultraviolet-curable mold for sub-100-nm lithography.* Journal of the American Chemical Society, 2004. **126**(25): p. 7744-7745.

[40] Kim, P., D.H. Kim, B. Kim, S.K. Choi, S.H. Lee, A. Khademhosseini, R. Langer, and K.Y. Suh, *Fabrication of nanostructures of polyethylene glycol for applications to protein adsorption and cell adhesion.* Nanotechnology, 2005. **16**(10): p. 2420-2426.

[41] Kim, D.H., P. Kim, I. Song, J.M. Cha, S.H. Lee, B. Kim, and K.Y. Suh, *Guided three-dimensional growth of functional cardiomyocytes on polyethylene glycol nanostructures.* Langmuir, 2006. **22**(12): p. 5419-5426.

[42] Ruiz, S.A. and C.S. Chen, *Emergence of Patterned Stem Cell Differentiation Within Multicellular Structures.* Stem Cells, 2008. **26**(11): p. 2921-2927.

[43] Langer, R. and J.P. Vacanti, *Tissue Engineering.* Science, 1993. **260**(5110): p. 920-926.

[44] Lutolf, M.P. and J.A. Hubbell, *Synthetic biomaterials as instructive extracellular microenvironments for morphogenesis in tissue engineering.* Nature Biotechnology, 2005. **23**(1): p. 47-55.

[45] Kim, D.H., H. Lee, Y.K. Lee, J.M. Nam, and A. Levchenko, *Biomimetic Nanopatterns as Enabling Tools for Analysis and Control of Live Cells.* Advanced Materials, 2010. **22**(41): p. 4551-4566.

[46] Vats, A., N.S. Tolley, J.M. Polak, and J.E. Gough, *Scaffolds and biomaterials for tissue engineering: a review of clinical applications.* Clinical Otolaryngology, 2003. **28**(3): p. 165-172.

[47] Kim, H.N., A. Jiao, N.S. Hwang, M.S. Kim, D.H. Kang, D.H. Kim, and K.Y. Suh, *Nanotopography-guided tissue engineering and regenerative medicine.* Advanced Drug Delivery Reviews, 2013. **65**(4): p. 536-558.

[48] Agarwal, S., J.H. Wendorff, and A. Greiner, *Progress in the Field of Electrospinning for Tissue Engineering Applications.* Advanced Materials, 2009. **21**(32-33): p. 3343-3351.

[49] Ashammakhi, N., A. Ndreu, Y. Yang, H. Ylikauppila, L. Nikkola, and V. Hasirci,

Tissue engineering: A new take-off using nanofiber-based scaffolds. Journal of Craniofacial Surgery, 2007. **18**(1): p. 3-17.

[50] Huang, L., R.A. McMillan, R.P. Apkarian, B. Pourdeyhimi, V.P. Conticello, and E.L. Chaikof, *Generation of synthetic elastin-mimetic small diameter fibers and fiber networks.* Macromolecules, 2000. **33**(8): p. 2989-2997.

[51] Huang, Z.M., Y.Z. Zhang, M. Kotaki, and S. Ramakrishna, *A review on polymer nanofibers by electrospinning and their applications in nanocomposites.* Composites Science and Technology, 2003. **63**(15): p. 2223-2253.

[52] Bashur, C.A., R.D. Shaffer, L.A. Dahlgren, S.A. Guelcher, and A.S. Goldstein, *Effect of Fiber Diameter and Alignment of Electrospun Polyurethane Meshes on Mesenchymal Progenitor Cells.* Tissue Engineering Part A, 2009. **15**(9): p. 2435-2445.

[53] Choi, J.S., S.J. Lee, G.J. Christ, A. Atala, and J.J. Yoo, *The influence of electrospun aligned poly(epsilon-caprolactone)/collagen nanofiber meshes on the formation of self-aligned skeletal muscle myotubes.* Biomaterials, 2008. **29**(19): p. 2899-2906.

[54] Corey, J.M., D.Y. Lin, K.B. Mycek, Q. Chen, S. Samuel, E.L. Feldman, and D.C. Martin, *Aligned electrospun nanofibers specify the direction of dorsal root ganglia neurite growth.* Journal of Biomedical Materials Research Part A, 2007. **83A**(3): p. 636-645.

[55] Dang, J.M. and K.W. Leong, *Myogenic induction of aligned mesenchymal stem cell sheets by culture on thermally responsive electrospun nanofibers.* Advanced Materials, 2007. **19**(19): p. 2775-+.

[56] Huang, N.F., S. Patel, R.G. Thakar, J. Wu, B.S. Hsiao, B. Chu, R.J. Lee, and S. Li, *Myotube assembly on nanofibrous and micropatterned polymers.* Nano Letters, 2006. **6**(3): p. 537-542.

[57] Lee, C.H., H.J. Shin, I.H. Cho, Y.M. Kang, I.A. Kim, K.D. Park, and J.W. Shin, *Nanofiber alignment and direction of mechanical strain affect the ECM production of human ACL fibroblast.* Biomaterials, 2005. **26**(11): p. 1261-1270.

[58] Yang, F., R. Murugan, S. Wang, and S. Ramakrishna, *Electrospinning of nano/micro scale poly(L-lactic acid) aligned fibers and their potential in neural*

tissue engineering. Biomaterials, 2005. **26**(15): p. 2603-2610.

[59] Katta, P., M. Alessandro, R.D. Ramsier, and G.G. Chase, *Continuous electrospinning of aligned polymer nanofibers onto a wire drum collector.* Nano Letters, 2004. **4**(11): p. 2215-2218.

[60] Li, D., Y.L. Wang, and Y.N. Xia, *Electrospinning of polymeric and ceramic nanofibers as uniaxially aligned arrays.* Nano Letters, 2003. **3**(8): p. 1167-1171.

[61] Theron, A., E. Zussman, and A.L. Yarin, *Electrostatic field-assisted alignment of electrospun nanofibres.* Nanotechnology, 2001. **12**(3): p. 384-390.

[62] Bisht, G., S. Nesterenko, L. Kulinsky, and M. Madou, *A Computer-Controlled Near-Field Electrospinning Setup and Its Graphic User Interface for Precision Patterning of Functional Nanofibers on 2D and 3D Substrates.* Jala, 2012. **17**(4): p. 302-308.

[63] Yang, D.Y., B. Lu, Y. Zhao, and X.Y. Jiang, *Fabrication of aligned fibirous arrays by magnetic electrospinning.* Advanced Materials, 2007. **19**(21): p. 3702-+.

[64] Park, S.H. and D.Y. Yang, *Fabrication of Aligned Electrospun Nanofibers by Inclined Gap Method.* Journal of Applied Polymer Science, 2011. **120**(3): p. 1800-1807.

[65] Park, S.H., T.G. Kim, H.C. Kim, D.Y. Yang, and T.G. Park, *Development of dual scale scaffolds via direct polymer melt deposition and electrospinning for applications in tissue regeneration.* Acta Biomaterialia, 2008. **4**(5): p. 1198-1207.

[66] Chapleau, N., B.D. Favis, and P.J. Carreau, *Measuring the interfacial tension of polyamide/polyethylene and polycarbonate/polypropylene blends: effect of temperature.* Polymer, 2000. **41**(17): p. 6695-6698.

[67] Kressler, J., C. Wang, and H.W. Kammer, *Structure formation in thin poly(epsilon-caprolactone) films.* Langmuir, 1997. **13**(16): p. 4407-4412.

[68] Simon, D., A. Holland, and R. Shanks, *Poly(caprolactone) thin film preparation, morphology, and surface texture.* Journal of Applied Polymer Science, 2007. **103**(2): p. 1287-1294.

[69] Kim, H.N., D.H. Kang, M.S. Kim, A. Jiao, D.H. Kim, and K.Y. Suh, *Patterning Methods for Polymers in Cell and Tissue Engineering.* Annals of Biomedical Engineering, 2012. **40**(6): p. 1339-1355.

[70] Park, S.H., J.W. Hong, J.H. Shin, D.Y. Yang, and Y. Yang, *Quantitatively Controlled Fabrication of Uniaxially Aligned Nanofibrous Scaffold for Cell Adhesion.* Journal of Nanomaterials, 2011.

[71] Ahn, S., Y.H. Koh, and G. Kim, *A three-dimensional hierarchical collagen scaffold fabricated by a combined solid freeform fabrication (SFF) and electrospinning process to enhance mesenchymal stem cell (MSC) proliferation.* Journal of Micromechanics and Microengineering, 2010. **20**(6).

[72] Moroni, L., R. Schotel, D. Hamann, J.R. de Wijn, and C.A. van Blitterswijk, *3D fiber-deposited electrospun integrated scaffolds enhance cartilage tissue formation.* Advanced Functional Materials, 2008. **18**(1): p. 53-60.

[73] Mota, C., D. Puppi, D. Dinucci, C. Errico, P. Bartolo, and F. Chiellini, *Dual-Scale Polymeric Constructs as Scaffolds for Tissue Engineering.* Materials, 2011. **4**(3): p. 527-542.

[74] Blackwood, K.A., R. McKean, I. Canton, C.O. Freeman, K.L. Franklin, D. Cole, I. Brook, P. Farthing, S. Rimmer, J.W. Haycock, A.J. Ryan, and S. MacNeil, *Development of biodegradable electrospun scaffolds for dermal replacement*. Biomaterials, 2008. **29**(21): p. 3091-3104.

[75] Levenberg, S., J. Rouwkema, M. Macdonald, E.S. Garfein, D.S. Kohane, D.C. Darland, R. Marini, C.A. van Blitterswijk, R.C. Mulligan, P.A. D'Amore, and R. Langer, *Engineering vascularized skeletal muscle tissue.* Nature Biotechnology, 2005. **23**(7): p. 879-884.

[76] Cho, M.H., K.S. Kim, H.H. Ahn, M.S. Kim, S.H. Kim, G. Khang, B. Lee, and H.B. Lee, *Chitosan gel as an in situ-forming scaffold for rat bone marrow mesenchymal stem cells in vivo.* Tissue Engineering Part A, 2008. **14**(6): p. 1099-1108.

[77] Yang, J., M. Yamato, T. Shimizu, H. Sekine, K. Ohashi, M. Kanzaki, T. Ohki, K. Nishida, and T. Okano, *Reconstruction of functional tissues with cell sheet engineering.* Biomaterials, 2007. **28**(34): p. 5033-5043.

[78] Yu, Q., Y.X. Zhang, H. Chen, F. Zhou, Z.Q. Wu, H. Huang, and J.L. Brash, *Protein Adsorption and Cell Adhesion/Detachment Behavior on Dual-Responsive Silicon Surfaces Modified with Poly(N-isopropylacrylamide)-block-polystyrene*

Copolymer. Langmuir, 2010. **26**(11): p. 8582-8588.

[79] Yamato, M., M. Utsumi, A. Kushida, C. Konno, A. Kikuchi, and T. Okano, *Thermo-responsive culture dishes allow the intact harvest of multilayered keratinocyte sheets without dispase by reducing temperature.* Tissue Engineering, 2001. **7**(4): p. 473-480.

[80] Lin, J.B., B.C. Isenberg, Y.K. Shen, K. Schorsch, O.V. Sazonova, and J.Y. Wong, *Thermo-responsive poly(N-isopropylacrylamide) grafted onto microtextured poly(dimethylsiloxane) for aligned cell sheet engineering.* Colloids and Surfaces B-Biointerfaces, 2012. **99**: p. 108-115.

[81] Takahashi, H., M. Nakayama, K. Itoga, M. Yamato, and T. Okano, *Micropatterned Thermoresponsive Polymer Brush Surfaces for Fabricating Cell Sheets with Well-Controlled Orientational Structures.* Biomacromolecules, 2011. **12**(5): p. 1414-1418.

[82] Choi, J.S., K.W. Leong, and H.S. Yoo, *In vivo wound healing of diabetic ulcers using electrospun nanofibers immobilized with human epidermal growth factor (EGF).* Biomaterials, 2008. **29**(5): p. 587-596.

[83] Ghasemi-Mobarakeh, L., M.P. Prabhakaran, M. Morshed, M.H. Nasr-Esfahani, and S. Ramakrishna, *Electrical Stimulation of Nerve Cells Using Conductive Nanofibrous Scaffolds for Nerve Tissue Engineering.* Tissue Engineering Part A, 2009. **15**(11): p. 3605-3619.

[84] Ma, Z.W., W. He, T. Yong, and S. Ramakrishna, *Grafting of gelatin on electrospun poly(caprolactone) nanofibers to improve endothelial cell spreading and proliferation and to control cell orientation.* Tissue Engineering, 2005. **11**(7-8): p. 1149-1158.

[85] Wang, N., J.D. Tytell, and D.E. Ingber, *Mechanotransduction at a distance: mechanically coupling the extracellular matrix with the nucleus.* Nature Reviews Molecular Cell Biology, 2009. **10**(1): p. 75-82.

[86] Arnaoutova, I. and H.K. Kleinman, *In vitro angiogenesis: endothelial cell tube formation on gelled basement membrane extract.* Nature Protocols, 2010. **5**(4): p. 628-635.

[87] Vailhe, B., X. Ronot, P. Tracqui, Y. Usson, and L. Tranqui, *In vitro angiogenesis*

is modulated by the mechanical properties of fibrin gels and is related to alpha(v)beta(3) integrin localization. In Vitro Cellular & Developmental Biology-Animal, 1997. **33**(10): p. 763-773.

[88] Tranqui, L. and P. Tracqui, *Mechanical signalling and angiogenesis. The integration of cell-extracellular matrix couplings.* Comptes Rendus De L Academie Des Sciences Serie Iii-Sciences De La Vie-Life Sciences, 2000. **323**(1): p. 31-47.

[89] Yamamura, N., R. Sudo, M. Ikeda, and K. Tanishita, *Effects of the mechanical properties of collagen gel on the in vitro formation of microvessel networks by endothelial cells.* Tissue Engineering, 2007. **13**(7): p. 1443-1453.

[90] Asakawa, N., T. Shimizu, Y. Tsuda, S. Sekiya, T. Sasagawa, M. Yamato, F. Fukai, and T. Okano, *Pre-vascularization of in vitro three-dimensional tissues created by cell sheet engineering.* Biomaterials, 2010. **31**(14): p. 3903-3909.

국문초록

본 학위 논문은 조직공학응용을 위한 멀티스케일의 2 차원 및 3 차원 제작 기법의 개발을 목적으로 한다. 세부적으로 모세관력 리소그라피 (Capillary force lithography, CFL)을 이용해 정밀하게 제작된 멀티스케일 패턴을 분석 플랫폼으로 이용하여, 세포의 기능 발현 향상을 위한 최적의 패턴 형상을 탐색하였다. 또한 기존의 전기방사 (Electrospinning) 기법에 기반하여, 세포가 부착된 나노 섬유를 말거나, 적층하는 새로운 제작 기법을 제시하여 세포 밀도가 높은 3 차원 체외 조직의 형성을 가능하게 하였다.

세포를 둘러싼 세포외기질 (Extracellular matrix, ECM)은 친수성의 나노섬유로 이루어진 구조를 가지며, 세포 부착, 증식, 이동, 분화 등의 다양한 세포 기능의 조절에 필수적인 기계적, 생화학적 자극을 제공하는 역할을 한다. 따라서, 조직공학에의 적용을 위해서는 세포외기질 환경이 모사된 2 차원, 3 차원 담체 (Scaffold) 제작 기법의 개발이 선행되어야 한다. 이를 위하여, 자외선 경화성 재료를 이용한 모세관력 리소그라피를 바탕으로 나노 구조물에 의한 세포 기능 조절 분석을 위한 2 차원 플랫폼의 제작

기술을 개발하고, 그 응용으로 나노 구조물의 기하학적 형상이 지방세포분화에 미치는 영향을 분석하였다. 그 결과, 세포가 선형 나노 패턴 사이로 침투하여 높은 접촉 유도 경향을 경우 향상된 분화 정도를 보이는 것을 확인할 수 있었다. 이는 향상된 세포와 표면간의 상호작용이 지방세포의 분화에 있어서 중요한 역할을 한다는 것을 의미한다.

다음으로, 세포외기질 환경을 반영한 세포 밀도가 높은 3 차원 체외조직의 형성을 위하여, 경사 갭 기법 (Inclined gap method)을 이용하여 제작된 나노 섬유를 세포와 함께 말거나 (Rolling-up), 적층 (Stacking)하는 기술을 개발하였다. 먼저 롤링업 공정의 경우, 전기방사, 스핀 코팅, 미세 용융 압출의 3 가지 기법을 융합하여 나노 섬유 기반의 멀티스케일 담체를 제작하고, 근아세포 (Myoblast)가 배양된 담체를 말아서 실린더 형상의 3 차원 체외 근육 조직의 제작을 가능하게 하였다. 담체 위에 부착된 세포들은 정렬된 나노 섬유에 의하여 접촉 유도되어 높은 정렬도를 보였으며, 이동 및 마는 공정 이후에도 세포의 형상이 유지됨을 알 수 있었다. 마지막으로, 정렬된 나노 섬유로 이루어진 멤브레인을 이용하여 배양된 세포막의 손상 및 세포의 형상 변화 없이 표면으로부터 분리, 전사 및 조작을

가능케 하는 기법을 개발하였다. 이를 바탕으로 형성된 세포막의 적층을 통하여 높은 세포 밀도를 가진 3 차원 체외 조직의 형성이 가능하였고, 나아가 여러 층의 근아세포가 적층된 체외 조직의 분화를 통하여 근섬유로 이루어진 3 차원 근육 조직의 형성이 가능하였다. 또한 섬유아세포막과 혈관세포막의 교차 적층 및 공배양을 통하여 혈관망이 내부에 형성되어 있는 3 차원 피부 조직의 형성 역시 가능하였다.

주요어: 세포외기질, 마이크로/나노패터닝, 모세관력 리소그라피, 전기방사, 롤 업 공정, 세포 막 공학, 세포막 적층, 지방세포분화, 근육분화, 혈관망 형성, 3 차원 체외 조직

학번: 2010-20657

공학박사학위논문

Development of multiscale 2D/3D fabrication methods for tissue engineering

조직공학응용을 위한 멀티스케일 2 차원/3 차원 제작 기법 개발

2015 년 2 월

서울대학교 대학원

기계항공공학부

김 민 성

Abstract

In this thesis, we suggested multiscale 2D and 3D fabrication methods for tissue engineering applications. In detail, we utilized precisely fabricated nanopatterns through capillary force lithography (CFL) as a screening platform for determining effects of nanotopography on cellular behavior. In addition, to overcome the limitations of present electrospinning methods for adopting tissue engineering field, we have developed new methods based on rolling and stacking process of cell-seeded nanofibers for formation of cell-dense 3D engineered tissues *in vitro*.

Extracellular matrix (ECM) is the nanofibrous environment surrounding cells which serve both mechanical and biochemical stimuli and the cells regulate their functions such as adhesion, proliferation, migration and differentiation by interaction with ECM. Multiscale fabrication methods for mimicking ECM environment in 2D/3D scaffold, therefore, have to be established first. For this aim, we developed nanopatterned 2D platform by using UV-assisted capillary force lithography for investigating adipogenic differentiation affected by geometrical variables. We observed that the cell

crawling into nanogrooves contributed substantially to an enhanced level of differentiation with higher contact guidance, suggesting that cell-to-surface interactions would play a role for the adipocyte differentiation.

To form 3D cell-dense engineered tissue *in vitro*, further, electrospun nanofibers fabricated inclined gap method was used because fabricated nanofibers could be easily transferred to other substrates so that they could be adoptable for 3D fabrication processes such as rolling and stacking with the cells. First, we reported new 3D fabrication method based on rolling of cell-seeded scaffold. It was demonstrated that this hybrid fabrication could produce uniaxially aligned nanofiber scaffolds supported by a thin film, allowing for stable manipulation with aligned cellular morphology. In addition, we successfully formed a cylindrical 3D engineered tissue by rolling up the cell seeded film type scaffold around a melt extruded microfiber. As another approach for 3D engineered tissue formation, we suggested a simple and versatile method for formation of various cell sheets and their layer-by-layer stacking based on electrospun nanofibers. By the performance of nanofibers as a role of structural support, the cell sheets on nanofibrous membrane could sustain their entire geometry even after detached from culture substrate.

In addition, 3D muscle and vascularized skin tissue was achieved by differentiating multilayered myocyte sheets or sandwiching endothelial cell sheet between fibroblast sheets respectively. Taken together, the experimental results indicated that this method provides universal and effective tools for not only stable formation and manipulation of the cell sheet structure but also formation of functional 3D engineered tissue.

Key Words : Extracellular matrix, Micro/nanopatterning, Capillary force lithography, Electrospinning, Rolling-up process, Cell sheet engineering, Layer-by-layer stacking, Adipogenesis, Myogenesis, Vascular network, 3D engineered tissue

Student Number: 2010-20657

Contents

List of Figures

Nomenclature

ECM	Extracellular matrix
CFL	Capillary force lithography
PUA	Polyurethane acrylate
PDMS	Polydimethylsiloxane
PNIPAAm	Poly-N-isopropylacrylamide
HMDS	Hexamethyldisilazane
DMF	Dimethylformamide
DMEM	Dulbecco's Modified Eagle's Medium
EBM	Endothelial basal medium
GM	Growth medium
EGM	Endothelial growth medium
DM	Differentiation medium
FBS	Fetal bovine serum
PS	Penicillin-streptomycin
PDL	Poly-D-lysine
SEM	Scanning electron microscope
AFM	Atomic force microscope
qRT-PCR	Quantitative real-time polymerase chain reaction
TR #n	Number of transfers (n times)
One-way ANOVA	One-way analysis of variance
LBL	Layer-by-layer

Chapter 1. Introduction

Extracellular matrix (ECM) is collection of extracellular molecules such as collagen/elastin nanofibers and proteoglycans. Collagen/elastin nanofibers serve adhesion sites for the cells and mechanical stimuli through cell-nanofiber interactions. Proteoglycans play a role in storage of biochemicals inside ECM by hydration due to their highly negative charged nature. Taken together, the cells receive not only mechanical stumuli but also biochemical stimuli as a result of cell-ECM interaction and regulate their functions such as proliferation, migration and differentiation [1]. Among them, mechanical properties of ECM such as nanotopographical features and matrix stiffness have considered as crucial stimuli which allow regulation of cellular functions through integrin-mediated mechanotransduction [2, 3]. For this reason, fabrication of three-dimensional (3D) scaffolds mimicking nanotopographical features of ECM have been considered as a major challenge in field of tissue engineering whose major aim is to

repair cellular functions of damaged tissues/organs or to replace them to engineered tissues/organs.

Recent development of nano/micropatterning methods accelerates the researches on effect of mechanical stimuli exerted on the cells by nanotopographical features. Especially, polymeric material based nanopatterning methods such as electron beam lithography, colloidal lithography, nanoimprint lithography and capillary force lithography have attracted great attentions because those fabrication methods have strengths of tunability of their mechanical properties and high transparency required for biological assays. Thus, many researchers have used nanopatterns as a tool for investigating effect of nanotopography on cellular functions of diverse cell types such as neural cells [4, 5], muscular cells [6, 7], fibroblasts [8] and stem cells [9, 10]. Fabrication of 3D structures, however, is still remaining limitation of patterning methods for application as a scaffold. Nonetheless, nanopatterns are worthwhile as a platform for determining geometrical characteristics of desired scaffold because their strength in fabricating nanostructures in a precise manner.

In conjunction with nano/micropatterning methods, electrospinning is an another representative method in tissue engineering field due to its strengths such as fibrous morphology similar with ECM, ease in controlling mechanical and chemical properties of nanofibers and capacity for fabricating 3D scaffold composed of random or aligned nanofibers. Unlike randomly oriented nanofibrous mesh, however, aligned nanofibers cannot sustain 3D structure due to their geometrical constraint so that application of electrospinning methods for tissues having uniaxially aligned ECM structures is limited. To address this problem, many fabrication methods such as air/insulator gap methods, pin/blade based methods, ring based methods, rotating disc/drum based methods and their hybrid methods. Among them, air gap methods and hybrid methods have attracted many attentions in tissue engineering field because nanofibers fabricated by air gap methods can be easily transferred to other substrate and resulting thickness and pore size can be controlled by differing number of transfer and fiber density of single transfer.

In addition, nanofibrous meshes have a critical limitation of cellular infiltration which results in different cellular populations according to depth of scaffolds due to their small pore size. To address this problem, many researchers suggested various methods for

increasing pore size such as sequential electrospinning of micro and nanofibers [11, 12] and selective dissolution of water soluble nanofibers from co-electrospun nanofibrous meshes [13], but cellular infiltration problem still remaining unsolved. Other approaches focusing on making 3D engineered tissues with evenly distributed cell populations have also been suggested by repetitive cell seeding and electrospinning on the cultured cell layer [14], but entire cellular populations through the engineered tissue are reduced due to thickness of the nanofibrous mesh.

In this thesis, we suggested various multiscale 2D and 3D fabrication methods to overcome described limitations of previous methods (Figure 1-1). We utilized precisely fabricated nanopatterns through capillary force lithography (CFL) as a tool for investigating cellular behaviors affected by nanotopography. Further, to overcome the limitations of present electrospinning methods, we have developed new methods based on rolling and stacking process of cell-seeded nanofibers for formation of cell-dense 3D engineered tissues *in vitro*.

In chapter 2, we present the effect of nanotopographically defined surfaces on adipocyte differentiation using various nanogroove patterns. Parallel nanogroove arrays with equal inter-groove distance (400 nm, 550 nm, 800 nm width) and varying distances (550 nm width with three different spaces of 550, 1100, and 2750 nm) were fabricated by UV-assisted capillary force lithography (CFL) on 18 mm diameter glass coverslips using biocompatible polyurethane (PU)-based material. After coating with fibronectin and subsequent culture of 3T3-L1 preadipocytes, the degree of adipocyte differentiation was determined by Oil Red O staining and adipogenic gene expression. We observed that adipocyte differentiation was slightly but substantially affected by culture on various nanogrooved surfaces. In particular, the cell crawling into nanogrooves contributed substantially to an enhanced level of differentiation with higher contact guidance, suggesting that cell-to-surface interactions would play a role for the adipocyte differentiation.

In chapter 3, we have successfully fabricated nanofiber-based scaffold complexes of rod and sheet type by combining the three microfabrication techniques of electrospinning, spin-coating, and polymer melt deposition. It was demonstrated that this

hybrid fabrication could produce uniaxially aligned nanofiber scaffolds supported by a thin film, allowing for a mechanically enforced substrate for cell culture as well as facile scaffold manipulation. The results of cell analysis indicated that nanofibers on spin-coated films could provide contact guidance effects on cells and retain them even after manipulation. As an application of the cell-laden nanofiber film, we built a rod type structure by rolling up the film around a mechanically supporting core microfiber which was incorporated by polymer melt deposition. A biocompatible and biodegradable polymer, polycaprolactone (PCL), was used throughout the processes and thus could be used as a directly implantable substitute in tissue regeneration.

Finally in chapter 4, we suggested a simple and versatile method for cell sheet manipulation and 3D engineered tissue formation *in vitro*. The technical result was achieved by integrating an array of electrospun nanofibers into a polydimethylsiloxane (PDMS) assembly containing an opened culture well so that the cultured cells could be peeled off with the nanofibers. By the performance of nanofibers as a role of structural support, the cell sheet-nanofiber complex could sustain its entire geometry even after detached from culture substrate. The nanofibers also allowed the cultured cells to be

oriented in the desired direction and this cell orientation was not impaired by the detachment regardless of cell types when the quantity of integrated nanofibers was offered by the line density of 173 fibers/mm. Compared with conventional methods based on poly-N-isopropylacrylamide (PNIPAAm) which is the most widely used thermoresponsive polymer, cell sheets generated by suggested method based on nanofibers showed almost identical properties and could be used as a building blocks to form 3D tissue constructs *in vitro* by stacking detached cell sheets layer-by-layer. Inspired from these results, we performed experiments for forming 3D engineered muscle tissue and vascularized skin tissue. As results, longitudinally well-developed myotubes were observed through entire muscle tissue and well-organized vascular network was formed inside skin tissue by differentiating multilayered myoblast sheets and co-culturing endothelial cell sheet between fibroblast sheets for 7 days.

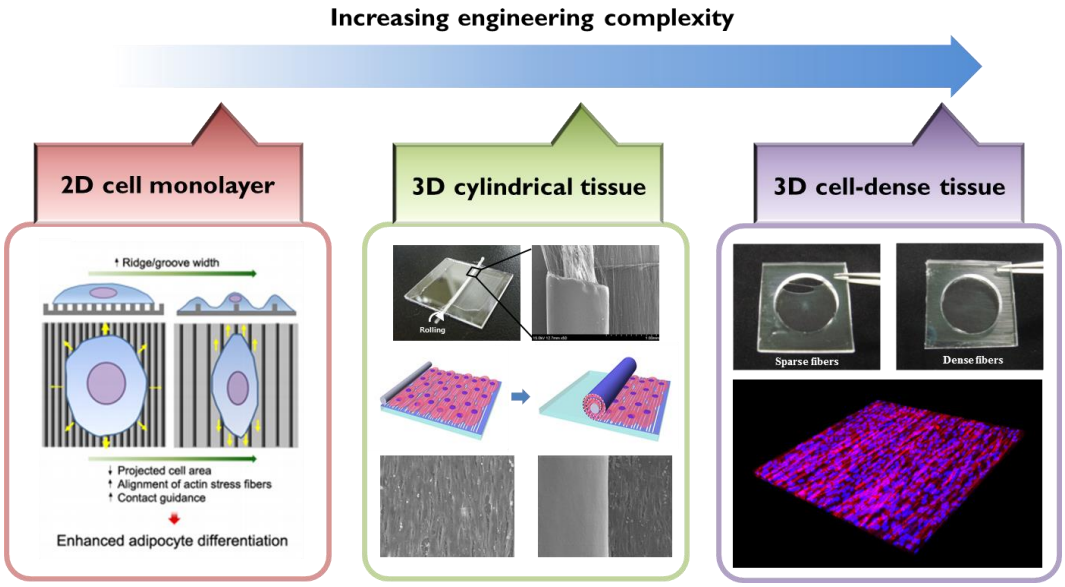

Figure 1-1. An illustration of the goal of this thesis. Multiscale 2D and 3D fabrication methods were suggested.

Chapter 2. Effect of nanogroove geometry on adipogenic differentiation

2.1. Introduction

Cellular response is exquisitely sensitive to the surrounding extracellular matrix (ECM) with nanoscale topographical features [15-18]. Also, cells contain nanoscale physical structures whose size is compatible with embedded ECM, including the intracellular organelles such as cytoskeletal elements (e.g., actin filaments and microtubules) and adhesive structures (e.g., focal adhesions). It is therefore quite reasonable to expect that functioning of many cell types can be regulated *in vitro* by the nanoscale features of the surrounding ECM.

Most of the previous *in vitro* studies have examined cells cultured on two-dimensional flat and rigid surfaces (e.g., Petri dish) despite that most cells *in vivo* are exposed to three-dimensional microenvironments with complex topographical features. In order to address some of the limitations, microfabrication and surface-chemistry-based approaches have provided a versatile set of tools to control the spatial organization and

temporal presentation of cellular cues on a microscale [19, 20]. To better understand the mechanism involved in cellular behavior and function in a microenvironment, nanoscale topographical features have been incorporated into the *in vitro* experimental platform to mimic various *in vivo* three-dimensional ECM environments with structural and mechanical similarity [16]. Previous experiments with various nanotopographic features such as grooves, ridges, pore, wells, and pillar, have shown that nanotopography can strongly influence cell morphology, adhesion, proliferation, and gene regulation [17, 21-24], but the underlying mechanism mediating this cell response still remains unclear.

Recently, we have shown that nanopatterned surfaces of UV-curable polyurethane acrylate (PUA) or polyethylene glycol (PEG) material can be used as a structured biomaterials interface to control various cell functions such in neuronal differentiation [4, 5], osteogenic differentiation [25], directed cell migration [26, 27], and cardiac tissue engineering [6]. The cell culture platform was fabricated by combining UV-assisted capillary force lithography (CFL) and self-replication as schematically illustrated in Figure 2-1. There are a number of advantages with the fabrication method. First, the UV-curable PUA and PEG materials provide excellent biocompatibility for many cell

types, allowing for a long-term cell culture without modification of cell function. Second, the patterned surface can be prepared on a large area, typically larger than 1×1 cm^2, with good uniformity, which is beneficial for various biochemical assays (e.g., Western blotting, RT-PCR, etc.). Third, the self-replication characteristic (i.e., replication from PUA to PUA material) allows a facile duplication of the PUA replica from positive to negative sense (or vice versa), indicating that dot and hole patterns can be prepared from the same silicon master [28, 29].

By taking advantage of the above benefits, we present here the role of nanoscale groove patterns on the adipocyte differentiation. Adipogenesis is referred to as differentiation into adipogenic lineage from preadipocytes. Adipocytes play crucial role in synthesis and storage of energy source in the form of neutral lipid metabolites. Regulation of adipogenesis has been implicated in obesity-related metabolic diseases such as hyperlipidemia, hypertension, and type 2 diabetes. Obese animals often exhibit increase in fat cell size and/or fat cell numbers. Several anti-obesity and/or anti-diabetic drugs such as berberine and thiazolidinediones show beneficial effects through regulating adipogenesis [30, 31]. Recently, *ex vivo* adipocyte differentiation has been intensively

studied for self-fat grafting in the part of cosmetic treatment. In this aspect, some core technologies to control the process of adipocyte differentiation are needed to be established.

Adipocyte differentiation is a complex process regulated by many transcriptional cascades and hormonal stimuli. For example, a certain hormonal change stimulates adipogenesis in concert with adipogenic transcription factors including peroxisome proliferator-activated receptor γ (PPARγ) and CCAAT/enhancer-binding proteins [32-36]. Moreover, it has been reported that ECM proteins or cytoskeleton proteins are also involved in adipocyte differentiation [37, 38]. Therefore, it is likely that the ECM nanoscale topography would affect adipogenesis in an *in vitro* culture platform. Our results demonstrate that the adipogenic differentiation can be up-regulated to a certain extent by changing the nanogroove geometry. In particular, the pattern spacing is more influential than the pattern width such that the largest spacing pattern (width:spacing = 1:5, width = 550 nm) showed the highest differentiation level. In this case, the cells penetrated into the grooves with the actin cytoskeleton being more aligned along the grooves, suggesting that cell-to-surface interactions as characterized by contact guidance

is closely related to the adipogenesis.

2.2. Materials and methods

2.2.1. Preparation of PUA mold

The silicon masters having various parallel arrays of nanogrooves were prepared by standard photolithography and reactive ion etching. A small amount of UV-curable PUA precursor (0.1 – 0.5 mL) was drop-dispensed on the silicon master and covered with a transparent poly(ethylene terephthalate) (PET) film of 50-μm thickness. To cure the resin, the assembly was exposed to UV light (λ = 200 ~ 400 nm, dose = 100 mJ/cm^2) for 25 s. After UV-curing, the PUA replica was peeled off from the silicon master using a sharp tweezer and further exposed to UV light for 10 h for complete annihilation of reactive acrylate groups. Glass coverslips that were used as substrate were sonicated in acetone for 1 h to remove organic contaminants and then dried with N_2 gas.

2.2.2. Fabrication of nanopatterned surfaces

A similar amount of PUA precursor was drop-dispensed on the 18 mm glass coverslip and a PUA mold with engraved nanogrooves was placed carefully to make a conformal contact, leaving behind a replica of the PUA mold after UV exposure for a few

tens of seconds followed by mold removal. To promote adhesion of the patterned layer, the glass coverslip was treated with an adhesion promoter (phosphoric acrylate or acrylic acid dissolved in propylene glycol monomethyl ether acetate (PGMEA), 10 vol %). The nanopatterned surfaces were treated with oxygen plasma for 1 min to make the surface hydrophilic. Then, the fibronectin (1 μg/mL) was coated to increase cell adhesions by dipping the surface for 1 h. To remove unbound fibronectin, the surface was washed with Dulbecco's phosphate buffered saline (DPBS) for 3 times. Prior to cell culture, the fabricated PUA nanopatterns were sterilized by rinsing with ethyl alcohol and D.I. water.

2.2.3. Cell culture

3T3-L1 preadipocytes were maintained in Dulbecco's Modified Eagle's Medium (DMEM) supplemented with 10% bovine calf serum (BCS). To induce adipocyte differentiation, at 2 days post-conflucence, 3T3-L1 cells were incubated with DMEM containing 10% fetal bovine serum (FBS), 0.5 mM 3-isobutyl-1-methylxanthine (IBMX), 1 M dexamethasone and 1 g/ml insulin for 2 days. Then, the culture medium was replaced with DMEM containing 10% FBS and 1 g/ml insulin and the cells were cultured for

additional 2 days. In this manner, the culture medium was changed every two days with DMEM containing 10% FBS.

2.2.4. Oil Red O staining

3T3-L1 cells were washed with PBS and fixed for 5 min with 3.7% formaldehyde solution. Cells were dehydrated with 100% propylene glycol for 5 min. Oil Red O (0.5% in propylene glycol) was incubated with fixed and dehydrated cells for 1 h at room temperature. Cells were re-hydrated with 85% propylene glycol for 5 min and washed with PBS. The stained fat droplets in the cells were visualized under optical microscopy. For statistical significance, each experiment was repeated at least 5 times.

2.2.5. RNA isolation and quantitative real-time PCR (RT-PCR)

Total RNA was isolated with Iso-RNA lysis reagent (5 PRIME, Hamburg, Germany) and subjected to cDNA synthesis using RevertAid M-MuLV reverse transcriptase (Fermentas, Glen Burnie, MD, USA). Relative amounts of mRNA were measured using the CFX96^{TM} Real-Time System (Bio-Rad Laboratories, Hercules, CA.

USA) and calculated by normalization to the level of cyclophilin mRNA. The primer sequences used for quantitative real-time PCR analysis were as follows: PPARγ2-forward (f), 5'-GCATGGTGCCTTCGCTGA-3'; PPARγ2-reverse (r), 5'-TGGCATCTCTGTGT CAACCATG-3'; adiponectin-f, 5'-GGCAGGAAAGGAGAACCTGG-3'; Adiponectin-r, 5'-AGCCTTGTCCTTCTTGAAGAG-3'; aP2-f, 5'-AAG AAGTGGGAGTGGGCTTT-3'; aP2-r, 5'-GCTCTTCACCTTCCTGTCGT-3'; FASN-f, 5'-GCCTACACCCAGAGCTAC CG-3'; FASN-r, 5'-GCCATGGTACTTGGCCTTG-3'; cyclophilin-f, 5'-CAGACGCCAC TGTCGCTTT-3'; cyclophilin-r, 5'-TGTCTTTGGAACTTTGTCTG-3'. The RT-PCR experiment was repeated three times.

2.2.6. Scanning electron microscopy (SEM)

3T3-L1 cells were gently rinsed with DPBS and fixed by 5% glutaraldehyde solution in DPBS containing 0.1 M sodium cacodylate and 0.1 M sucrose for 30 min at 4 °C. After the fixation process, the cells were washed with DPBS for 3 times and dehydrated by sequentially immersing them in gradient ethanol solutions and hexamethyldisilazane (HMDS). The samples were dried in fume hood for 10 h and

observed with SEM (S-48000, Hitachi, Japan).

2.2.7. Quantification of lipid droplet accumulation and projected cell area

To quantify lipid droplet accumulation and projected cell area, ImageJ software (NIH) was used. The images of 3T3-L1 cells stained by Oil Red O were taken for 15 points for each nanopatterned substrate. With the aid of appropriate image processing, stained lipid droplets in the images were highlighted and then the occupied portion of the lipid droplets was calculated. The projected cell area was calculated in a similar manner from arbitrary selection of the cell boundaries for about 100 cells in each SEM image.

2.2.8. Immunofluorescence staining

3T3-L1 cells were washed with PBS for 2 times and fixed with 3.7% formaldehyde solution for 15 min. Fixed cells were treated with 0.1% Triton X-100 in PBS for 10 min to make cells permeable and then treated with antibody buffer (2% bovine serum albumin (BSA) and 0.1% Triton X-100 in PBS) for 30 min to block unspecific bindings. After washing 3 times with PBS, the cells were incubated for 1 h

with tetramethylrhodamine isothiocyanate (TRITC)-phalloidin solution (1:400 in antibody buffer) to stain actin filaments (F-actin).

2.3. Results and Discussion

2.3.1. Preparation of nanogroove patterns on 18 mm glass coverslip

As described earlier, the PUA material has been extensively used for cell culture due to its several excellent properties such as transparency, tunable surface energy [39] and biocompatibility for various cell types [4, 5, 25]. Figure 2-1 shows a schematic diagram for the fabrication of nanopatterned substrates using UV-assisted CFL. Representative SEM images of the nanopatterns are shown in figure 2-2(A-E). In the experiment, five types of nanogroove patterns were used with different width and inter-groove spacing: (A) 400nm 1:1, (B) 550nm 1:1, (C) 800nm 1:1, (D) 550nm 1:2 and (E) 550nm 1:5 (width:spacing). Therefore, for equally-spaced dense nanogroove pattern, the width varied from 400, 550, to 800 nm. For nanogrooves with varying spaces, the width was fixed at 550 nm, while changing the distance from 550 to 2750 nm. For all patterns, the pattern height was fixed at 600 nm. As shown in Figure 2-2(A-E), the patterns exhibited high structural fidelity over large areas (see Figure 2-2F) showing well-defined nanopatterns on 18 mm glass coverslip). To fabricate uniform patterns, it is important to remove trapped air from PUA precursor during replication steps. This is because PUA

precursor cannot fill the cavity occupied by the air trap. To resolve this problem, the rubber roller was mildly rolled on the PET film support before UV-curing process [40].

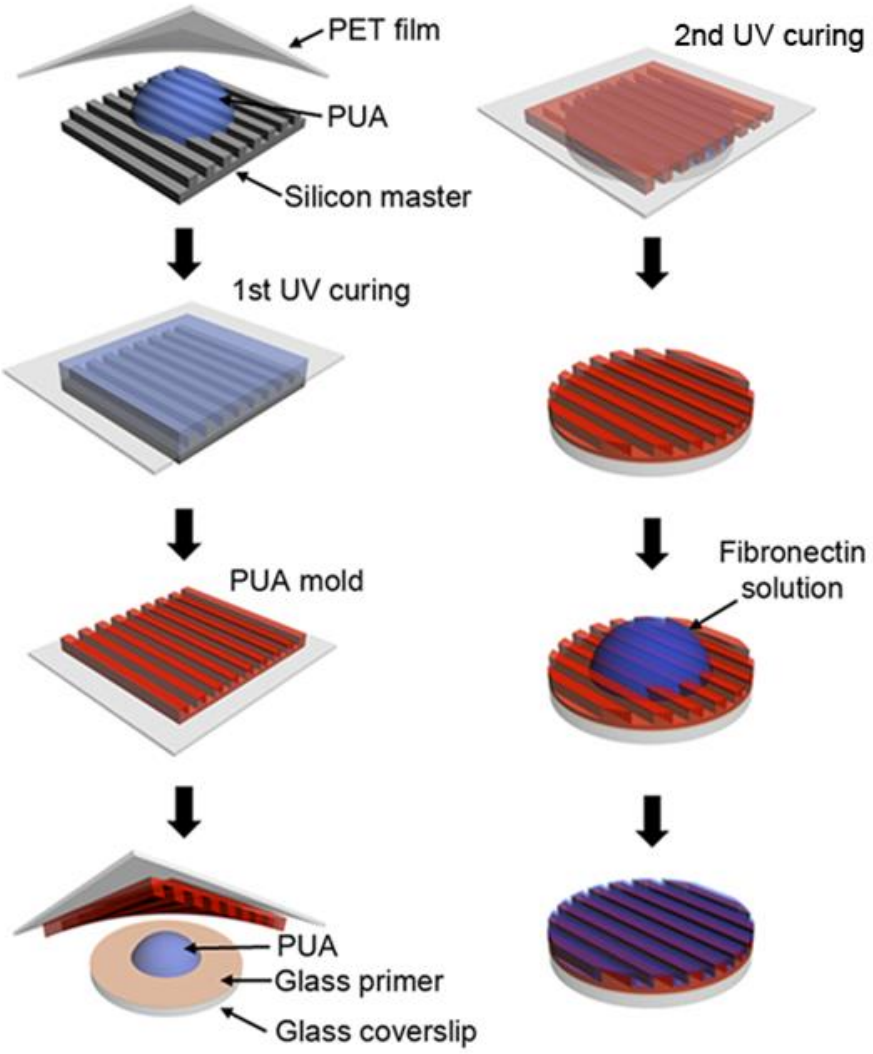

Figure 2-1. A schematic diagram for the fabrication of polyurethane acrylate (PUA) nanogroove patterns using UV-assisted capillary force lithography (CFL).

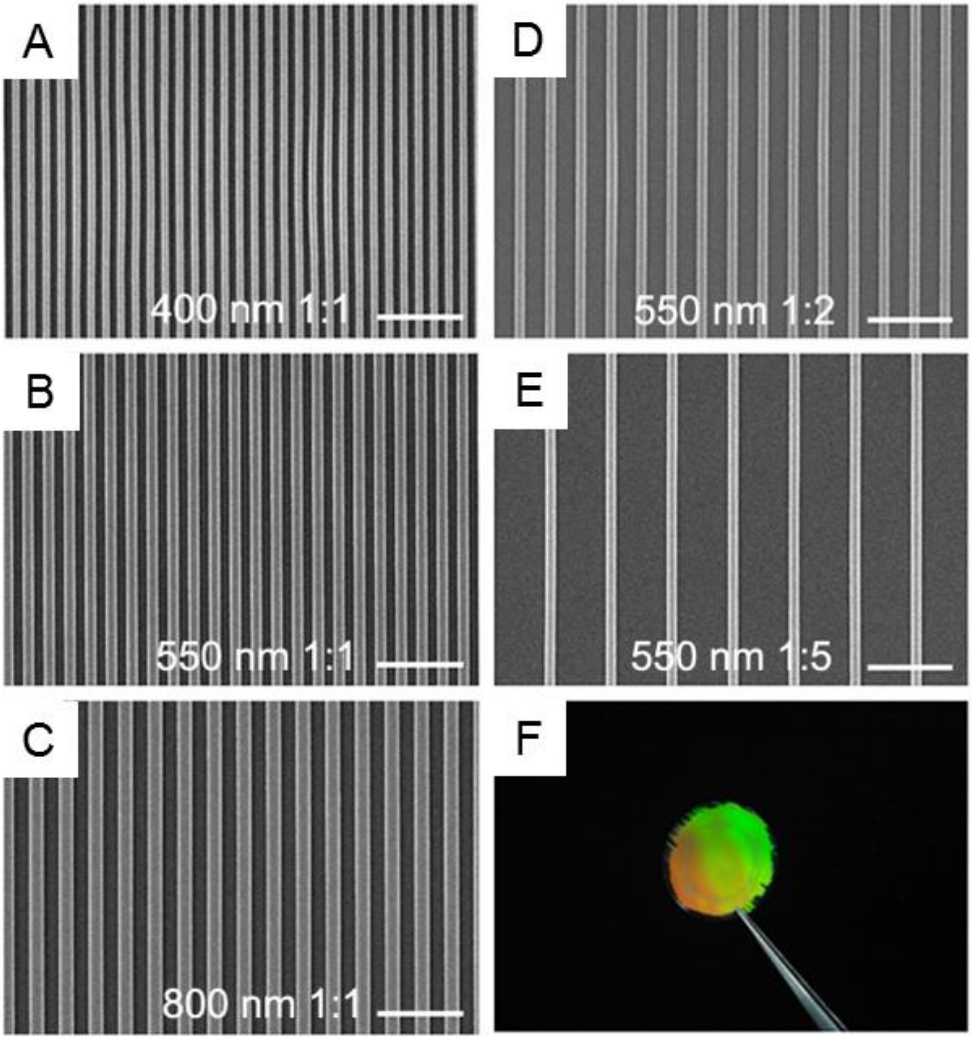

Figure 2-2. Representative SEM images of various PUA nanogrooves: (A) 400 nm 1:1, (B) 550 nm 1:1, (C) 800 nm 1:1, (D) 550 nm 1:2, and (E) 550 nm 1:5 (width : spacing). Scale bars indicate 5 μm. (F) Example of large-area fabrication on 18 mm diameter glass coverslip.

2.3.2. Quantification of adipogenic differentiation on nanogroove patterns

To investigate whether nanotopography would influence adipocyte differentiation, we cultured 3T3-L1 preadipocytes on the various nanogroove surfaces, first for 2 days for confluency and additional 5 days under induction media for adipogenesis. Without the induction media, no appreciable differentiation was observed, suggesting that the effect of media is crucial for the 3T3-L1 preadipocytes. Prior to cell culture, fibronectin was incubated on the surfaces, which turned out to render a uniform coating over the topography without notable difference between ridge and bottom regions [4, 41]. To measure the level of adipocyte differentiation, Oil Red O staining was conducted to stain accumulated intracellular lipid droplets and the results are displayed in Figure 2-3(A-F). For the quantification, two different methods were used: direct calculation of the portion occupied by lipid droplets through image processing (Figure 2-4A and B) and quantitative RT-PCR analysis of the expression of key adipocyte marker genes including PPARγ and its target genes which were up-regulated during adipogenesis (Figure 2-5).

We first examined the effect of groove width on the differentiation. As can be

seen from the Oil Red O stained images shown in Figure 2-3(A-D) and relative amount of lipid accumulation (Figure 2-4A), the differentiation was slightly suppressed compared with control (bare PUA surface, Figure 2-3A) when the cells were cultured on the dense 400 nm and 500 nm 1:1 pattern. In contrast, the differentiation was somewhat enhanced on the largest 800 nm 1:1 pattern, but the level of differentiation was marginal. Next, we examined the effect of groove spacing (Figure 2-3(D-F)). Additionally, we revealed that the level of differentiation was slightly increased with the increase of inter-groove spacing from 550 nm 1:1 to 550 nm 1:5 nanogrooves as evidence by the relative amount of lipid accumulation (Figure 2-4B). In conjunction with the staining results, a similar trend was observed from the quantitative RT-PCR even though the change of marker gene expression was not dramatic (Figure 2-5). Here, relative mRNA levels of several adipogenic marker genes such as PPARγ, adiponectin, aP2, and FASN were measured with respect to that on the control surface.

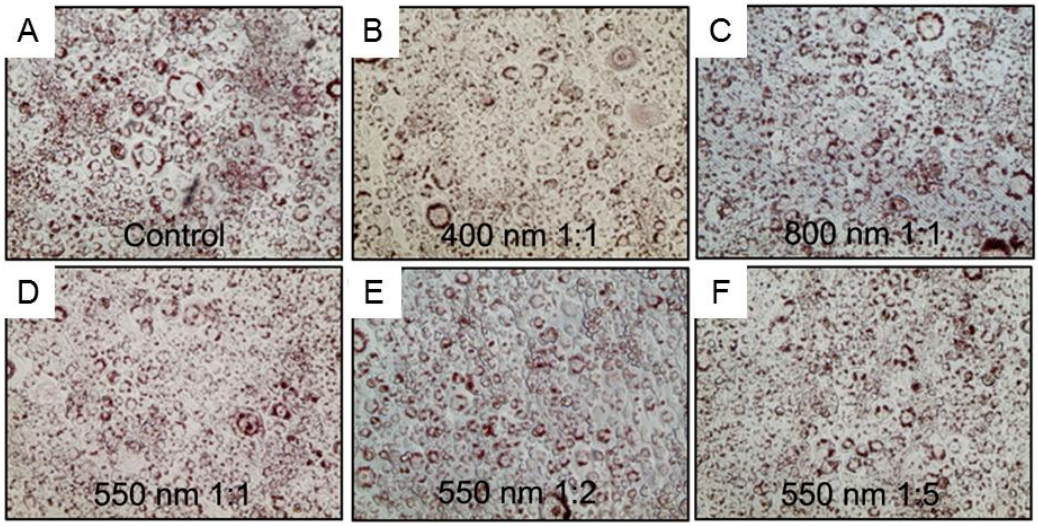

Figure 2-3. Microscopic view of Oil Red O stained 3T3-L1 adipocytes on various nanogroove patterns after culture of 5 days.

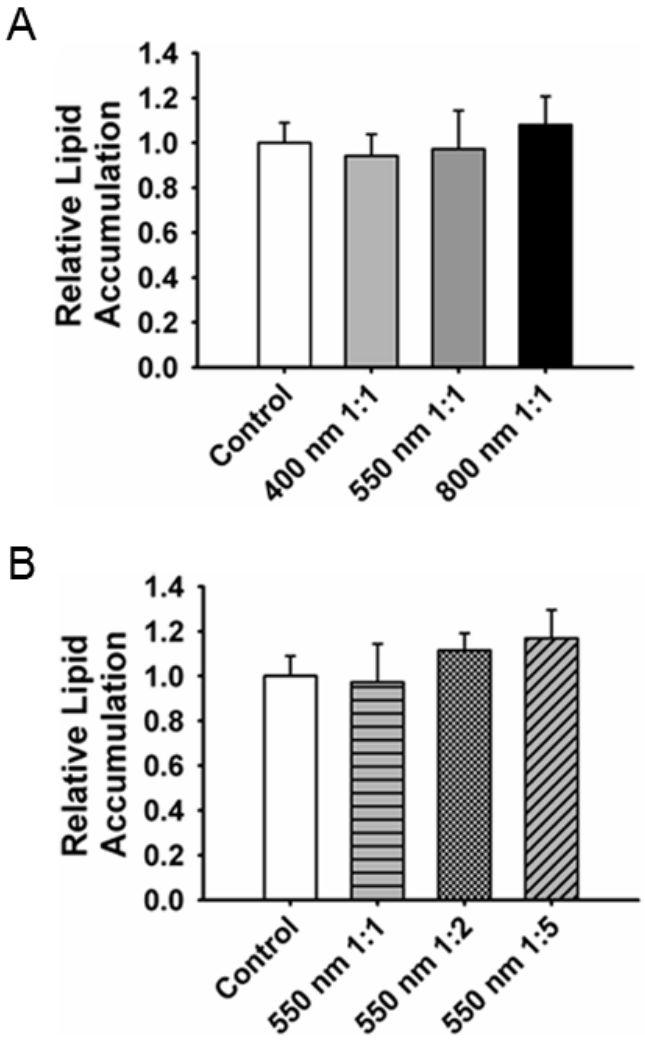

Figure 2-4. Quantitative analysis of relative lipid accumulation obtained by image processing for varying groove width with the same spacing (A) and varying groove spacing with the same width (B).

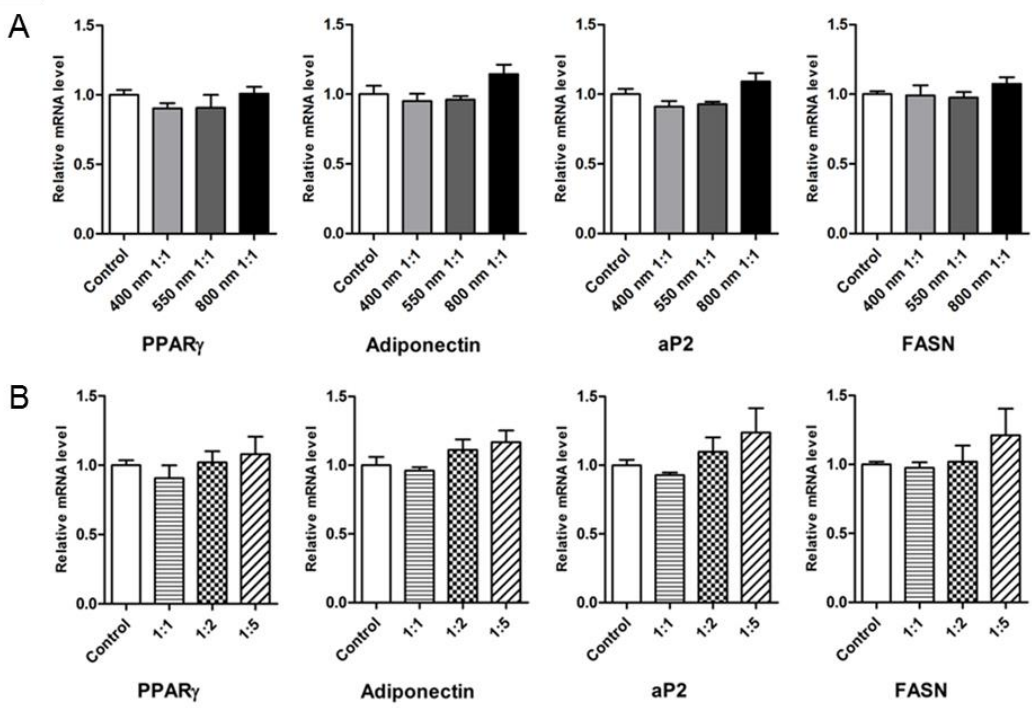

Figure 2-5. Relative mRNA levels of several adipogenic marker genes by quantitative real-time RT-PCR for the dense nanogroove patterns (A) and the nanogrooves of varying spaces (B). The amounts were normalized with respect to that on the control sample.

2.3.3. Effect of cellular morphology on adipogenic differentiation

Based on the observations thus far, it appears that the adipogenesis is associated with the width and spacing of nanogrooves or the geometry of the underlying nanoscale features. To link the geometrical change of nanotopography to cell shape, we measured apparent cell projected area and detailed cell morphology onto nanogrooves by SEM. Representative planar SEM images of the cells cultured for 2 days after plating (i.e., just before the induction of adipogenesis) are shown in Figure 2-6(A-F). According to the SEM images, the cells were less spread with the increase of groove width for the equally-spaced nanogrooves, and with the increase of inter-groove spacing with the same groove width (Figure 2-7(A-B)). For the equally-spaced patterns (Figure 2-6(B-D)), the topographical guidance along the groove direction was less pronounced except for the 800 nm 1:1 pattern, in which a certain degree of cell alignment is apparent. For the various inter-spacing patterns, a dramatic change of cellular morphology was observed (Figure 2-6(D-F)). As the inter-spacing was increased, the projected cell size became smaller with enhanced contact guidance along the groove direction.

For the quantification, the orientation of cell morphology with respect to the

nanogroove direction was plotted in an angular mapping diagram as shown in Figure 2-8. It is seen that the orientation slightly became narrower and directional as the pattern size was increased from 400 to 800 nm. For the nanogrooves with varying spaces, the contact guidance was distinctively enhanced with the increase of the inter-groove spacing from 1:1 to 1:5. Such enhanced contact guidance resulted in relatively reduced cell spreading areas (Figure 2-7(A-B)), which were calculated based on the cell boundaries from the images.

To elaborate on the contact guidance of nanogrooves, the cross-sectional images of the cells were obtained as shown in Figure 2-9. For this experiment, the nanopatterned glass coverslips with dehydrated cells were slightly frozen in a refrigerator (-80℃) for 15 min. A distinct and notable finding from the figure is that the cells only penetrated into the nanogrooves for the largest spacing of 550 nm pattern, in accordance with the enhanced contact guidance shown in Figure 2-6F. This suggests that the cell crawling into the nanogrooves apparently assists in contact guidance. For the less penetrating dense patterns, a careful examination reveals that the cell penetration was slightly increased for the 800 nm 1:1 pattern as compared to the other smaller patterns. Therefore, it is hypothesized that the contact guidance plays a critical role in regulating the adipocyte

differentiation presented in this study.

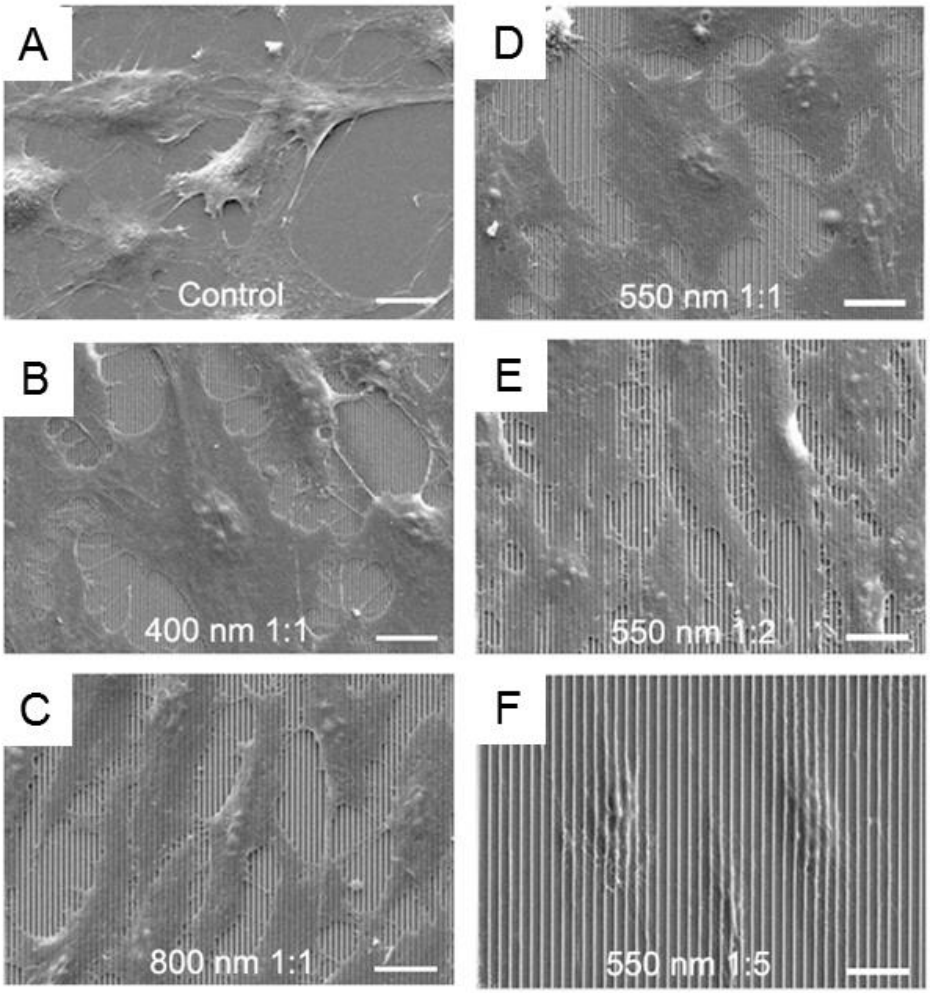

Figure 2-6. Representative SEM images of the 3T3-L1 cells cultured on various nanogroove patterns. The cells were observed after culture for 2 days (before induction of adipogenesis). Scale bar indicates 20 μm.

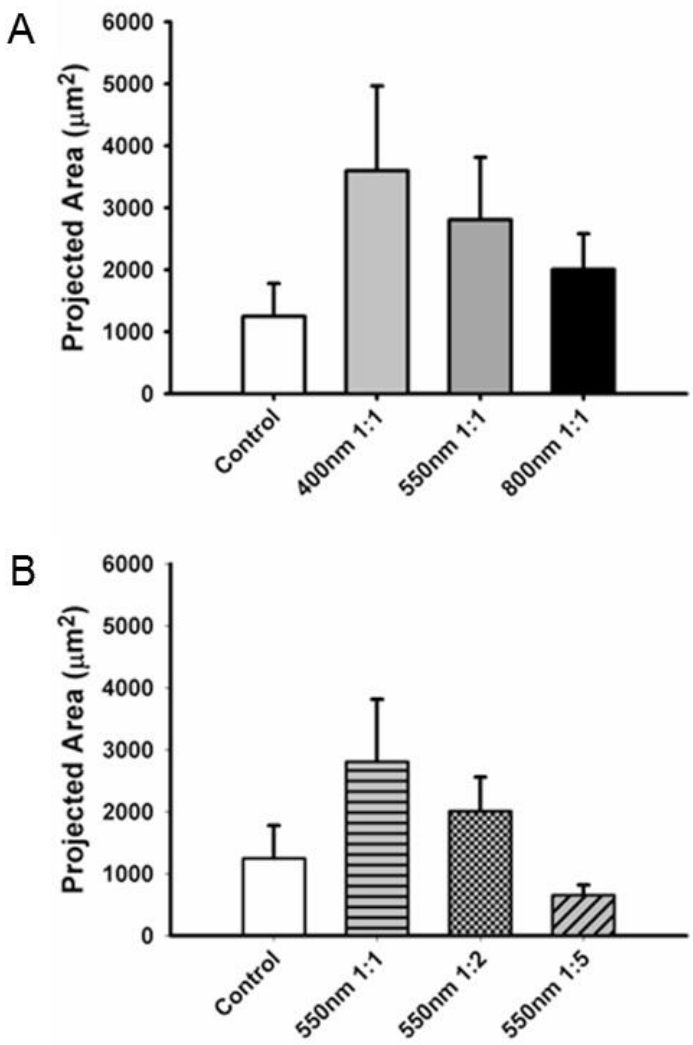

Figure 2-7. Projected cell spreading areas calculated from the SEM images for the dense nanogroove patterns (A) and the nanogrooves of varying spaces (B).

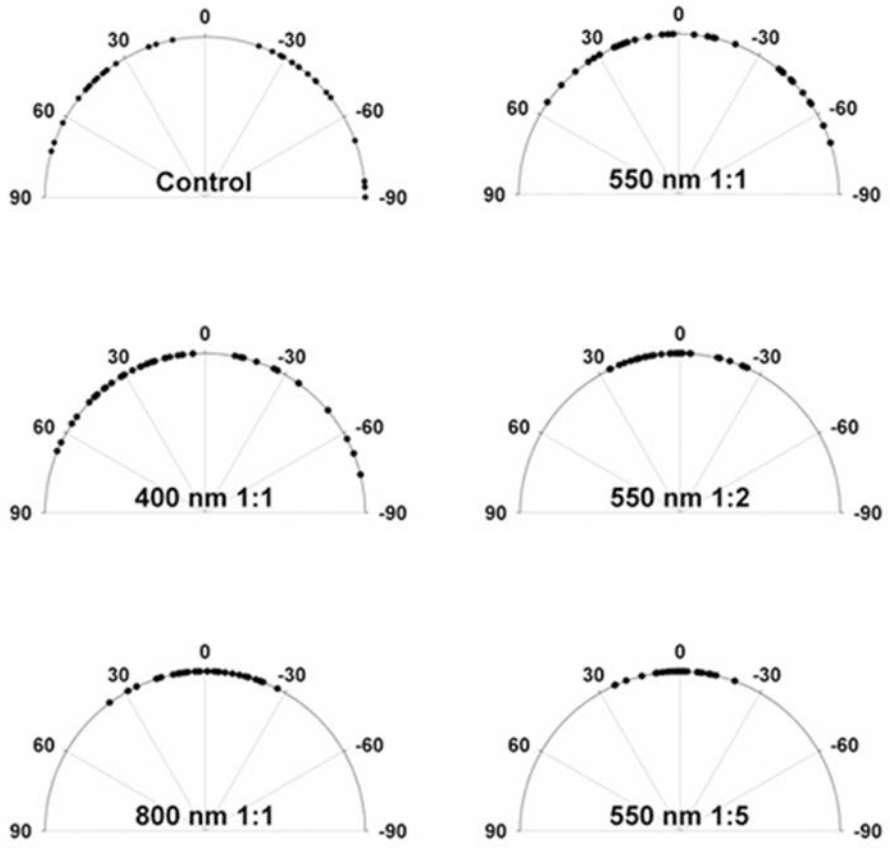

Figure 2-8. Quantification of cellular orientation in angular mapping diagrams for control and various nanogroove patterns. (n = 40).

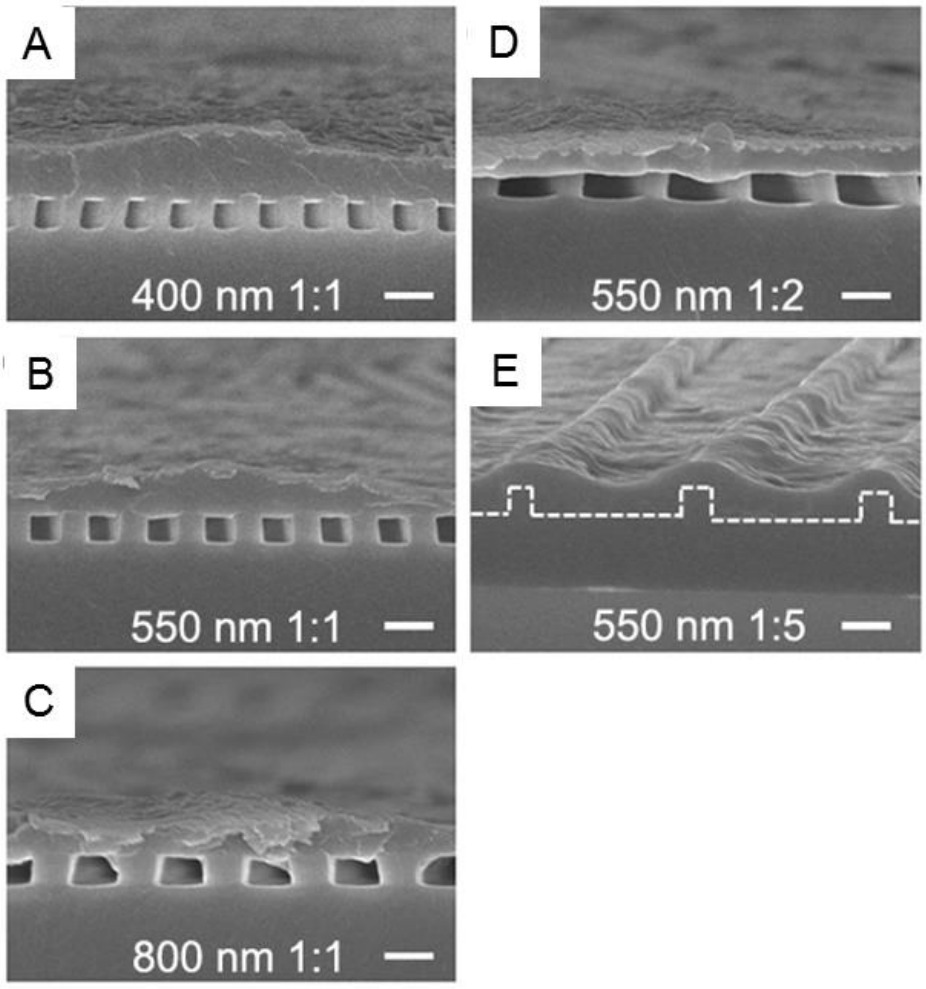

Figure 2-9. Cross-sectional SEM images of the 3T3-L1 cells cultured on various nanogroove patterns. Depending on the width and space of nanogrooves, the cells were spreading only on the ridge regions or penetrated into the grooves. In the case of the 550 nm 1:5 pattern, the cells crawled into the spaces and formed tighter cell adhesions and contact guidance along the groove direction. Scale bar indicates 1μm.

2.3.4. On the role of contact guidance in adipogenic differentiation

The pioneering work by Chen and coworkers revealed that the cell shape can dictate the differentiation of mesenchymal stem cells by modulating cytoskeletal tension and contractility [20, 42]. They reported that as the degree of cell spreading was increased by culturing on large ECM islands, the degree of cytoskeletal tension and contractility was enhanced, which resulted in reduced adipogenesis. In this respect, the degree of actin stress fiber formation can be used as an index for the cytoskeletal tension and contractility [24]. Following the observation by Chen and coworkers, it is expected that the formation of actin filaments would be reduced for the larger width or inter-spacing nanogroove patterns.

To evaluate the degree of cytoskeletal organization, we conducted immunofluorescent staining for actin filaments as shown in Figure 2-10(A-D). While some alignment was seen for the 800 nm pattern, well-organized and aligned actin fibers were mainly observed on the 550 nm 1:5 pattern in contrast with the other dense nanogrooves and PUA control. This suggests that a simple nanogroove pattern has ability to down- or up-regulate adipocyte differentiation by modulating cell shape and cytoskeletal organization. Further, the contact guidance can be used as an indicator to determine the

degree of adipocyte differentiation.

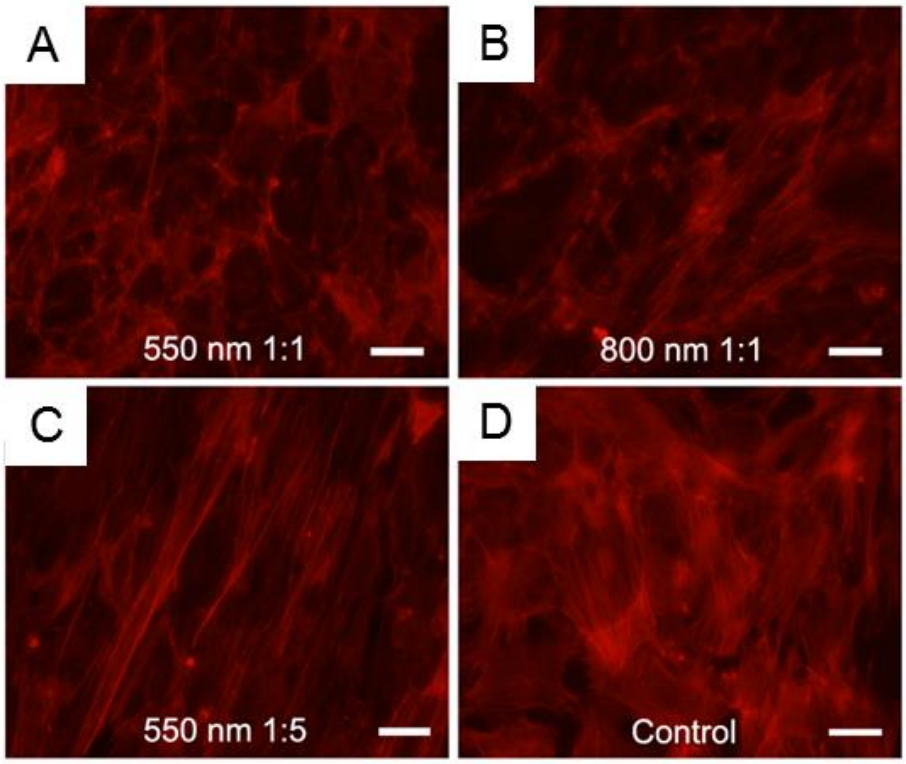

Figure 2-10. Fluorescence images of the 3T3-L1 cells immunostained for F-actin. Well-organized actin stress fibers were observed for the largest spacing of the 550 nm pattern. Scale bar indicates 100 μm.

2.4. Summary

We have presented the role of ECM nanotopographical features in the form of parallel nanogroove arrays on the adipocyte differentiation of 3T3-L1 preadipocytes. Data from Oil Red O staining, relative amount of lipid accumulation, and adipogenic marker gene expression have implied that the adipogenesis could be modulated by culture on various nanogroove patterns with different widths and spaces. In particular, the differentiation level was potentially enhanced on the 550 nm 1:5 pattern by 20 % as compared to the control without nanopatterns. Such small enhancement might be attributed to the dominant effect of the induction media that is needed for the differentiation. The SEM measurement has shown that the cell morphology was distinctly different on different nanogroove patterns. Surprisingly, the cells penetrated into the grooves with better contact guidance only for the 550 nm 1:5 pattern, in good correlation with the differentiation level. A cartoon in Figure 2-11 depicts the role of nanogroove geometry on adipogenic differentiation observed in this study. Although a detailed study elucidating biological mechanisms is required, the present study shows that contact guidance, which is closely related to integrin-mediated adhesions, plays a critical role in

regulating adipocyte differentiation. Therefore, a simple index for contact guidance might be useful to predict the level of differentiation.

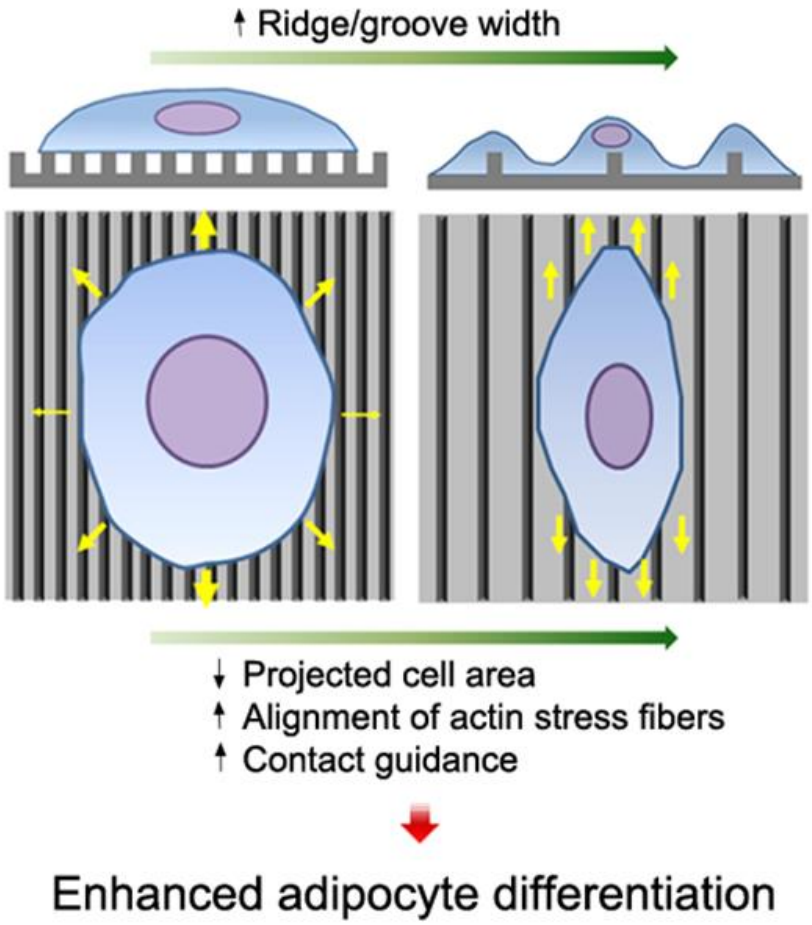

Figure 2-11. A cartoon depicting the role of nanogroove geometry on the adipocyte differentiation.

Chapter 3. Hybrid microfabrication of nanofiber-based sheets and rods for tissue engineering applications

3.1. Introduction

One of the important issues in the tissue engineering field is to provide cultured cells with a biocompatible template, or scaffold, which mimics the natural extracellular matrix (ECM), to regulate cell functions, such as adhesion, migration, proliferation, and differentiation [43-45]. Through the scaffold-based strategies, a wide range of research has been conducted to understand the cellular processes controlled by the surrounding microstructure as well as to develop scaffolds for practical applications in clinical settings [16, 46, 47]. Among many micro- and nano- processing tools for the scaffold fabrication, the electrospinning process has offered unique advantages due to its ability to produce nanofiber networks that closely simulate the ECM structure, which is a complex network with various nanoscale fibrils such as collagen, elastin, fibronectin and laminin [48-51]. The ECM mimicry is beneficial for cell activation and characterized by high productivity,

simplicity, and material universality in manufacturing the nanofibers.

Because the electrospinning process is driven by strong electrostatic force from high voltage, the as-spun fibers usually form a randomly configured nonwoven matrix. Recently, the nanofiber patterning technique has been diversified by modulating its configuration from simple random networks to uniaxially aligned form, which in turn can generate desired cell morphogenesis. The feasibility of aligned nanofiber scaffolds has been demonstrated using various cells such as fibroblasts, myoblasts, neuron cells, and mesenchymal stem cells [52-58]. Especially in the case of myoblasts, their native tissue, skeletal muscle, has a highly organized anatomical structure that consists of many parallel bundles formed by fusion of the myoblasts. It naturally follows a necessity of highly oriented nanofiber scaffold that resembles the native muscle architecture. In order to achieve the ordered fiber configuration, a variety of methods have been proposed by developing specific collecting mechanisms such as rotating cylinder, sharp-edged disk, wire-framed drum, near-field working distance, and parallel electrodes [59-63].

We previously reported a novel processing technique to acquire the ordered nanofiber array scaffold not only with better alignment but also with quantitatively

controlled fiber density [64]. The multiple transfers of nanofibers, by which the nanotopographic spacing could be modulated, were a favorable feature to demonstrate the contact guidance effect of nanofiber pattern. In particular, the well-aligned nanofiber pattern with the controlled configuration showed improved biological functions in cellular adhesion and morphogenesis [65]. However, the previous nanofiber manufacturing methods need to be assisted by some post-processing procedures, allowing for facile manipulation of the produced nanofibers. While the random mesh has a number of overlapping junctions on the constituent nanofibers, the structural interconnections in the aligned mesh are not abundant so that it cannot be handled as an individual entity. The sparse connectivity between aligned nanofibers implies that a supportive structure should be incorporated to prevent a possible distraction of nanofibers.

Here, we introduce an effective hybrid fabrication method to build a new kind of rod- or sheet-type composite scaffold that consists of a spin-coated polymer film and an array of electrospun nanofibers. A series of polycaprolactone (PCL) solutions with diluted concentrations were used for fabricating thin films with varying thicknesses from 1.5 to 35 μm. The polymer films over 20 μm thickness turned out to exhibit favorable stiffness

that allowed manipulation with tweezers. By using a relatively thick film as an underlying substrate, the mechanically stable scaffold was achieved in combination with the transferred electrospun nanofibers. C2C12 myoblasts were cultured to confirm the cellular morphogenesis such as cell alignment and elongation, which may be guided by the nanofiber configuration. In addition to the sheet-type scaffold, the films with thickness less than 10 μm were transformed into a rod-type scaffold by rolling up with the cell-fiber complex sheet. To facilitate the rolling manipulation with thin structures, a cylindrical core of microscale diameter was thermally extruded through a micro needle and deposited at one edge of the nanofiber film. Taken together, some potential obstacles associated with handling fragile nano-sized scaffold materials were alleviated by employing the microfabricated supportive structures with controllable size. For additional manipulations including folding and laminating, the current hybrid scaffolds are fully composed of biodegradable polymers, which could potentially meet the needs of tailored scaffolds for tissue engineering applications.

3.2. Materials and methods

3.2.1. Spin coating process

For spin coating solutions, polycaprolactone (PCL, Mw = 80,000 g/mol, Aldrich) was dissolved in chloroform (Sigma) at three different concentrations of 5, 10, and 20 wt%. As shown in Figure 3-1A, a certain quantity of PCL solution drop was deposited on the glass substrate on the spin-coating machine (JD tech) before spin coating at different speeds in the range from 1000 to 4000 rpm. The spinning time had no significant effect on the film thickness; thus it was fixed at 30 sec. Most of the solvent was evaporated while spinning, because chloroform is a highly volatile solvent. To remove the possible residue of the solvent in the film, the specimens were kept in a fume hood for one hour. The films coated on the glass substrate were incised using a sharp blade for thickness measurement. The film thickness was measured by an Alpha step surface profiler (Nanospec AFT/200, KLA TENCOR), which was determined by the height difference between the top of the coated film and the glass substrate.

3.2.2. Electrospinning process and nanofiber transfer

The PCL was also dissolved in the mixture of chloroform (Sigma) and dimethylformamide (Junsei) at a volume ratio of 75/25. Here, dielectric properties generated from the dimethylformamide enhanced electrospinning capability. The solution concentration was chosen to be ~20 wt%, which had been confirmed as a proper condition in the previous work [64, 65]. The PCL solution was stored in a syringe equipped with a 23-gauge metal needle which was connected to a high voltage DC power supply. The syringe module was loaded on a syringe pump and infused at a rate of 1.5 mL/h. The DC voltage of 15 kV was applied to the solution drop formed at the needle tip. The collector for crop of aligned nanofiber was designed as shown in Figure 3-1B. Two separate aluminum strips were perpendicularly arranged, and the ejected nanofibers were suspended across the air gap between the strips. Due to the repulsive interaction between the adjacent nanofibers hanging on the strips, well-aligned nanofibers could be obtained. More detailed information about the collecting mechanisms and conditions are described in our previous work [64]. The nanofibers were transferred onto the as-prepared PCL film via spin-coating. To vary the scaffold line density, which is determined by the number of

nanofibers along a unit distance perpendicular to the direction of nanofiber alignment, the overlapping transfer was carried out in a repetitive manner. The electrospinning time for each transfer was fixed at 1 min, and 3 and 12 transfers were performed respectively for low and high density. The resultant nanofiber scaffolds were measured using scanning electron microscope (SEM, S-48000, Hitachi). From the SEM images, the fiber alignment was analyzed by measuring the angles between the longitudinal and vertical directions of the fibers.

3.2.3. Thermal extrusion of core structure for rolled-up scaffold

The PCL has good formability for thermal processing due to its low melting temperature at 60℃. We previously developed a polymer melt deposition system for fabricating a three dimensional woodpile shape scaffold that was comprised of a number of thermally extruded microfibers [65]. In this approach, the microfiber-shaped structure was used not only as a core template to provide a tool for rolling manipulation but also as a mechanical support of the overall hybrid architecture. Figure 3-1C illustrates the thermal extrusion procedure following the prior processes for nanofiber-patterned film

fabrication. The system consists of a thermally conductive metal syringe equipped with a micro precision needle, a coil heater surrounding the syringe module, a pneumatic dispenser delivering compressed air, and a micro-positioning system driven by step motors. When the air pressure was applied to the polymer melts stored in the syringe, the microfiber-shaped polymer melts were extruded out through the micro needle. The initially molten state microfiber was then deposited onto the pre-processed nanofiber film surface, and fused with the film as solidified at ambient conditions. The inner diameter of the micro needle was 400 μm and the processing temperature of the coil heater was set up at 150℃. The applied pressure and the moving velocity of the micro needle were controlled in the range of 550~750 kPa and 0.5~2 mm/sec, respectively. Subsequently, the nanofiber film structure, even with cultured cells on its surface, could be easily rolled up along the fabricated microfiber core structure.

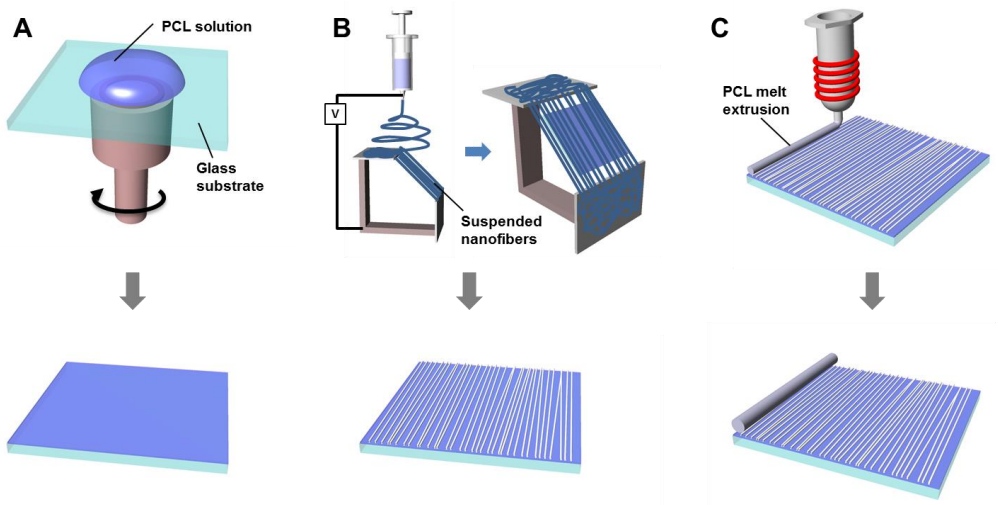

Figure 3-1. Fabrication process of hybrid nanofiber scaffold: (A) spin coating process to fabricate a PCL thin film, (B) electrospinning process to secure aligned nanofibers and transfer onto the film, and (C) polymer melt deposition process to place a microfiber core structure for subsequent rolling process.

3.2.4. Cell culture

All reagents used in the experiments related to cell culture were purchased from Sigma Aldrich, unless otherwise specified. C2C12 mouse myoblasts were purchased from ATCC and maintained in Dulbecco's Modified Eagle's Medium (DMEM, GIBCO) supplemented with 20 % fetal bovine serum (FBS, GIBCO) and 1 % penicillin-streptomycin (PS, GIBCO). Prior to cell seeding, all scaffolds were sterilized for one hour under ultraviolet irradiation, treated with oxygen plasma for 1 min, and coated with fibronectin of 10 mg/mL for one hour at room temperature. The cells were seeded onto the prepared scaffold at the density of 2×10^5 cells/cm^2 and cultured for two days until the cells formed a confluent monolayer.

3.2.5. Immunostaining

C2C12 cells on the scaffolds were gently washed with PBS and fixed with 3.7 % formaldehyde solution for 10 min. Fixed cells were washed with PBS three times and immersed in antibody buffer (0.1 % Triton X-100 and 2 % bovine serum albumin (BSA) in PBS) for 15 min to make the cells permeable and prevent unspecific binding of

antibodies. After washing three times with PBS, the cells were then sequentially stained with 4′,6-diamidino-2-phenylindole dihydrochloride (DAPI) solution (1:1000) for nucleus and phalloidin-TRITC solution (1:400) for actin cytoskeleton for 40 min each. To prevent photobleaching, the cells were embedded with a small amount of ProLong Gold antifade reagent (Invitrogen) and observed with fluorescence microscopy (Eclipse Ti, Nikon).

3.2.6. Scanning electron microscopy (SEM) measurement

The nanofiber film scaffolds with C2C12 cells were rinsed with PBS and rolled up using the developed method. The samples were fixed with 5 % glutaraldehyde solution supplemented with 0.1 M sodium cacodylate and 0.1 M sucrose for 30 min. For further fixation, the samples were treated with 1 % osmium tetroxide solution containing 0.1 M sodium cacodylate and 0.1 M sucrose for 1 h. After washing three times with PBS, the samples were slowly dehydrated by immersing them in ethanol solutions of increasing concentration and hexamethyldisilazane (HMDS, J.T.Baker) to prevent collapse of cell morphology. The samples were completely dried in a fume hood overnight and were observed using SEM (S-48000, Hitachi).

3.2.7. Quantitative analysis

The images of the C2C12 cells stained with DAPI were taken 5 times for each sample and used for analysis. Cell orientation was determined by the angle of long axis of nuclei against nanofiber alignment direction. Nucleus elongation was calculated by dividing the short axis length over the long axis length. In a similar manner, SEM images of nanofibers were taken 10 times for each sample and used for calculating nanofiber orientation.

3.3. Results and discussion

3.3.1. Spin-coating of PCL films

Figure 3-1 illustrates the process for fabricating a hybrid scaffold consisting of electrospun nanofibers supported on a thin film. The overall scaffolds were made of a well-known biodegradable and biocompatible polymer, PCL, which is widely used for various biomedical applications. Since it has a low glass transition temperature of -60℃ and exists in a rubbery state at room temperature, the PCL based structure has better mechanical compliance than other biodegradable polymers. This property makes it ideal for use as a flexible scaffold material. In this research, we exploited the shape-deformable characteristic of PCL by employing and integrating three consecutive microfabrication methods of spin-coating, electrospinning and deposition of polymer melt.

At first, we fabricated a thin PCL film using the spin coating method with variables such as angular speed of spinning and polymer solution concentration. It was observed that the increase of spinning duration time beyond 30 sec had no significant effect on the film thickness (data not shown) because the solution almost solidified from the fast evaporation of chloroform that was used as the solvent. Figure 3-2 shows the

correlation between film thickness and spinning speed at three different solution concentrations of 5, 10, and 20 wt%. As seen from the figure, the relatively thin films made from 5 and 10 wt% solutions displayed less dependency on the spinning speed. The variations of film thickness between 1000 and 4000 rpm appeared to be approximately 15% and 18% in the cases of 5 and 10 wt% solutions, respectively. As the solvent evaporation occurred in a very short period of time during the spinning, the film thicknesses at lower concentrations were less sensitive to the change of spinning speed and thus their standard deviations were very small below 0.3 μm. As with the typical spin coating process, thicker films were obtained as the solution concentration became higher. In the case of 20 wt% concentration, the thickness of all specimens exceeded 15 m from 1000 to 4000 rpm, and the thickness at 1000 rpm was two times higher than that at 4000 rpm, suggesting a significant dependency on the spinning speed. Figure 3-3A shows an example of the coated film peeled off from the glass substrate. We found that the film thicker than 20 μm was sufficiently rigid to manipulate by any tweezers, which was used as a basement substrate for a free standing nanofiber-transferred scaffold. As observed in other works [66-68], a certain degree of crystallization was found on the surface of PCL

film after spin coating as shown in Figure 3-3B and C. Here, the spherulitic crystals that were formed regularly on the entire films are believed to yield good mechanical stability and formability. When a thick film was spun from 20 wt% solution, however, some defects such as trapped or burst bubbles were frequently observed. To remove such defective bubbles, the films were heated on a hot plate above the PCL melting temperature (100℃) and held undisturbed for 10 min. After cooling back to room temperature, a uniform membrane was obtained without bubble defects as shown in Figure 3-3D.

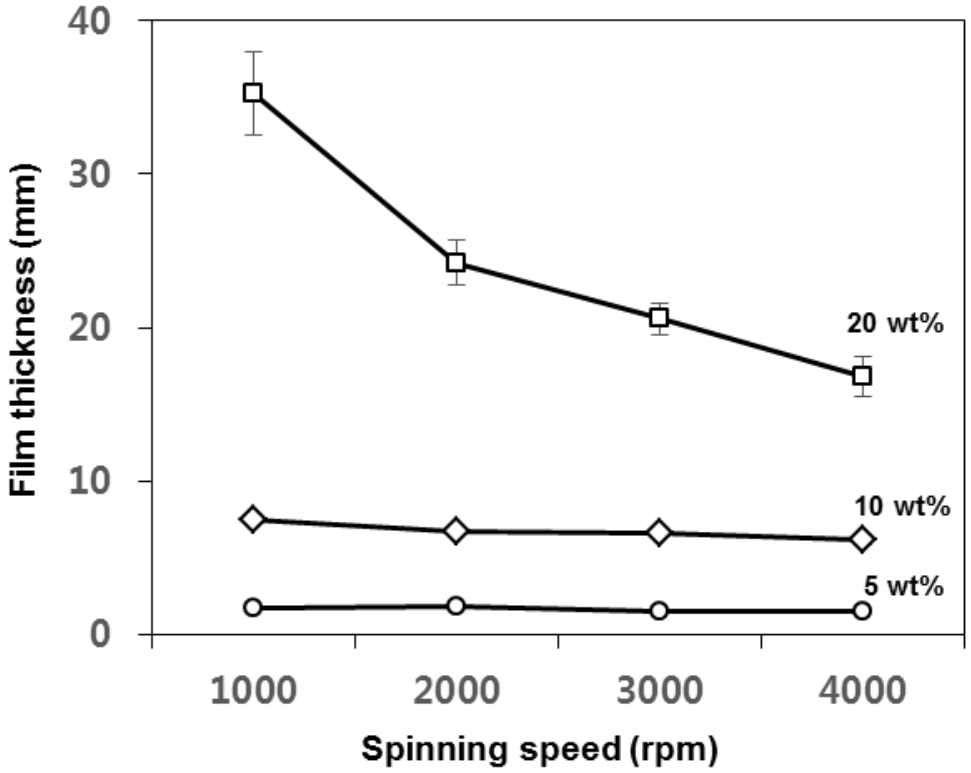

Figure 3-2. Relationship between film thickness and spinning speed at three different PCL solution concentrations of 5, 10 and 20 wt%.

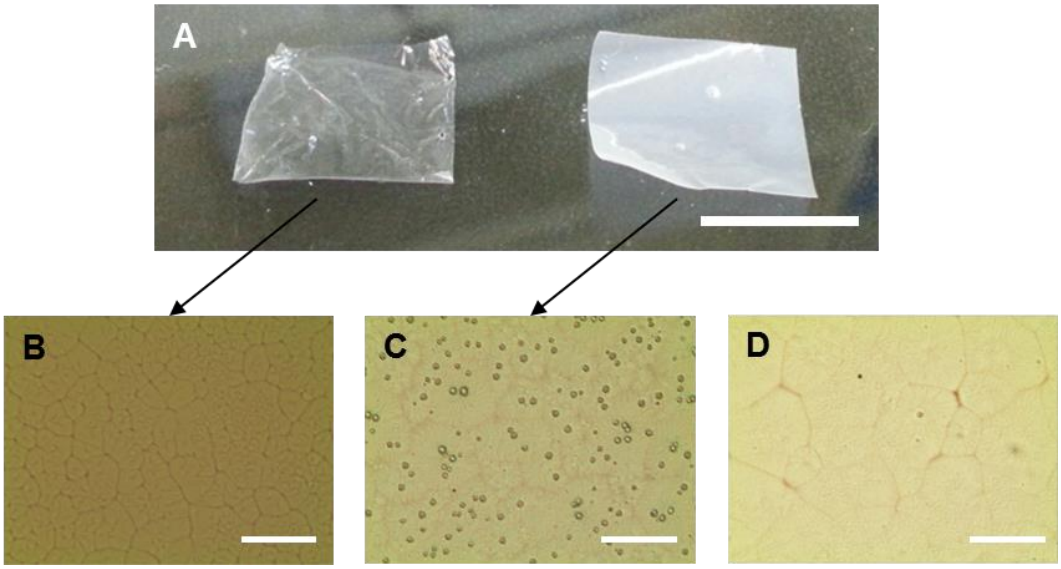

Figure 3-3. (**A**) Thin (left) and thick (right) films were respectively made from 5 and 20 wt% solutions at a speed of 3000 rpm. The scale bar is 5 mm. Optical microscope images of the PCL film surfaces made from (B) 5 and (C) 20 wt% solutions. (D) The thick film surface (case D) after removing bubble defects by heat treatment. The scale bar in B is 50 μm with the same magnification in C and D.

3.3.2. Electrospinning of PCL nanofibers for sheet-type scaffold

Next, nanofiber-microfilm hybrid constructs were generated by multiple transfers of nanofibers hanging on the void gap collector (Fig. 3-1B). In this way the density of collected nanofibers could be controlled in a quantitative fashion. Figure 3-4A and B show the resulting fibers of average densities of 108 and 384 fibers/mm with 3 and 12 transfers, respectively. Such different densities are expected to yield different contact guidance cues in the cell seeding experiments. As for nanofiber orientation in this scaffold, the fibers placed on PCL film were quantified by measuring the inclined angles with respect to the reference direction. As shown in Figure 3-4C and D, all of the transferred fibers were distributed within a narrow range of ±25° and more than 90% of the fibers were oriented within ±10° to the reference direction. The fiber alignment was nearly reproducible for every single-step electrospinning process, indicating that the nanofiber transfer repetition in both cases of 3 and 12 transfers did not significantly impair the fiber alignment.

Recently, a number of studies on contact guidance have been conducted via template-assisted techniques such as electrochemical deposition, soft lithography, and

nanoimprinting [69]. Although they provide reproducible construction of nanoscaffolds with high precision, the electrospun nanofibers have an advantage in terms of direct transplantation in their initial architecture. In order to demonstrate the feasibility of the developed nanofiber-based scaffold, C2C12 myoblasts were cultured for two days and morphological changes were analyzed from immunofluorescent imaging. We employed three types of scaffolds: i) flat film without nanofiber, ii) nanofiber scaffold of low density (3 transfers) and iii) that of high density (12 transfers). As shown in Figure 3-5, the nuclei and cytoskeletons of cells appeared to align along the unidirectionally oriented nanofibers. Also, the nuclei stained with DAPI showed that the nanofibers on film gave rise to elongated morphology in the direction along the fiber alignment. In contrast, neither the cell alignment nor elongated morphology was shown for the cells cultured on a flat PCL film surface without fibers.

For quantification, the distribution of aligned cell morphology was analyzed using angular mapping plots as shown in Figure 3-6 (A-B). On the scaffolds without nanofibers, it is seen that the cell alignment and elongation were hardly observed (Figure 3-6A and D). On the other hand, the cells grown on nanofiber scaffolds with 3 and 12

transfers showed distinct alignment and elongation guided by the nanofibers as shown in Figure 3-6 (B-D). As the nanofiber density increased from 108 (3 transfers) to 384 nanofibers/mm (12 transfers), both morphological changes of alignment and elongation became more pronounced. The correlations between fiber density and cell morphology were identified in accordance with the previous work [70]. It is noteworthy that a nanofiber set of relatively low density also provided the desired morphological changes similar to a high-density fiber set, while recognizing that a considerable amount of cells were still not affected by the fibers due to the larger fiber spacing. When considering the confluent state of cultured cells as shown in Figure 3-5, the cells aligned directly by nanofibers seemed to affect the shape of adjacent cells due to tight cell-cell interactions even in the presence of the low-density fiber network.

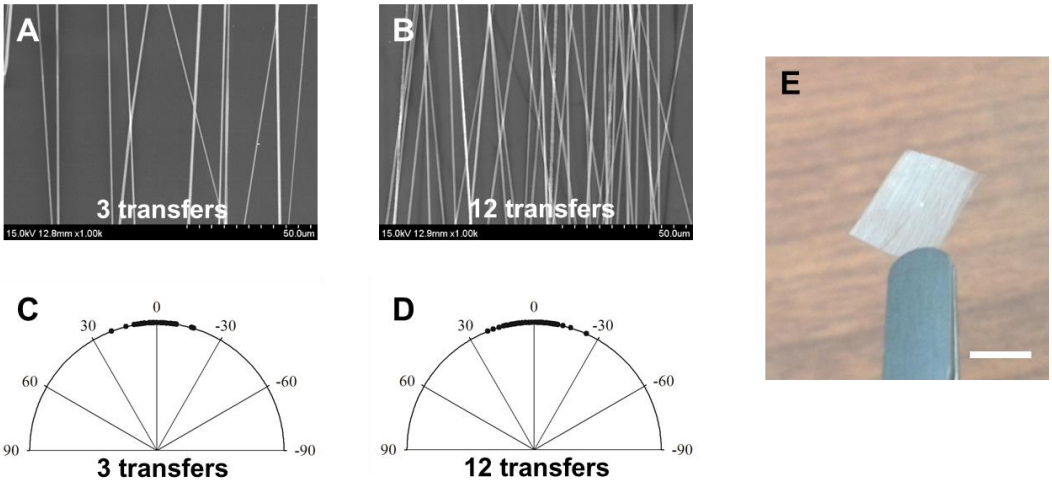

Figure 3-4. SEM images of the repetitively cropped nanofibers on PCL films: (A) 3 transfers and (B) 12 transfers. Angular mapping plots to quantify nanofiber alignment: (C) 3 transfers (n=70) and (D) 12 transfers (n=100). (E) Photograph of sheet-type hybrid scaffold integrated with aligned nanofibers. The scale bar is 5 mm.

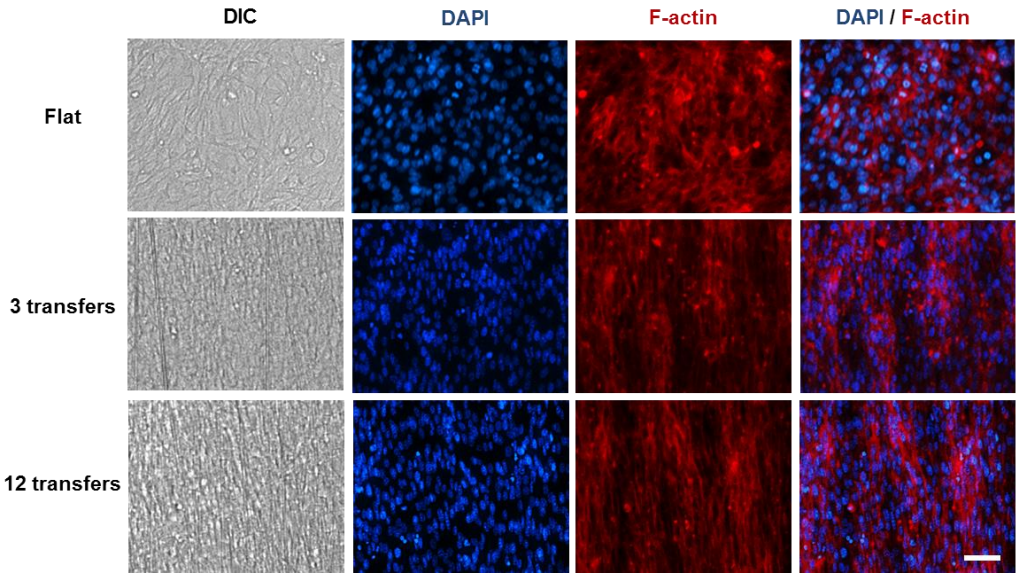

Figure 3-5. Diffraction interference contrast images (first column) and immunofluorescent staining images of cells cultured on flat PCL film (first row), nanofiber-integrated scaffold with 3 transfers (second row) and 12 transfers (third row). DAPI, F-actin and their merged stack are arranged in the second, third, and fourth column, respectively. The scale bar in A is 25 μm, and the other images are at the same magnification.

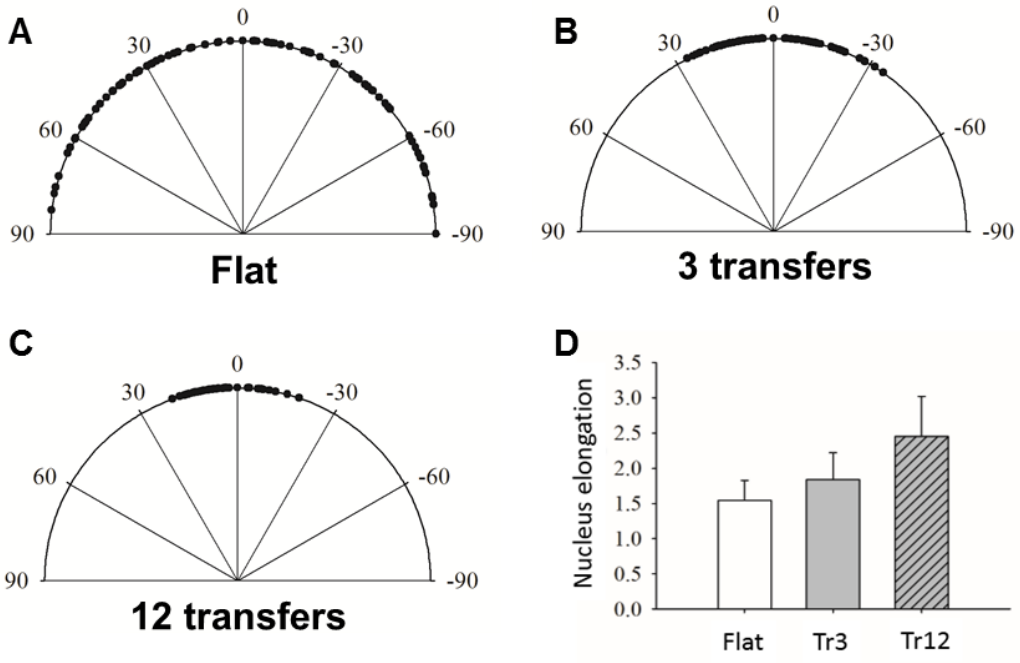

Figure 3-6. Angular mapping plots to quantify cell alignments of (A) flat PCL film and (B) nanofiber-integrated scaffold with (B) 3 transfers and (C) 12 transfers. (D) Degree of nucleus elongation of each scaffold. Data shown as mean ± standard deviation (n=100 in each scaffold).

3.3.3. Rolling of PCL nanofibers for rod-type scaffold

One of the crucial factors for an ideal scaffold is to offer a three-dimensional (3D) mechanical support for tissue growth. Since electrospun nanofiber structures are too subtle to provide the mechanical support for scaffolds, a number of studies have been made towards a stiff microstructure so as to overcome the inherent delicacy and two-dimensional limitation of nanofibers [64, 71-73]. To this end, 3D roll-type nanofiber scaffolds are demonstrated here by incorporating a core microfiber structure by polymer melt extrusion. Figure 3-7A shows the relation of the extruded microfiber radius versus the velocity of needle movement at two different applied air pressures. These results imply that the dimension of core structure could be adjusted as shown in Figure 3-7B and C, allowing for a simple route to controlling the final size of rolled scaffold. The dimensional variation could be further tailored by adopting different sizes of micro needles. As mentioned earlier, the microfiber structure was aimed to facilitate the rolling-up process; it was used to pack the planar nanofiber film around the core microfiber as shown in Figure 3-8A and B. For the basement substrate, a thin film made from 10 wt% solution yielding a thickness less than 10 μm was used for its enough flexibility to be

rolled up.

The rolling-based manipulation was even possible after culturing cells on the nanofiber film. As the region of cell-nanofiber construct on the film could be intact in the course of careful handling of microfiber, the cell structures on the nanofiber scaffold were not damaged during the rolling procedure as shown in Figure 3-9. Also, the nanofiber-induced cell alignments in both cases of 3 and 12 transfer scaffolds were not impaired (Fig. 3-9(C-F)). The mechanical properties of constituent components, such as nanofiber and micro thin film, were fairly compliable and flexible enough to retain their assembly. It is worthwhile nothing that the ability to embed cells in a rolled 3D scaffold would be beneficial when it is needed to retain the final shape of scaffolds after completing cell culture. If the cell culture is carried out on a 3D shape scaffold by simple top-seeding method, one would encounter various problems such as difficulties of cell penetration and nutrient/waste exchange. In future studies, more detailed cell experiments with handling the sheet scaffolds will be performed to determine the potential biofunctional significance based on the aforementioned issues of mass transfer through scaffold.

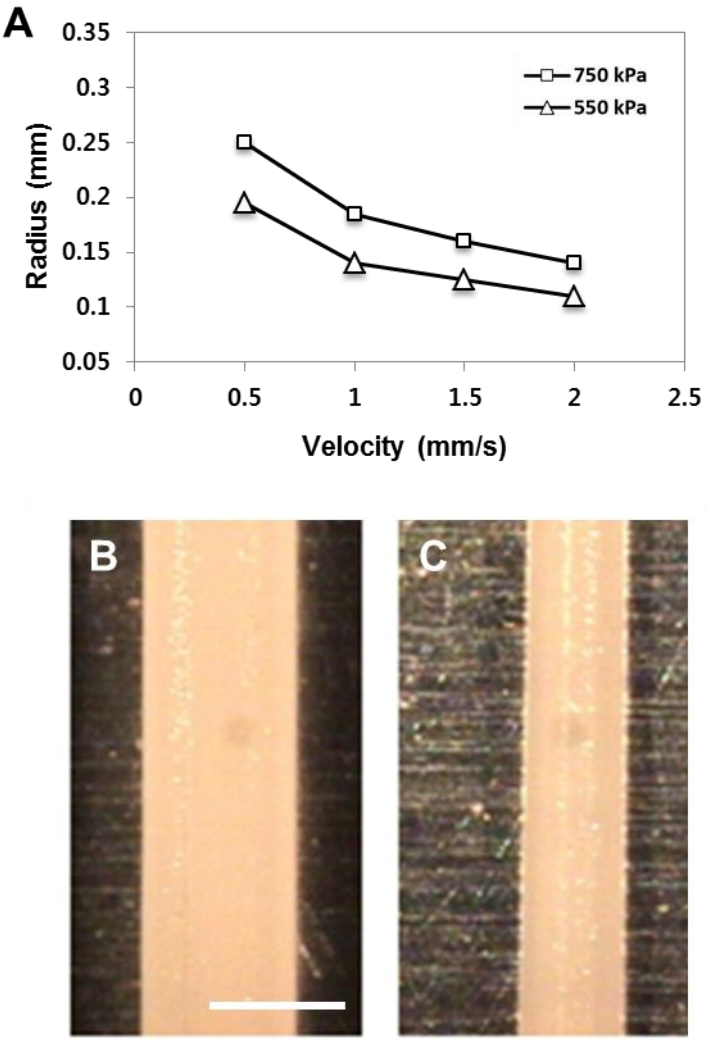

Figure 3-7. Results of thermally extruded microfibers. (A) Plots of microfiber radius vs. needle movement velocity at different applied pressures of 550 and 750 kPa. Optical microscopy images of microfibers fabricated by needle movement of (B) 0.5 and (C) 1.5 mm/sec at an air pressure of 750 kPa. The scale bar indicates 500 μm.

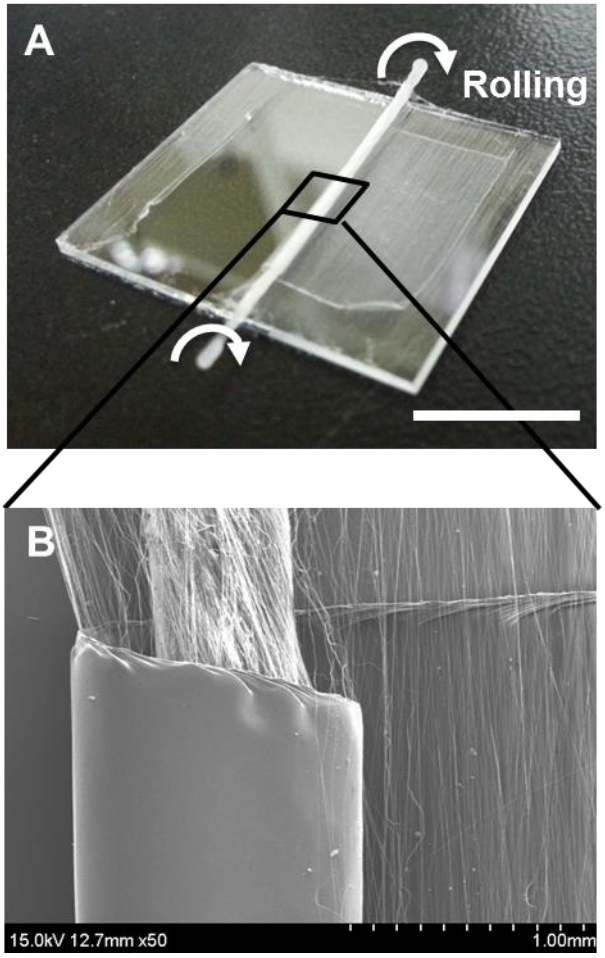

Figure 3-8. Photograph of rolling process and (E) SEM image of the resulting roll scaffold. The scale bar indicates 10 mm.

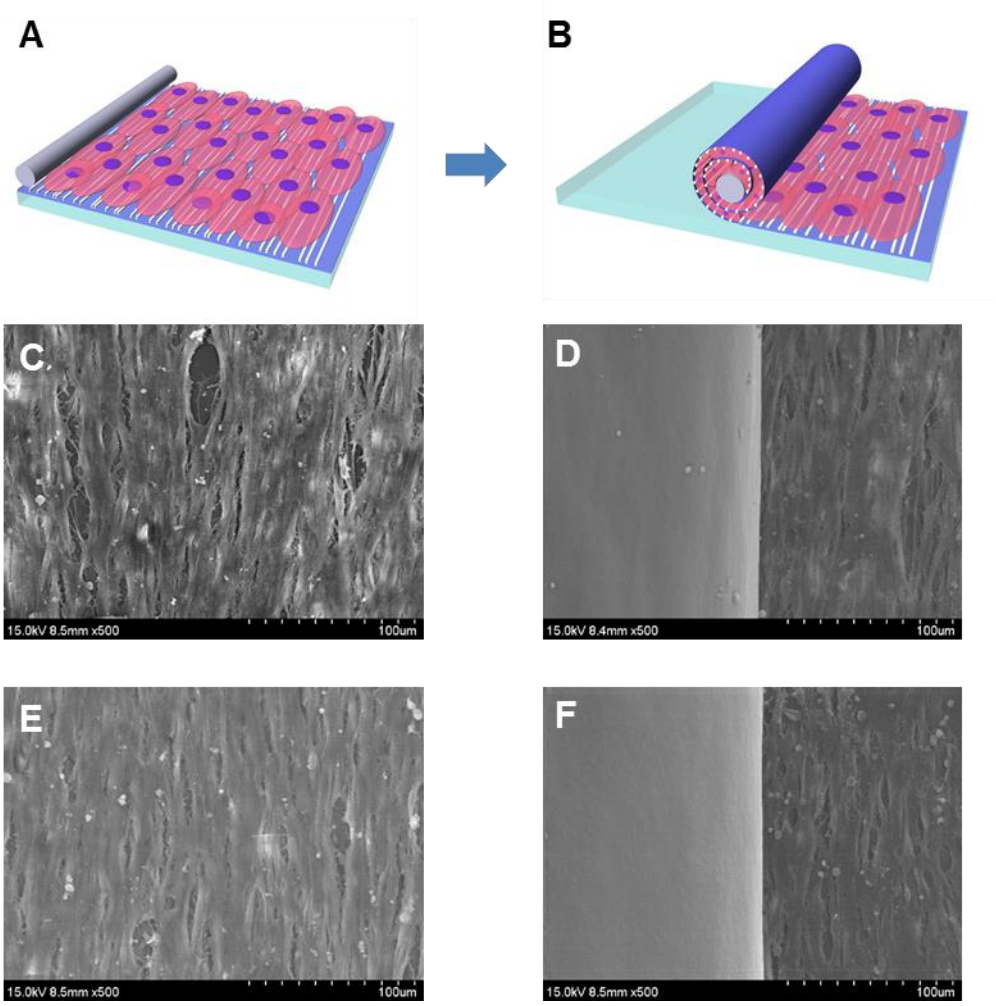

Figure 3-9. (A, B) Schematic diagrams of rolling process with embedding cells on nanofiber film scaffold. SEM images of the cultured cells (C, E) before and (E, F) after the rolling process. (C, D) 3 transfers and (E, F) 12 transfers of nanofibers were respectively performed on the scaffold for cell culture.

3.4. Summary

The present study has introduced our initial effort to utilize nanofiber scaffold in practical ways via some physical manipulation such as nanofiber alignment or scaffold rolling. Spin-coated PCL films with varied thicknesses enabled nanofiber manipulation for the development of sheet-type scaffolds. The film thickness could be modulated by adjusting solution concentration rather than spinning speed because of the highly volatile property of chloroform used as the solvent. Well-aligned nanofibers were transferred onto the film with multiple times ($\leq$ 12), which have proven effective to provide contact guidance cues on cultured cells. As expected, the presence of nanofibers yielded morphological changes of myoblasts into aligned and elongated shapes. In addition to sheet-type scaffolds, we developed rod-shaped roll constructs by exploiting the mechanical support of thermally extruded microfiber and the flexibility of nanofiber-film complex. The rolling process could be carried out without any appreciable damage to cultured cells. These results collectively suggest that the hybrid fabrication method presented here has the potential to overcome various obstacles involved in practical uses of the nanofibrous scaffold in clinical settings or other tissue engineering applications.

Chapter 4. Aligned nanofibrous membrane as a versatile tool for cell sheet manipulation and cell-dense 3D engineered tissue formation

4.1. Introduction

Current tissue engineering technology has matured with two major techniques, namely, the application of premade porous scaffolds seeded with or without cells [74, 75] and the direct transplantation of cells with hydrogels [76]. The former, namely scaffold-based strategy, possesses great advantages for regulation of cellular activity amechanical support by virtue of the scaffold micro- and macro- architecture. Although a number of biomaterials and processing techniques have been successful for a lot of clinical trials, they still have concerns for inflammatory responses caused by physiological and mechanical mismatch of the implanted scaffold material with host diseased area.

As another approach to the cell-based regenerative therapy, cell sheet engineering with no use of scaffold, or at least, has attracted much attention. The cell sheet engineering aims to harvest confluently cultured cells in an intact sheet-like form

without any damage of cell-cell attachment. The thermoresponsive culture surface, representatively poly-N-ispropylacrylamide (PNIPAAm), has been exploited for dissociation of the cell sheet which is a core procedure in the cell sheet engineering [77]. PNIPAAm becomes switchable between hydrophilic and hydrophobic surface at a critical temperature of 32℃, thus the cell attachment and detachment from culture substrate can be modulated by simple temperature changes. In contrast to enzymatic digestion as a usual method for cell dissociation, the cell sheet detachment using thermoresponsive polymer substrate allows to preserve not only the cell-to-cell junction but also the extracellular matrix (ECM) underlying the cell sheet. Taking advantage of this characteristic, PNIPAAm surfaces have been developed in a variety of forms, including silicon, tiissue culture polystyrene (TCPS), and polydimethylsiloxane (PDMS) [78-80]. Although the cell sheet techniques have been successful for various tissue engineering applications, the inherent mechanical instability and delicacy of cell sheets still make it difficult to manipulate them for practical transplantation. Furthermore, the preparation of such thermoresponsive surface could require labor-consuming tasks and cautious optimization of the processing parameters.

Some of native tissues, such as skeletal muscle tissue, have a unidirectional alignment in their anatomic microstructures. As the anisotropic organization of cell or ECM determines the physiological functions of tissues, it is extremely important to realize the biomimetic anisotropy in the cell sheets. Recently, a growing number of patterning techniques based on the thermoresponsive polymer have been introduced to produce the cell alignment in the cell sheets. For instance, Lin et al. presented a PNIPAAm-grafted surface based on microtextured PDMS substrate using traditional soft lithography [80]. Takahashi et al. showed a PNIPAAm stripe micropattern utilizing site-specific grafting method with hydrophilic polymer that has a repellent property for cell adhesion [81]. In those works, they discussed the shrinkage of detached cell sheets. The stresses on the aligned cell sheet caused more shrinkage along the direction of pattern alignment. It naturally follows the need for a mechanical support frame to prevent the uneven shrinkage in the cell sheets.

Here we introduce a simple method to build and manipulate cell sheets utilizing electrospun nanofibrous membrane as a tool. The nanofibers were integrated with a PDMS assembly involving a well for cell culture. After myoblasts were cultured to a

confluent state and formed a sheet-like structure, the cell sheet could be detached without any damage and contraction of the sheet structure by lifting off the nanofiber sieve. We demonstrated the feasibility of this dissociation method by immunofluorescent microscopic visualization of the cell morphology and the live/dead cell assay. Furthermore, it was observed that the nanofiber configuration optimized by control of fiber density could strengthen the structural stability of cell sheet and the nanofiber-guided cell orientation. Finally, we verified that even ordinary PDMS surface provided the same availability for base substrate of cell dissociation as PNIPAAm-grafted surface. These characteristics reported in this article would be appropriate for creating more effective and practical applications to cell sheet based tissue engineering.

4.2. Materials and methods

4.2.1. Fabrication of aligned nanofibrous membrane

Figure 4-1A illustrates the overall procedures to fabricate the device for cell sheet formation and manipulation. The device was comprised of a set of nanofiber array and two PDMS blocks involving a cell culture well in the upper block. The silicon resin and the curing agent (Sylgard 184 PDMS kit, Dow Corning, Midland, MI) were mixed at 10:1 weight ratio. A certain quantity of the PDMS prepolymer mixture was poured over petri dish to obtain approximately 2 mm and 5 mm thick slabs, which were used as base substrate and well barrier respectively. After curing at 70℃ for 1 h, the PDMS slabs were peeled off from the dishes and cut into square-shape blocks with a sharp blade. Hole was punched through the each 5 mm thick block for forming the cell culture well.

Polycaprolactone (PCL, average MW 80000, Sigma) was employed as the electrospun nanofiber material. Base solvent was prepared by mixing chloroform (Sigma) and N,N-dimethyformamide (DMF, Sigma) at a volume ratio of 75/25. The PCL granules were dissolved into the base solvent at a concentration of 20 wt%. The PCL solution was electrospun from the system consisting of a 23-gauge needle, a high-voltage power

supply and a syringe pump. The applied voltage and the infusion rate were 15 kV and 1.5 ml/h respectively. We previously reported on the fabrication process to build a well-aligned nanofiber array [64]. Using two separate metal strips arranged perpendicularly, we could obtain well-oriented nanofibers across the strip gap and transfer the nanofibers onto any kind of substrate. The more detailed information about the collecting mechanisms is described in our previous works [64, 70]. In order to crop the well aligned nanofiber, we used the developed electrospinning method and fixed the spinning time at 1 min. The nanofibers were transferred onto a surface of the punched PDMS block prepared in advance. Prior to the nanofiber transfer, the PDMS block surface was treated with oxygen plasma for 1 min (0 W, PDC-32G, Harrick Scientific) to enhance the charge-induced adhesion with positively charged nanofibers. The nanofiber sieves with quantitatively controlled fiber densities were fabricated by varying the number of transfers from 1, 3 to 6.

4.2.2. Characterization of aligned nanofibrous membrane

To investigate fiber diameter and orientation of fabricated nanofibrous membranes, samples were observed with scanning electron microscope (SEM, S-48000, Hitachi) and analyzed using ImageJ software. For measurement of membrane thickness, images of the samples were obtained using atomic force microscope (AFM, Park systems) and analyzed using XEI software (Park systems).

4.2.3. Cell culture

Murine skeletal muscle cell line (C2C12), mouse embryo fibroblast cell line (NIH-3T3) and human foreskin fibroblast cell line (HS68) were purchased from American Type Culture Collection (ATCC). Human umbilical vein endothelial cells (HUVECs) were purchased from Lonza. The cells except for HUVECs were maintained with Dulbecco's modified eagle medium (DMEM, Gibco) supplemented with 10 % fetal bovine serum (FBS, Hyclone) and 1 % penicillin-streptomycin (PS, Hyclone) (growth medium, GM) and HUVECs were maintained with EBM-2 medium supplemented with EGM-2 bullet kit (endothelial growth medium, EGM, Lonza).

To induce myogenic differentiation, the cultured C2C12 cells were shifted to DMEM supplemented with 2 % donor equine serum (Hyclone) and 1 % PS (differentiation medium, DM) cultured for 7 days with changing DM every other day.

4.2.4. Manipulation and layer-by-layer stacking of detached cell sheets

Nanofibrous membrane and base PDMS substrate assemblies were treated with oxygen plasma for 1 min to enhance surface hydrophilicity and sterilized with UV light for 2 h. Sequentially, the samples were treated with poly-D-lysine solution for enhancing initial cell adhesion and washed with 1X phosphate buffered saline (PBS, Hyclone) for 2 times. After washing steps, cells were seeded at a density of 1×10^5 cells/cm^2 for C2C12 cells and 5×10^5 cells/cm^2 for other cells. After the cells reached confluent state, nanofibrous membrane with cell sheet, upper part of assemblies, was carefully detached from base PDMS substrate using sharp tweezers and transferred to cell culture dish.

Layer by layer stacking procedures were schematically described in figure 4-1B. Because aligned nanofibers maintained their morphology by applied tension, removal of tension by cutting or detaching from structural frame resulted in loss of nanofiber

alignment. In conjunction with nanofibers, detached cell sheets on nanofibrous membranes lost their morphology when detached from structural frame. Thus structural frame was essential for stable manipulation of detached cell sheet during layer-by-layer stacking procedures. Punched PDMS frame, however, was not adaptable for stacking process due to its low mechanical property and difficulty of precise fabrication. Thus, we used three types of laser-cutted acrylic frame instead of punched PDMS frame used in above (i. e. 23 × 23 mm^2 with 20 × 20 mm^2 through hole, 26 × 26 mm^2 with 23 × 23 mm^2 through hole and 29 × 29 mm^2 with 26 × 26 mm^2 through hole). All of other parameters except for frame were identical. Layer-by-layer staking of detached cell sheet was accomplished by assembling smaller frame with cell sheet to bigger one.

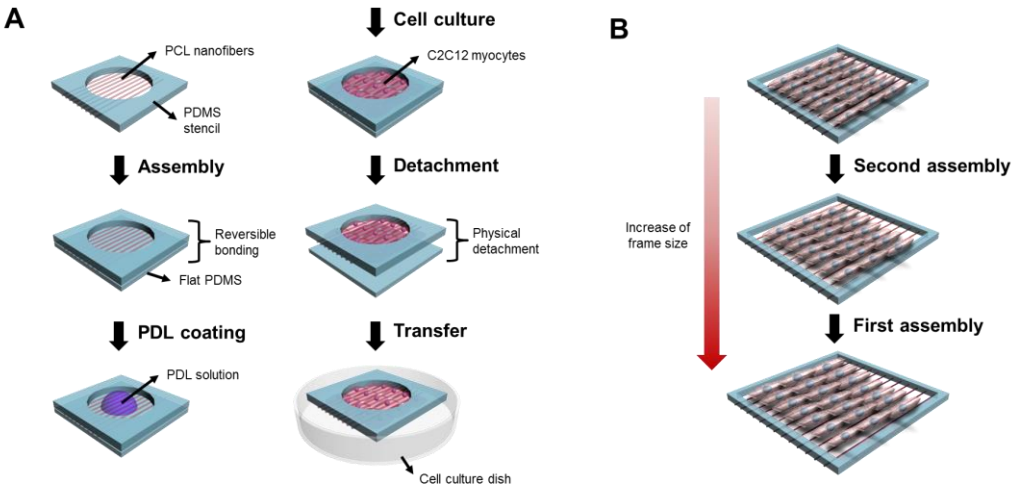

Figure 4-1. Schematic diagrams of (A) cell sheet detachment and manipulation using nanofibrous membranes and (B) layer-by-layer stacking of detached cell sheets to form 3D engineered tissue *in vitro*.

4.2.5. Tube formation assay

Growth factor reduced basement membrane matrix (Matrigel) was purchased from BD Biosciences. A small amount of Matrigel was dropped on prechilled glass coverslip with PDMS reservoir and then carefully covered with detached endothelial cell sheet. Consequently, same amount of Matrigel was dropped on the cell sheet and incubated to induce gelation for 30 min. After gelation, the samples were immersed with EGM and cultured for 5 days.

4.2.6. Immunostaining

For immunostaining, cultured cells at appropriate time point were washed with PBS for 3 times and fixed with chilly 4 % paraformaldehyde solution for 15 min at room temperature. Fixed cells were permeabilized with 0.2 % Triton-X solution (Sigma) for 15 min and blocked with blocking solution containing 3 % bovine serum albumin (BSA, Sigma) in PBS to prevent non-specific binding of antibodies for 1 h. Then, the samples were immersed in antibody solutions and incubated for 1 h. Antibodies used in this study are phalloidin-TRITC (1:500, Sigma) for f-actin, 4',6-diamidino-2-phenylindole (DAPI,

1:1000, Sigma) for nucleus, anti-arcomeric α-actinin produced in mouse (1:500, Sigma) as a primary antibody for myotube, anti-mouse IgG conjugated with Alexa 488 produced in goat (1:500, Invitrogen), anti-mouse IgG conjugated with Cy3 produced in goat (1:500, Molecular Probes) as a secondary antibody for myotube, and Alexa 488 anti-human CD31 antibody conjugated with Alexa 488 (1:200, clone WM59, BioLegend) for platelet endothelial cell adhesion molecule-1 (PECAM-1). Immunofluorescent images were taken using FluoView FV1000 confocal laser scanning unit with the IX81 inverted microscope (Olympus) and EVOS® FL (Life technologies) fluorescent microscope. To get 3D reconstructed images of fabricated engineered tissues, IMARIS software (Bitplane) was used.

4.2.7. Quantitative and statistical analysis of the cells

The quantification analysis presented in this study such as cellular orientation, nucleus elongation, number of myotubes and maturation index were analyzed with ImageJ software. For statistical analysis, Kruskal-Wallis one-way ANOVA on rank test for comparison of more than three groups were performed using Sigmaplot software.

4.3. Results and discussion

4.3.1. Fabrication and analysis of aligned nanofibrous membrane

To mimic extracellular matrix environment surrounding muscle cells, polycaprolactone (PCL), one of biodegradable polymers was selected due to its properties of electrospinning suitability and functional modification [82-84]. To fabricate aligned nanofibers, electrospinning based on inclined gap method which enabled transfer of nanofibers for nanofiber density control was used. In general, the longer spinning time in the electrospinning process, the more increased nanofibers can be collected. However, loss in nanofiber alignment was observed at longer collection time. Thus, we controlled the density of collected nanofibers by repetitive transfer at a fixed spinning time of 1 min.

As shown in figure 4-2A, electrospun nanofibers showed ~ 750 nm in diameter and increased fiber density (number of nanofibers perpendicular to alignment axis) as repeating transfers. A single transfer of nanofibers served the fiber density of 32 fibers/mm in average. The number of transfer times was increased up to 3 and 6, the higher line densities were followed respectively to 79 and 173 fibers/mm in average. In addition, distributions of nanofiber orientation shown in figure 4-2B suggest that all of

nanofibers were within 25 ˚ to the alignment axis regardless of the number of transfer.

To investigate thickness of fabricated nanofibrous membranes with various nanofiber densities (TR #1, #3 and #6), samples were analyzed by atomic force microscope. Through 3D profiles and cross-sectional profiles of the samples shown in figure 4-3, thickness of nanofibrous membrane was ~ 750 nm at single nanofibers and ~ 1.5 μm at points where two nanofibers were overlapped, which is summed value of diameters of two nanofibers. Points which were overlapped more than three nanofibers were barely observed in low magnification optical images.

In addition, porosity and distance between nanofibers of nanofibrous membranes were analyzed due to demonstration of their potentials as a tool which could serve enough spaces for cellular infiltration. Nanofibrous membranes showed very high porosity of 95.250, 88.229 and 76.214 % for TR #1, #3 and #6 respectively (figure 4-4A). Distance between nanofibers distributed in a wide range from 0 μm to several hundreds μm and showed average distance of 26.836, 9.684 and 6.465 μm, which values were smaller than average diameter of the cells except for TR #1 (figure 4-4B). However, cellular infiltration seemed to be possible because there were many points wider than diameter of

the cells overdue to their wide distribution.

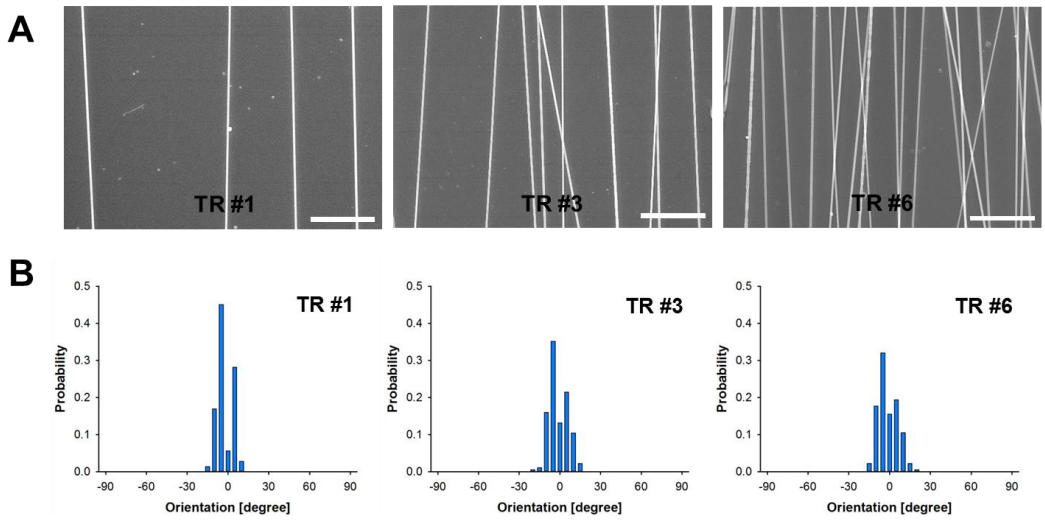

Figure 4-2. (A) Representative SEM images of nanofibrous membranes with various number of transfers (1, 3 and 6 times). (B) Distributions of nanofiber orientation of each nanofibrous membranes (n = 142, 182 and 181 for TR #1, #3 and #6 respectively). The scale bar indicates 25 μm.

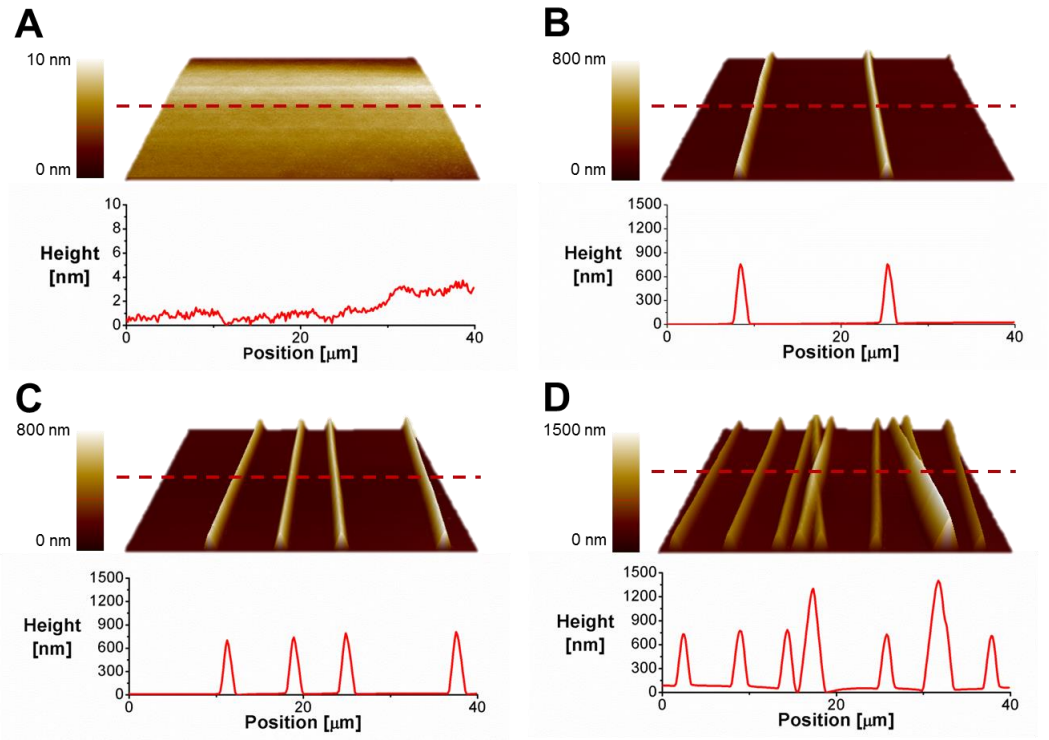

Figure 4-3. Representative atomic force microscope images and cross-sectional profiles of (A) flat, (B) TR #1, (C) TR #3 and (D) TR #6. Thickness of nanofibrous membranes was ~ 750 nm which was identical value of single nanofiber except for overlapped points of 2 nanofibers. Overlapped points of more than 3 nanofibers were barely observed.

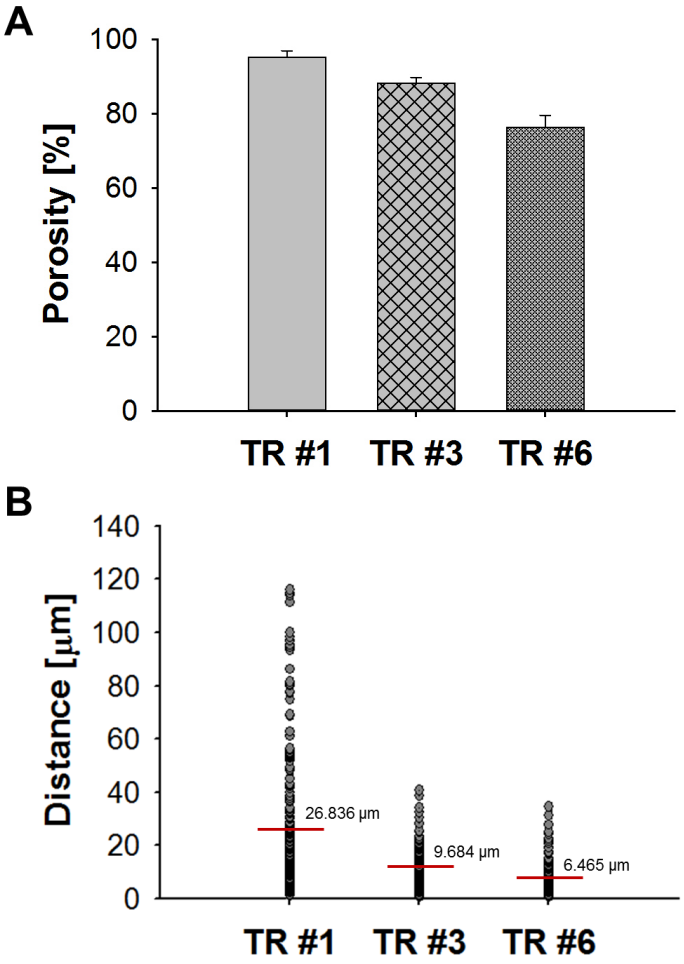

Figure 4-4. (A) Porosity and (B) distribution of distance between nanofibers. 5 samples for each case were analyzed for porosity analysis and total 200 points of 5 samples for each case were measured for distance analysis.

4.3.2. Detachment of various types of cell sheet

Though PDMS has widely used in biological researches due to its biocompatibility, additional chemical/ECM protein treatment is required to compensate its poor cell adhesion property. In accordance with previous researches, we observed that confluent C2C12 cell layer on PDMS substrate was easily delaminated from the surface as a sheet when slight deformation was applied to the substrate (figure 4-5). Inspired from this finding, we hypothesized that there may be minimal nanofiber density which enables stable manipulation of detached cell sheet with maintenance of induced cellular morphology. To verify our hypothesis, we cultured various types of cells including myoblasts, fibroblasts and endothelial cells on nanofibrous membranes with different densities and detached when they formed confluent cell sheet. Entire procedures of cell sheet detachment and manipulation is illustrated in figure 4-1A.

As shown in figure 4-6A, all of cell types cultured on TR #6 were successfully detached as a sheet without notable defects. In addition, fluorescent images of transferred cell sheets except for HUVECs sustained their aligned morphology as before detachment (figure 4-6B). In case of HUVECs, the cells seemed to be aligned along nanofibers just

after cell seeding, however, morphology of the cells was gradually changed to polygonal shape as the cells reached confluent state. Thus transferred endothelial cell sheet also showed polygonal cell shape as before detachment (figure 4-6B).

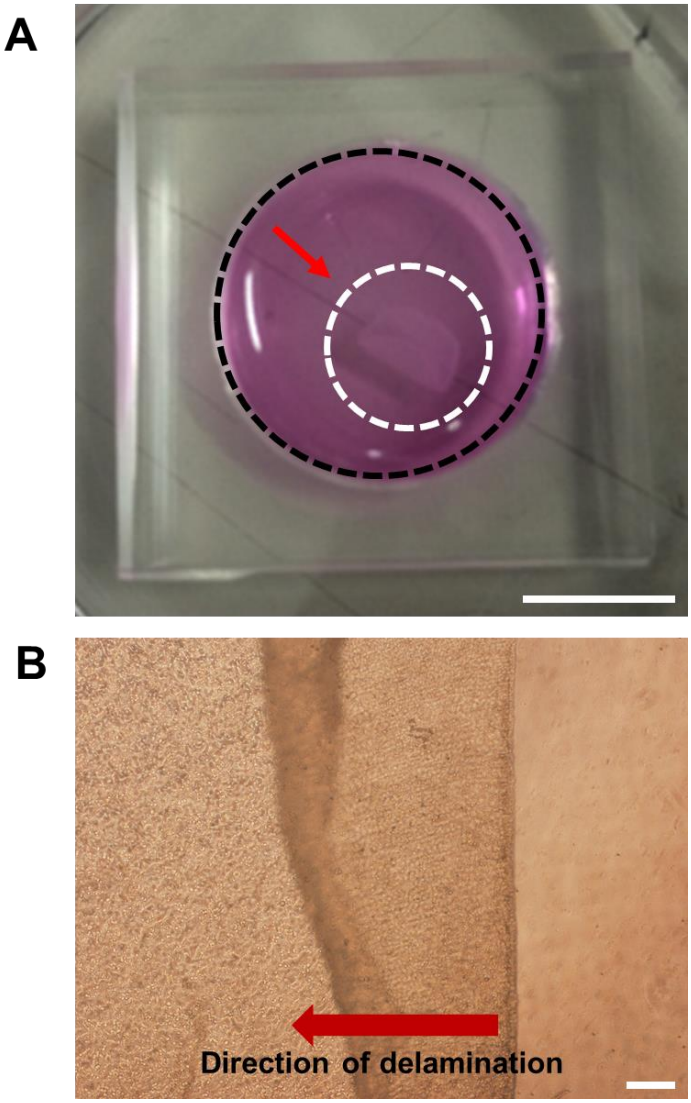

Figure 4-5. (A) Photograph of delaminated C2C12 cell sheet cultured on PDMS substrate. Significantly reduction in size was observed due to loss of cellular morphology after delamination. (B) Microscopic images of cell sheet during delamination.

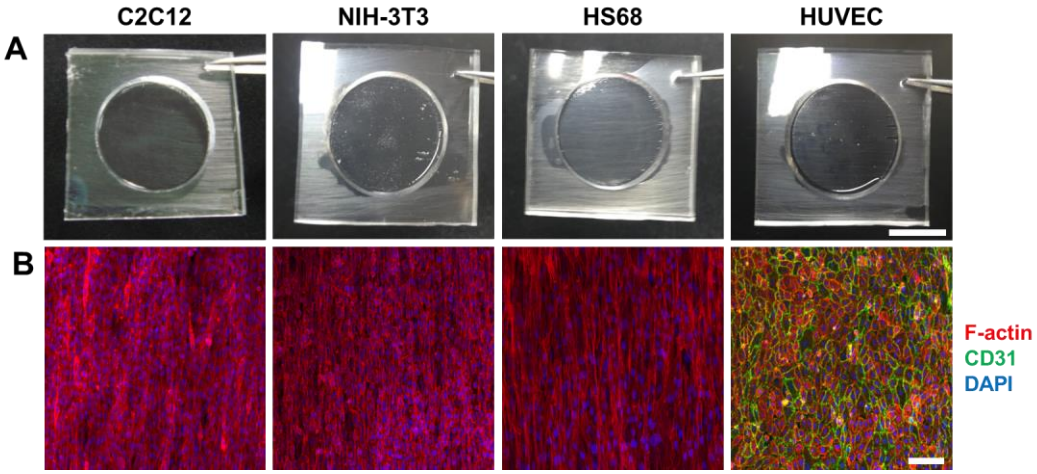

Figure 4-6. (A) Photographs of detached various cell sheets using TR #6 nanofibrous membrane. (B) immunofluorescent images of transferred cell sheets for f-actin cytoskeleton, endothelial cell-specific CD31 and DAPI. Morphologies of the cells were preserved after transfer. The scale bars indicate 1 cm for A and 100 μm for B.

4.3.3. Formation of 3D engineered muscle tissue

4.3.3.1. Effect of nanofiber density on morphological change of C2C12 cells

To investigate effects on cellular orientation and elongation according to various nanofiber densities, we cultured C2C12 myoblasts on various densities of nanofibers and analyzed cellular orientation and nucleus elongation from immunofluorescent images.

Figure 4-7 shows representative fluorescent images for the cells cultured on bare PDMS substrate for control and nanofibrous membrane with various densities. The cells on bare PDMS substrate showed randomly oriented and round morphology. In contrast, the cells on relatively high fiber densities (TR #3 and TR #6) showed highly aligned and elongated morphology with well-developed actin stress fiber along nanofiber direction but the cells on relatively low fiber density (TR #1) showed intermediate state between control and high fiber densities. To verify these findings, we analyzed distributions of cellular orientation for all cases and plotted in figure 4-8A together. As expected, the cells showed increased alignment ratio (number of highly aligned cells within ± 20˚ / total cell number) of 0.361, 0.469, 0.777 and 0.890 for control, TR #1, TR #3 and TR #6 respectively.

Similarly, nuclei of the cells showed more elongated shape and increased average nucleus aspect ratio (length of long axis/length of short axis) of 1.520, 1.533, 1.976 and 2.057 for control, TR #1, TR #3 and TR #6 respectively (figure 4-8B). Notable finding was that there were statistical significances of nucleus elongation between control group and relatively high nanofiber density groups (TR #3 and TR #6), whereas no statistical significance was observed between control group and TR #1 group. These results indicate that there is minimal fiber density for inducing sufficient nucleus elongation for mechanical regulation of cellular functions [85].

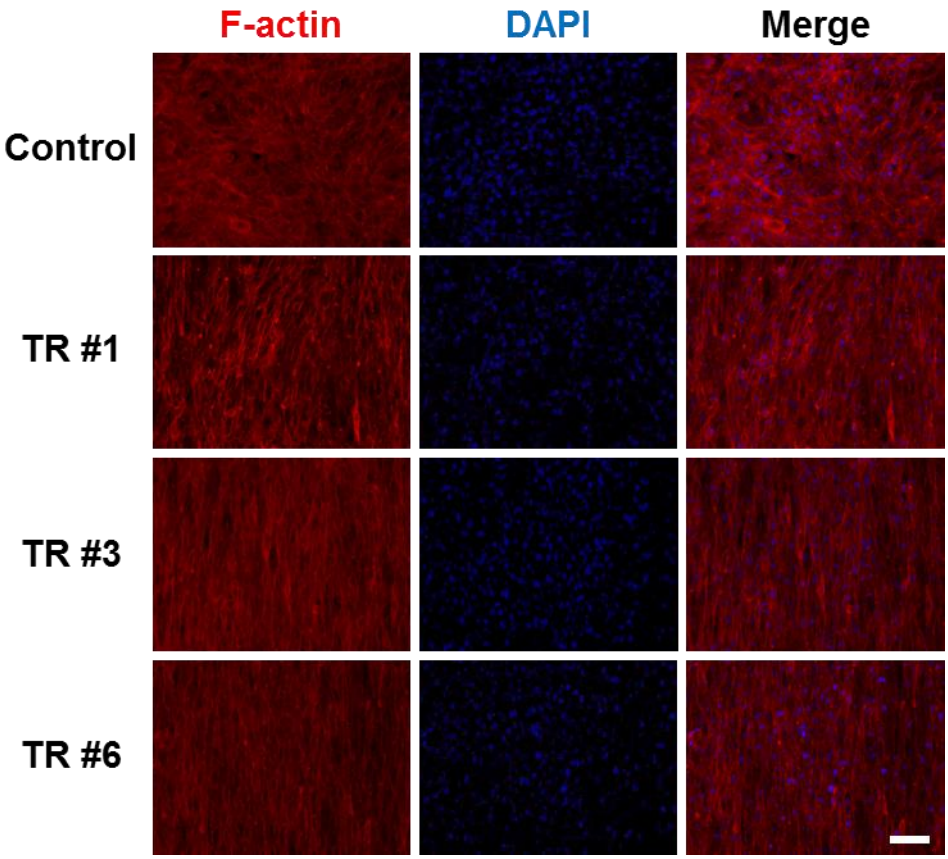

Figure 4-7. Representative immunofluorescent images of f-actin cytoskeleton and nucleus for identification of cellular alignment. As increasing of number of transfers, well-developed actin stress fibers along nanofibers were observed. The scale bar indicates 100 μm.

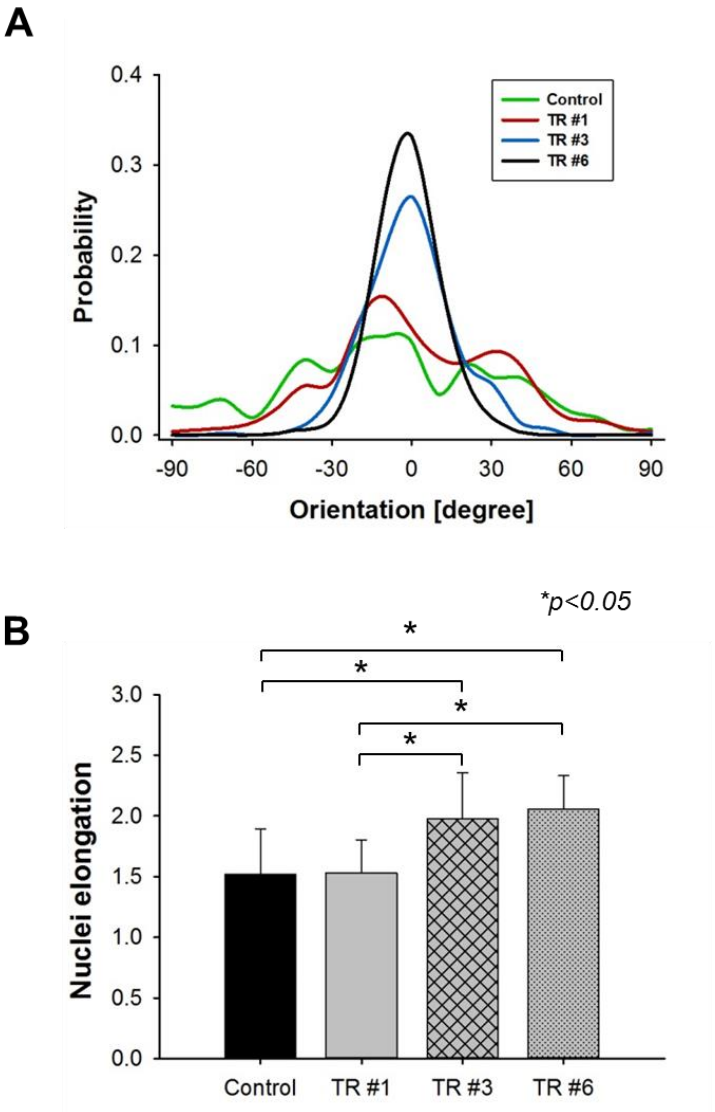

Figure 4-8. Results of (A) cellular orientation and (B) nucleus elongation analysis (n = 200). Enhanced cellular alignment and nucleus elongation were observed as increasing nanofiber density. For comparison of nucleus elongation between groups, Kruskal-Wallis one-way ANOVA on rank test was performed. Asterisk indicates *p < 0.05.

4.3.3.2. Effect of nanofiber density on myogenic differentiation

Structural feature of native skeletal muscle tissue is a densely packed bundle of uniaxially aligned multinucleate myotubes which play a role in generating uniaxial contractile force. Thus, uniaxial alignment and formation of large numbers of myotubes in unit area are key issues in muscle tissue engineering. To investigate effect of nanofibrous membrane with various nanofiber densities on myogenic differentiation, we carried out immunostaining for identifying myotube sturcture, quantification of myotube orientation for determining degree of alignment and quantification of number of myotubes in unit area and maturation index for determining degree of differentiation.

Figure 4-9 shows representative images of myotubes on various densities of nanofibrous membrane. Similar to alignment tendency of myoblasts, increased alignment tendency was observed as increasing nanofiber density. Alignment ratio of the myotubes was 0.199, 0.778, 1 and 1 for control, TR #1, TR #3 and TR #6 respectively (figure 4-10). Namely, all of the myotubes on intermediate and high nanofiber density were within 20 ˚ with respect to axis of nanofiber alignment.

Average number of myotubes per mm^2 was 83.4, 120.6, 115.6 and 104.8 and

average maturation index (number of myotubes with more than 5 nuclei/total number of myotubes) was 0.775, 0.659, 0.818 and 0.810 for control, TR #1, TR #3 and TR #6 respectively (figure 4-11A and B). Taken together, cellular fusion of the cells on control occurred in not only longitudinal but also horizontal direction which resulted in thick but less myotube formation. In contrast, long but relatively thin myotubes along nanofibers were observed on TR #3 and TR #6, which indicated that longitudinal cellular fusion was dominantly occurred.

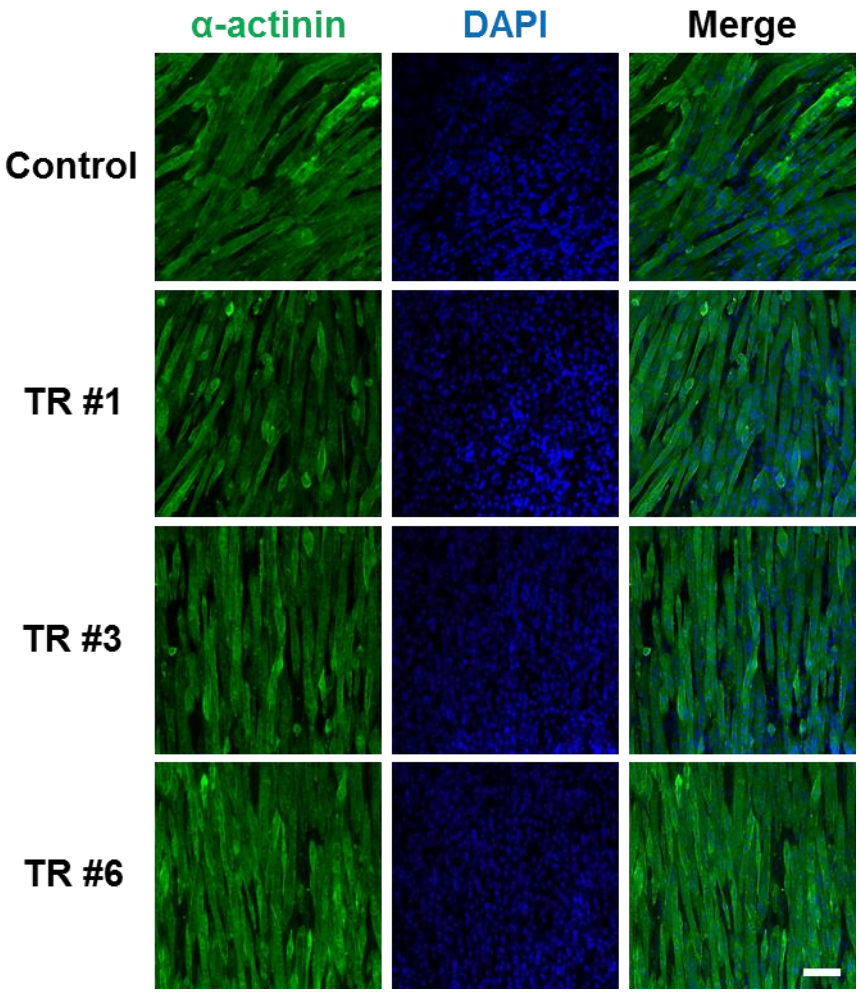

Figure 4-9. Representative immunofluorescent images of differentiated myotubes on nanofibrous membranes with various nanofiber densities. Well-developed multinucleated myotubes along nanofiber direction was observed on TR #3 and #6. The scale bar indicates 100 μm.

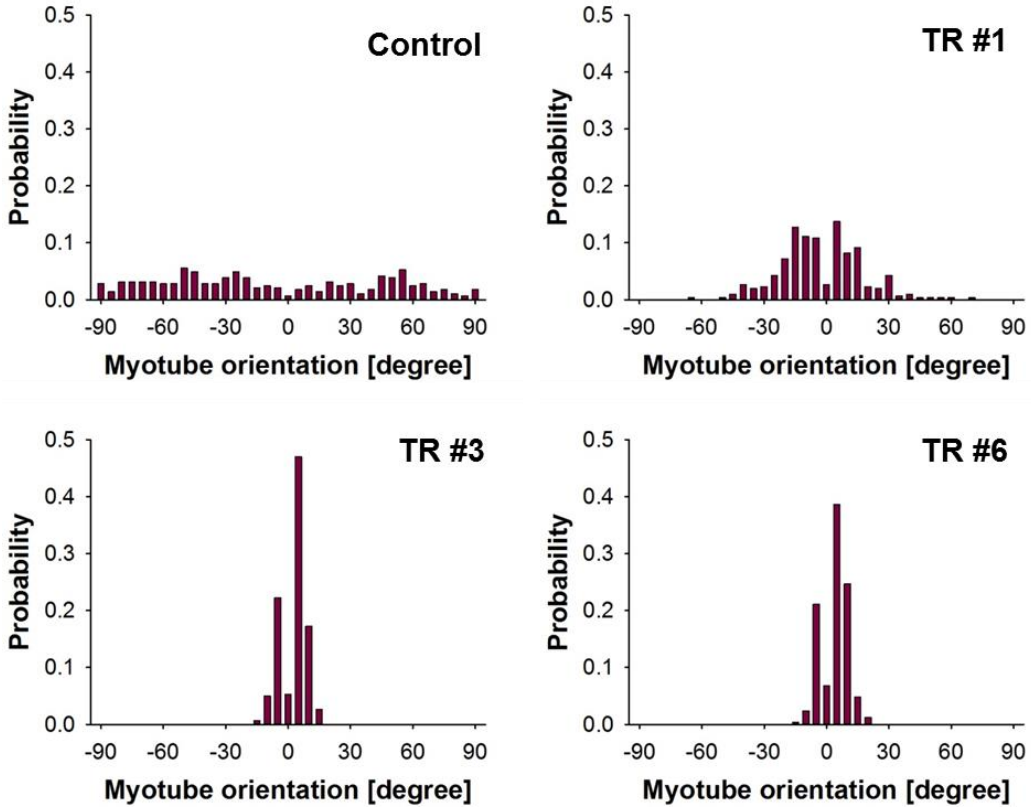

Figure 4-10. Distributions of myotube orientations on nanofibrous membranes with various nanofiber densities.

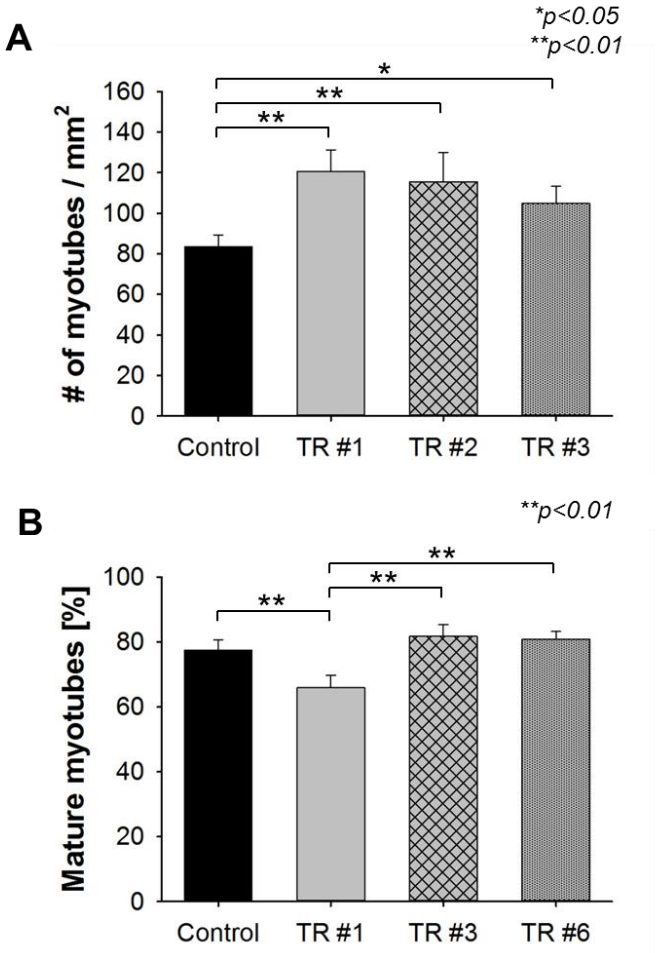

Figure 4-11. Quantitative analysis of (A) number of myotubes in unit area and (B) ratio of mature myotubes with more than 5 nuclei for investigating degree of differentiation. . For comparison of groups, Kruskal-Wallis one-way ANOVA on rank test was performed. Asterisks indicate *p < 0.05 and **p < 0.01.

4.3.3.3. Formation of 3D engineered muscle tissue by LBL stacking

As shown in figure 4-12A, detached cell sheets on the membrane with low and intermediate nanofiber density (TR #1 and TR #3) were fractured during or after detachment. In contrast, detached cell sheets on the membrane with high nanofiber density (TR #6) were stably maintained sheet form with high viability (figure 4-12B). Success rates of cell sheet detachment were 0 %, 15 % and 100 % in 20 trials for TR #1, TR #3 and TR #6 respectively. This result indicated that nanofiber density of TR #6 (173 fibers/mm) was minimal density for stable cell sheet detachment and manipulation.

To investigate whether cellular morphology and nucleus elongation maintained after transfer, detached cell sheets were transferred to cell culture dish and stabilized for 2 h then analyzed. From representative fluorescent images of transferred cell sheets shown in figure 4-12B and C, aligned actin stress fibers and elongated nucleus were clearly observed with high viability. In addition, there was no significant difference between distribution of cell orientation at before and after transfer (figure 4-13A). Nucleus elongation was slightly decreased from 2.057 to 1.909 after transfer. It might be local recovery of nucleus elongation at nanofiber-free area (figure 4-13B). However, decreased

value of nucleus elongation after transfer showed no statistical significance compared with value of nucleus elongation on TR #3. This result indicated that mechanical stimulus exerted on the cells is sustained in similar degree with TR #3.

Using detached cell sheets as building blocks, 3D engineered tissues were successfully fabricated by layer-by-layer stacking. As mentioned above, stacking process was achieved by assembling cell sheet with smaller frame to cell sheet with bigger frame. Three dimensional engineered tissues with two and three layers of cell sheets stacked in parallel and perpendicular manners were shown in figure 4-14 and 4-15. Each cell sheet in engineered tissue shows sustained cellular morphology as before detachment. Resulting thicknesses were ~ 10 um and ~ 15 um for two and three layers respectively.

To fabricate functional engineered muscle tissue, samples with two layers of myocytes were differentiated for 7 days. Similar with the result of myogenic differentiation in 2D, longitudinally well-developed myotubes along nanofibers were observed through entire 3D engineered tissue (figure 4-16 and 4-17).

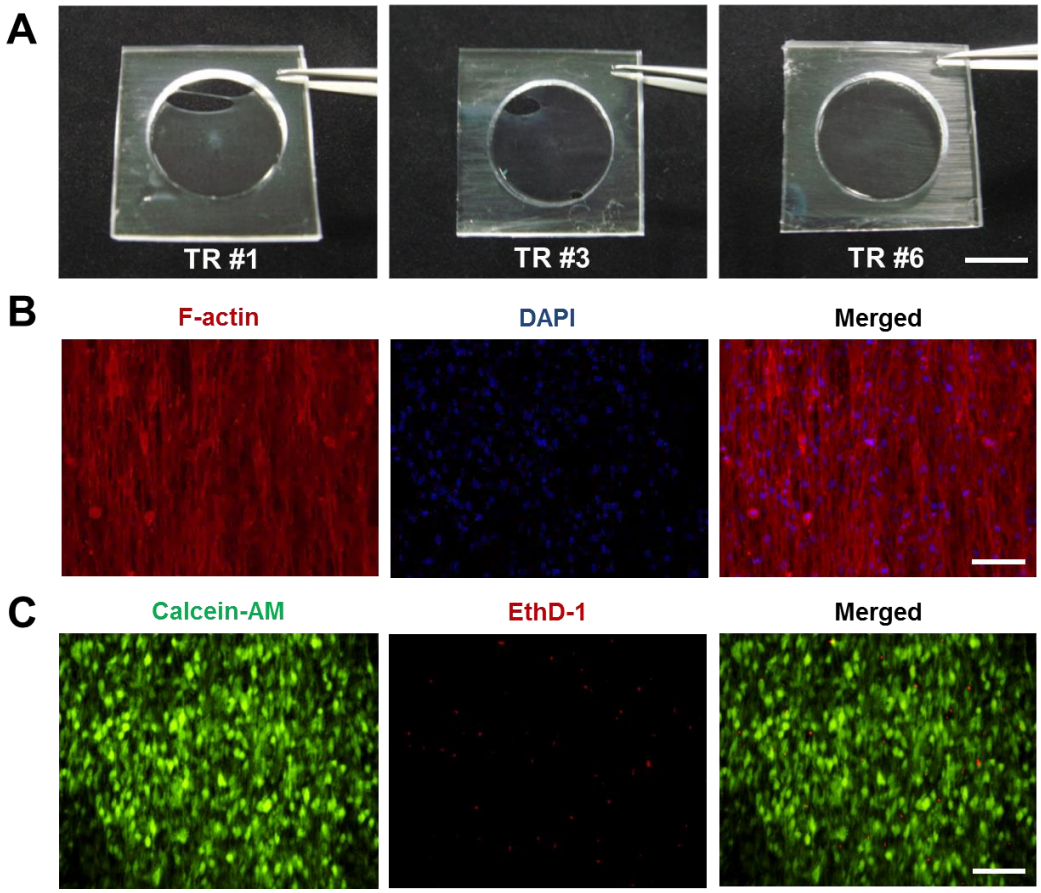

Figure 4-12. (A) Photographs of detached cell sheets using various nanofibrous membranes. Only cell sheet on TR #6 successfully detached from base PDMS substrate. Notable morphological changes and damages were not observed through (B) immunofluorescent images of f-actin cytoskeleton and viability test. The scale bars indicate 1 cm for A and 100 μm for B and C.

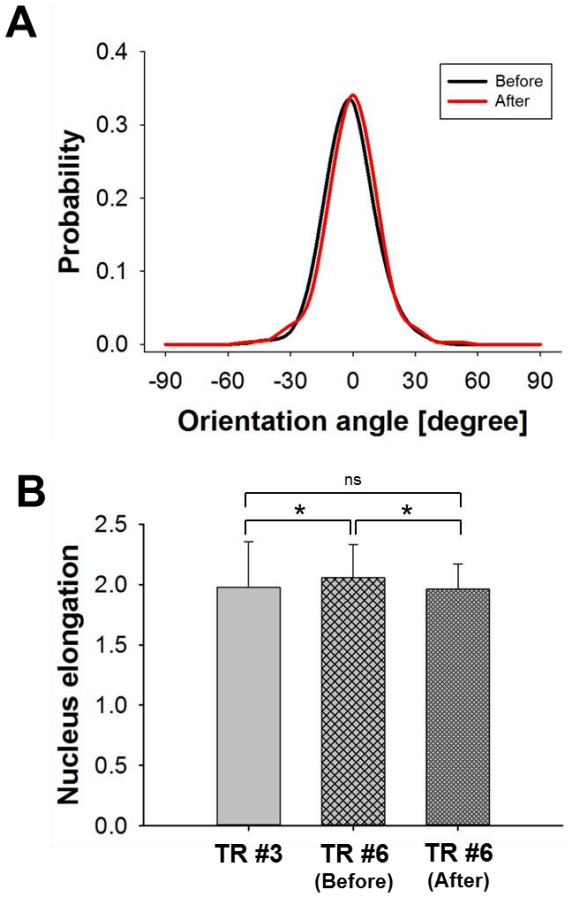

Figure 4-13. (A) Comparison of cellular orientation distributions between before and after detachment. Cellular alignment sustained after detachment. (B) Nucleus elongation was slightly decreased after detachment, but sustained the level similar with the cells on TR #3 before detachment. For comparison of nucleus elongation between groups, Kruskal-Wallis one-way ANOVA on rank test was performed. Asterisk indicates *p < 0.05.

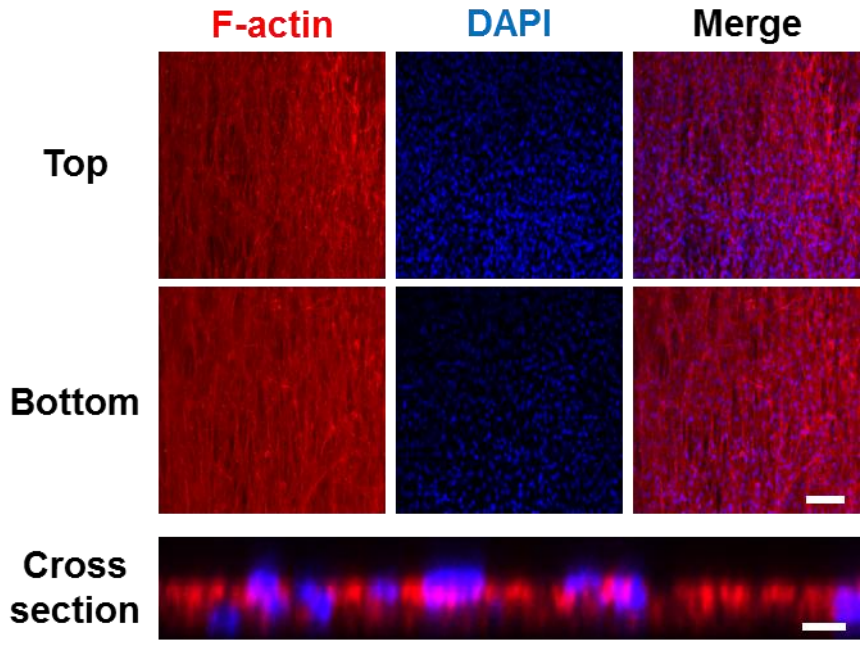

Figure 4-14. Immunofluorescent images of 3D engineered tissue formed by stacking 2 layers of cell sheets in parallel manner. The scale bars indicate 100 μm in planar images and 10 μm in cross-sectional image.

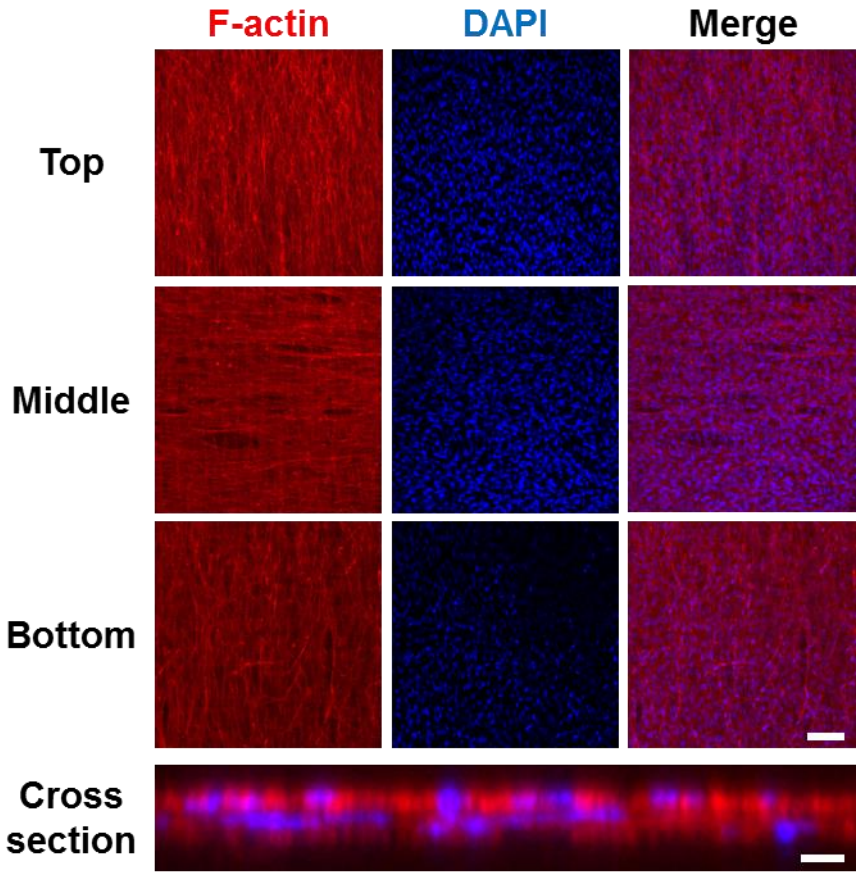

Figure 4-15. Immunofluorescent images of 3D engineered tissue formed by stacking 3 layers of cell sheets in perpendicular manner. The scale bars indicate 100 μm in planar images and 10 μm in cross-sectional image.

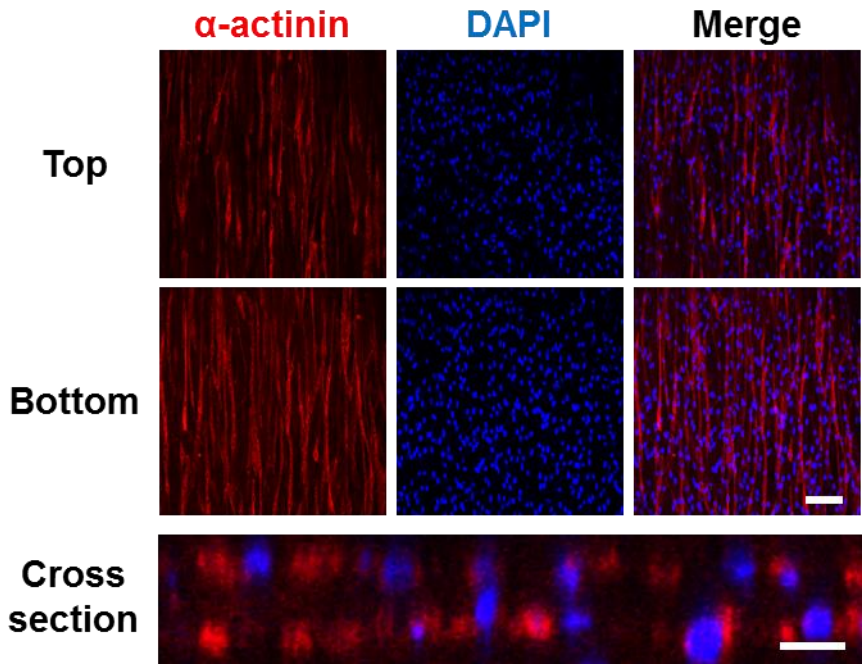

Figure 4-16. Immunofluorescent images of functional 3D engineered tissue formed by induction of myogenic differentiation of 2-layered tissue. The scale bars indicate 100 μm in planar images and 10 μm in cross-sectional image.

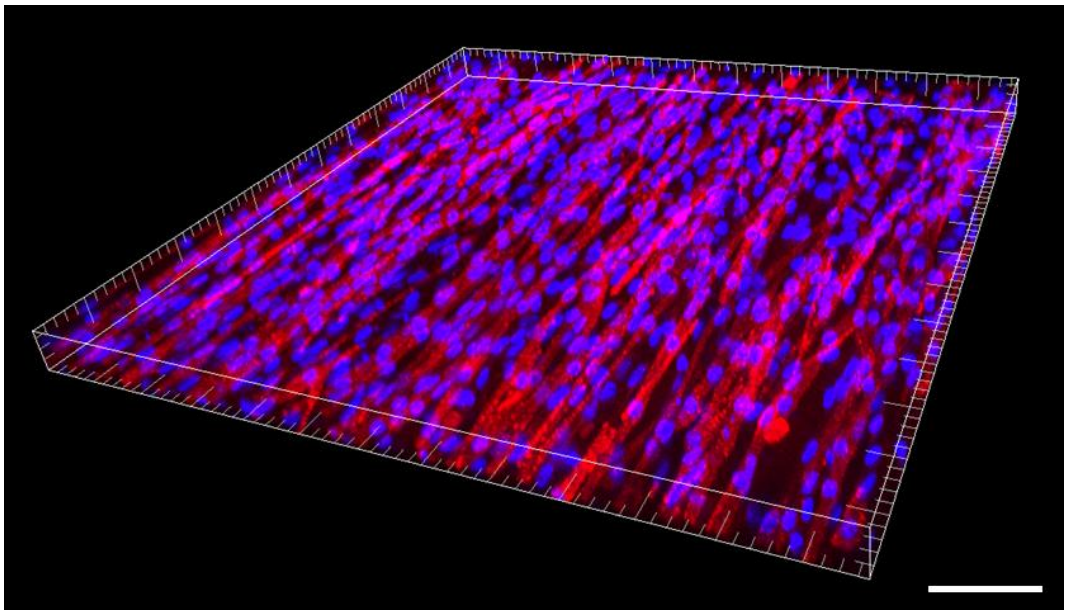

Figure 4-17. 3D reconstructed image of functional 3D engineered tissue. The scale bar indicates 100 μm.

4.3.4. Formation of vascularized 3D engineered skin tissue

4.3.4.1. Tube formation of endothelial cell sheet embedded in Matrigel

In vitro tube formation assay based on Matrigel have been widely used due to not only Matrigel itself has a potential of inducing vasculogenesis but also it is convenient to screen the effect of various factors [86]. Therefore, detached endothelial cell sheet was embedded in Matrigel matrix as shown in figure 4-18A to determine whether the endothelial cells maintained their ability of forming vascular networks or not.

At day 0, embedded endothelial cell sheet maintained their interconnected morphology as before detachment. However, local disconnection of cellular junctions and formation of tube-like structures were observed at day 1 and well-organized tube-like structures were formed over the entire region at day 5 (figure 4-18B). To evaluate 3D structure of formed tube-like structures, immunostaining was performed at day 5 and analyzed using confocal microscope. Similar with optical microscope images, well-organized tube-like structures were observed from the fluorescent images and 3D reconstructed image shown in figure 4-19A and B. These results indicated that detached endothelial cell sheet sustained their ability to form vascular networks. Interestingly,

endothelial cells did not penetrate into the gel layers which resulted in restricted formation of tube-like structures on nanofibrous membrane (figure 4-19A). These results might be related with stiffness of surrounding Matrigel matrix. On soft matrix such as Matrigel and low concentration collagen gel, endothelial cells were known to show suppressed proliferation and invasion which were essential cellular behaviors for angiogenesis and form tube-like structures through vasculogenesis [87-89].

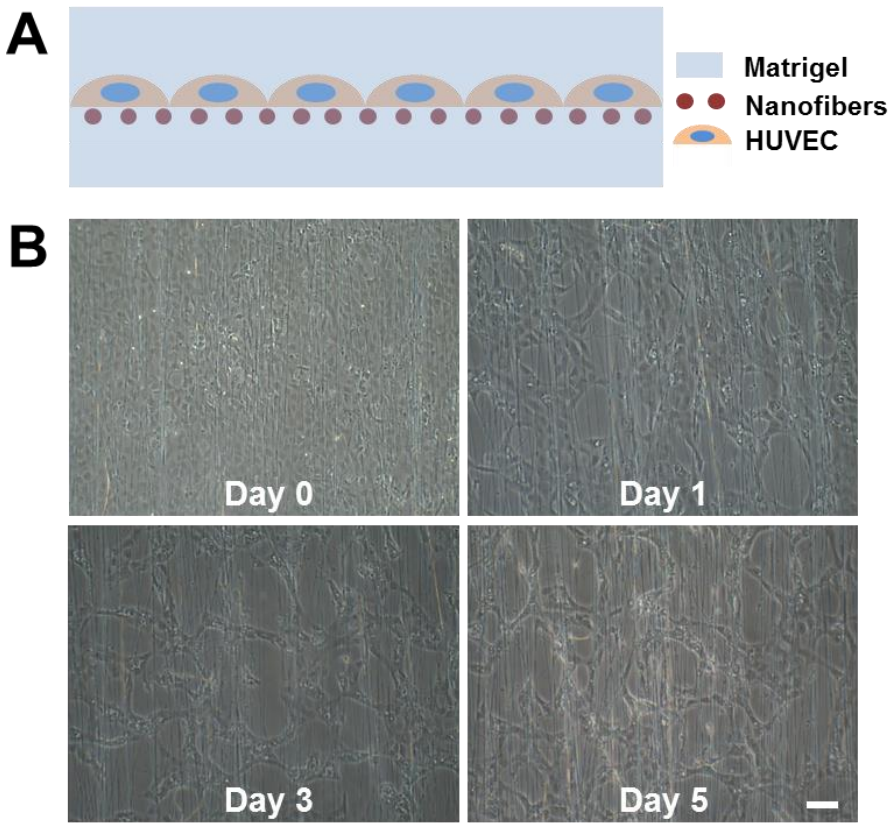

Figure 4-18. (A) Schematic illustration of tube formation assay for endothelial cell sheet embedded in Matrigel. (B) Time-lapse microscope images of transferred endothelial cell sheet. The scale bar indicates 100 μm.

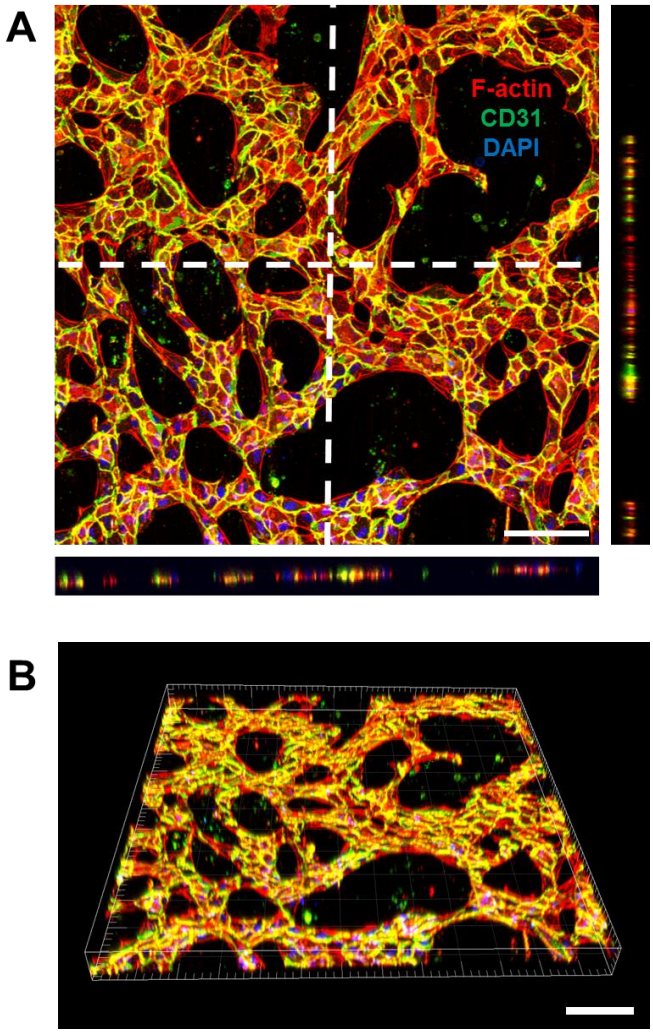

Figure 4-19. (A) Planar and cross-sectional fluorescent images and (B) 3D reconstructed image of tube-like structures at day 5. The scale bars indicate 100 μm.

4.3.4.2. Vascularized 3D engineered skin tissue formation by LBL stacking

In this experiments, mouse embryo fibroblast cell line (NIH-3T3) and human foreskin fibroblast cell line (HS68) was used as a model cells for making 3D skin tissue *in vitro*. To determine feasibility of stacking different cell sheets, detached endothelial cell sheet was stacked on HS68 cell sheet. Fluorescent images shown in figure 4-20 and reconstructed 3D image shown in figure 4-21 which were taken 4 h after stacking confirmed that stacking process was successfully accomplished without any morphological change. To investigate vasculogenic behavior inside 3D engineered skin tissue, furthermore, endothelial cell sheet was stacked between two HS68 sheets and two NIH-3T3 sheets and entire tissue constructs were cultured for additional 5 days. As shown in figure 4-22, sandwiched endothelial cells between HS68 sheets successfully formed lumenized vascular networks. These results were well coincident with previous research which demonstrated that endothelial lumens could be detectable after culturing 5 more days after stacking process [90]. In contrast, endothelial cells between NIH-3T3 sheets formed tube-like structures at day 3 (figure 4-23A), but they cannot sustained their structures and degenerated at day 5 (figure 4-23B). Taken together, formation and

stabilization of lumenized vascular networks might be strongly influenced surrounding cells.

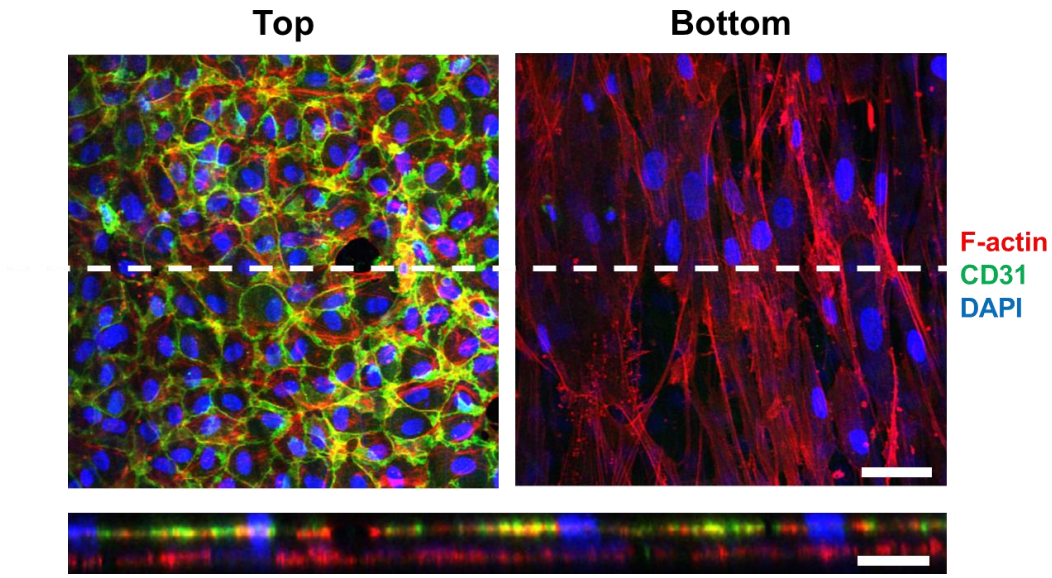

Figure 4-20. Immunofluorescent images of HUVEC sheet stacked on HS68 human fibroblast sheet in parallel manner. The scale bars indicate 50 μm in planar images and 25 μm in cross-sectional image.

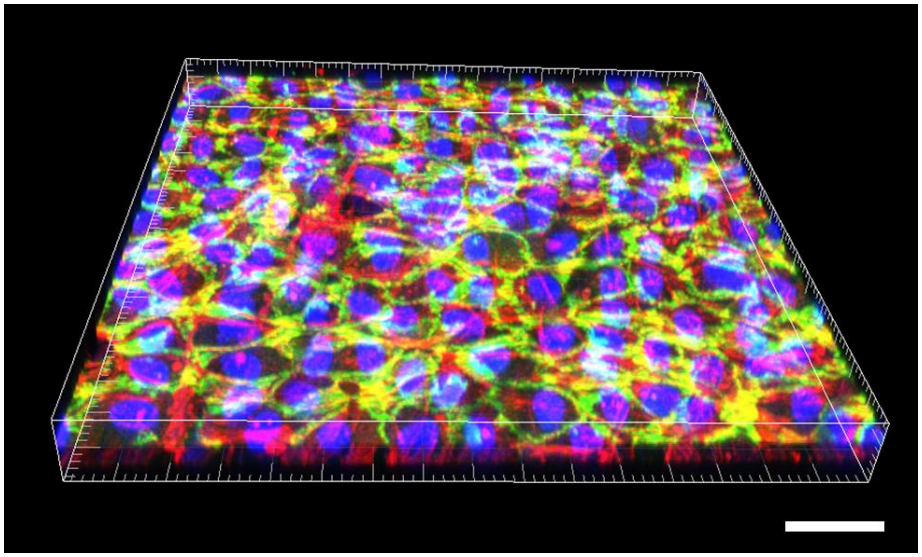

Figure 4-21. 3D reconstructed image of HS68-HUVEC tissue construct. The scale bar indicates 50 μm.

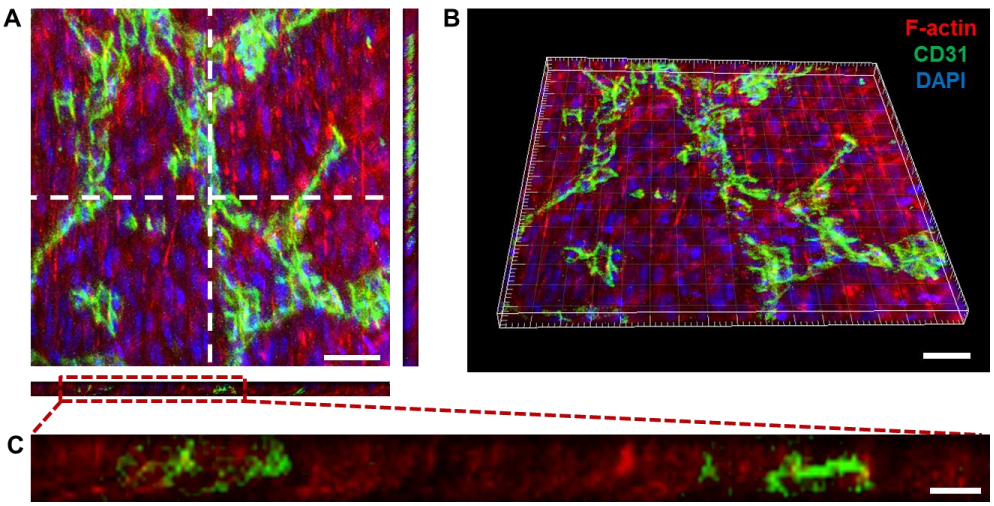

Figure 4-22. Immunofluorescent images of HS68-HUVEC-HS68 tissue construct stacked in parallel manner at day 5. (A) Planar image and (B) 3D reconstructed image of vascularized tissue construct. (C) Cross-sectional image of vascular lumens inside tissue construct. The scale bars indicate 50 μm (A, B) and 10 μm (C).

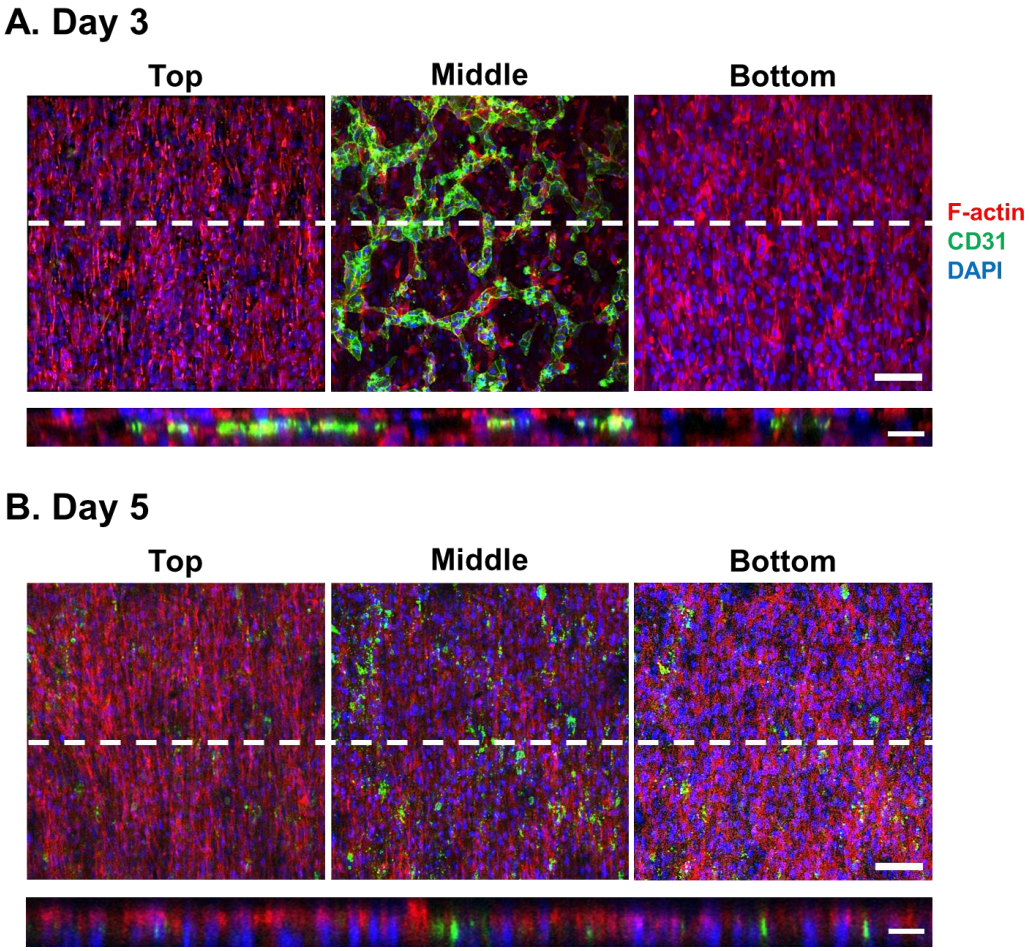

Figure 4-23. Immunofluorescent images of 3T3-HUVEC-3T3 tissue construct stacked in parallel manner at (A) day 3 and (B) day 5. Degeneration of formed tube-like structures was observed at day 5. The scale bars indicate 100 μm in planar images and 25 μm in cross-sectional images.

4.4. Summary

The major aim of this study was to demonstrate that thin, highly porous and aligned nanofibrous membrane could be used as a tool for cell sheet manipulation and formation of various cell-dense 3D engineered tissues *in vitro*.

Since cell sheet engineering based on PNIPAAm which is one of thermoresponsive polymers was suggested by Okano group, cell sheet engineering have attracted great attentions as a reliable method for formation of diverse 3D engineered tissues such as cardiac, skeletal muscle and skin tissue with vascular network for the reasons of simple cell sheet formation by dropping temperature below 20 ˚C, capacity of thick cell-dense 3D engineered tissue formation and easy implantation. Compared with previous researches, our method suggested in this study is noteworthy as another approach which enables cell sheet engineering based on well-known electrospinning method without any morphological changes between before and after transfer. In addition, because electrospinning method has a potential for fabricating functional nanofibers by adopting various growth factors and/or drugs, we expect that enhancement of cellular functions and controlled release of loaded drugs could be achieved.

Undoubtedly, because the current experimental method requires frame for maintaining tension of nanofibers, effective area is reduced as increasing number of stacking. In relation to tensional maintenance, collection problem of 3D engineered tissues without any morphological changes for *in vitro* implantation has to be solved through future researches.

References

[1] Kleinman, H.K., D. Philp, and M.P. Hoffman, *Role of the extracellular matrix in morphogenesis.* Current Opinion in Biotechnology, 2003. **14**(5): p. 526-532.

[2] Jalali, S., M.A. del Pozo, K.D. Chen, H. Miao, Y.S. Li, M.A. Schwartz, J.Y.J. Shyy, and S. Chien, *Integrin-mediated mechanotransduction requires its dynamic interaction with specific extracellular matrix (ECM) ligands (vol 98, pg 1042, 2001).* Proceedings of the National Academy of Sciences of the United States of America, 2001. **98**(9): p. 5369-5369.

[3] Orr, A.W., B.P. Helmke, B.R. Blackman, and M.A. Schwartz, *Mechanisms of mechanotransduction.* Developmental Cell, 2006. **10**(1): p. 11-20.

[4] Jang, K.J., M.S. Kim, D. Feltrin, N.L. Jeon, K.Y. Suh, and O. Pertz, *Two Distinct Filopodia Populations at the Growth Cone Allow to Sense Nanotopographical Extracellular Matrix Cues to Guide Neurite Outgrowth.* Plos One, 2010. **5**(12).

[5] Lee, M.R., K.W. Kwon, H. Jung, H.N. Kim, K.Y. Suh, K. Kim, and K.S. Kim, *Direct differentiation of human embryonic stem cells into selective neurons on nanoscale ridge/groove pattern arrays.* Biomaterials, 2010. **31**(15): p. 4360-4366.

[6] Kim, D.H., E.A. Lipke, P. Kim, R. Cheong, S. Thompson, M. Delannoy, K.Y. Suh, L. Tung, and A. Levchenko, *Nanoscale cues regulate the structure and function of macroscopic cardiac tissue constructs.* Proceedings of the National Academy of Sciences of the United States of America, 2010. **107**(2): p. 565-570.

[7] Yang, H.S., N. Ieronimakis, J.H. Tsui, H.N. Kim, K.Y. Suh, M. Reyes, and D.H. Kim, *Nanopatterned muscle cell patches for enhanced myogenesis and dystrophin expression In a mouse model of muscular dystrophy.* Biomaterials, 2014. **35**(5): p. 1478-1486.

[8] Kim, H.N., Y. Hong, M.S. Kim, S.M. Kim, and K.Y. Suh, *Effect of orientation and density of nanotopography in dermal wound healing.* Biomaterials, 2012. **33**(34): p. 8782-8792.

[9] Il Cho, Y., J.S. Choi, S.Y. Jeong, and H.S. Yoo, *Nerve growth factor (NGF)-conjugated electrospun nanostructures with topographical cues for neuronal*

differentiation of mesenchymal stem cells. Acta Biomaterialia, 2010. **6**(12): p. 4725-4733.

[10] You, M.H., M.K. Kwak, D.H. Kim, K. Kim, A. Levchenko, D.Y. Kim, and K.Y. Suh, *Synergistically Enhanced Osteogenic Differentiation of Human Mesenchymal Stem Cells by Culture on Nanostructured Surfaces with Induction Media.* Biomacromolecules, 2010. **11**(7): p. 1856-1862.

[11] Kim, S.J., D.H. Jang, W.H. Park, and B.M. Min, *Fabrication and characterization of 3-dimensional PLGA nanofiber/microfiber composite scaffolds.* Polymer, 2010. **51**(6): p. 1320-1327.

[12] Pham, Q.P., U. Sharma, and A.G. Mikos, *Electrospun poly(epsilon-caprolactone) microfiber and multilayer nanofiber/microfiber scaffolds: Characterization of scaffolds and measurement of cellular infiltration.* Biomacromolecules, 2006. **7**(10): p. 2796-2805.

[13] Baker, B.M., A.O. Gee, R.B. Metter, A.S. Nathan, R.A. Marklein, J.A. Burdick, and R.L. Mauck, *The potential to improve cell infiltration in composite fiber-aligned electrospun scaffolds by the selective removal of sacrificial fibers.* Biomaterials, 2008. **29**(15): p. 2348-2358.

[14] Yang, X.C., J.D. Shah, and H.J. Wang, *Nanofiber Enabled Layer-by-Layer Approach Toward Three-Dimensional Tissue Formation.* Tissue Engineering Part A, 2009. **15**(4): p. 945-956.

[15] Wheeldon, I., A. Farhadi, A.G. Bick, E. Jabbari, and A. Khademhosseini, *Nanoscale tissue engineering: spatial control over cell-materials interactions.* Nanotechnology, 2011. **22**(21).

[16] Bettinger, C.J., R. Langer, and J.T. Borenstein, *Engineering Substrate Topography at the Micro- and Nanoscale to Control Cell Function.* Angewandte Chemie-International Edition, 2009. **48**(30): p. 5406-5415.

[17] Sniadecki, N., R.A. Desai, S.A. Ruiz, and C.S. Chen, *Nanotechnology for cell-substrate interactions.* Annals of Biomedical Engineering, 2006. **34**(1): p. 59-74.

[18] Kim, D.H., P.K. Wong, J. Park, A. Levchenko, and Y. Sun, *Microengineered Platforms for Cell Mechanobiology.* Annual Review of Biomedical Engineering, 2009. **11**: p. 203-233.

[19] Raghavan, S. and C.S. Chen, *Micropatterned environments in cell biology.* Advanced Materials, 2004. **16**(15): p. 1303-1313.

[20] McBeath, R., D.M. Pirone, C.M. Nelson, K. Bhadriraju, and C.S. Chen, *Cell shape, cytoskeletal tension, and RhoA regulate stem cell lineage commitment.* Developmental Cell, 2004. **6**(4): p. 483-495.

[21] Chung, S.H., S.J. Son, and J. Min, *The nanostructure effect on the adhesion and growth rates of epithelial cells with well-defined nanoporous alumina substrates.* Nanotechnology, 2010. **21**(12).

[22] Hu, W., A.S. Crouch, D. Miller, M. Aryal, and K.J. Luebke, *Inhibited cell spreading on polystyrene nanopillars fabricated by nanoimprinting and in situ elongation.* Nanotechnology, 2010. **21**(38).

[23] Dalby, M.J., A. Hart, and S.J. Yarwood, *The effect of the RACK1 signalling protein on the regulation of cell adhesion and cell contact guidance on nanometric grooves.* Biomaterials, 2008. **29**(3): p. 282-289.

[24] Dalby, M.J., *Topographically induced direct cell mechanotransduction.* Medical Engineering & Physics, 2005. **27**(9): p. 730-742.

[25] You, M.H., M.K. Kwak, D.H. Kim, K. Kim, A. Levchenko, K.Y. Suh, and D.Y. Kim, *Synergistically Enhanced Osteogenic Differentiation of Human Mesenchymal Stem Cells by Culture on Nanostructured Surfaces with Induction Media.* Biomacromolecules, 2010. **11**(7): p. 1856-1862.

[26] Kim, D.H., K. Han, K. Gupta, K.W. Kwon, A. Levchenko, and K.Y. Suh, *Mechanosensitivity of fibroblast cell shape and movement to anisotropic substratum topography gradients.* Biomaterials, 2009. **30**(29): p. 5433-5444.

[27] Kim, D.H., C.H. Seo, K. Han, K.W. Kwon, A. Levchenko, and K.Y. Suh, *Guided Cell Migration on Microtextured Substrates with Variable Local Density and Anisotropy.* Advanced Functional Materials, 2009. **19**(10): p. 1579-1586.

[28] Suh, K.Y., S.J. Choi, S.J. Baek, T.W. Kim, and R. Langer, *Observation of high-aspect-ratio nanostructures using capillary lithography.* Advanced Materials, 2005. **17**(5): p. 560-+.

[29] Suh, K.Y., M.C. Park, and P. Kim, *Capillary Force Lithography: A Versatile Tool for Structured Biomaterials Interface Towards Cell and Tissue Engineering.*

Advanced Functional Materials, 2009. **19**(17): p. 2699-2712.

[30] Kletzien, R.F., S.D. Clarke, and R.G. Ulrich, *Enhancement of adipocyte differentiation by an insulin-sensitizing agent.* Mol Pharmacol, 1992. **41**(2): p. 393-8.

[31] Lee, Y.S., W.S. Kim, K.H. Kim, M.J. Yoon, H.J. Cho, Y. Shen, J.M. Ye, C.H. Lee, W.K. Oh, C.T. Kim, C. Hohnen-Behrens, A. Gosby, E.W. Kraegen, D.E. James, and J.B. Kim, *Berberine, a natural plant product, activates AMP-activated protein kinase with beneficial metabolic effects in diabetic and insulin-resistant states.* Diabetes, 2006. **55**(8): p. 2256-64.

[32] Rosen, E.D., C.H. Hsu, X. Wang, S. Sakai, M.W. Freeman, F.J. Gonzalez, and B.M. Spiegelman, *C/EBPalpha induces adipogenesis through PPARgamma: a unified pathway.* Genes Dev, 2002. **16**(1): p. 22-6.

[33] Rosen, E.D., P. Sarraf, A.E. Troy, G. Bradwin, K. Moore, D.S. Milstone, B.M. Spiegelman, and R.M. Mortensen, *PPAR gamma is required for the differentiation of adipose tissue in vivo and in vitro.* Mol Cell, 1999. **4**(4): p. 611-7.

[34] Tanaka, T., N. Yoshida, T. Kishimoto, and S. Akira, *Defective adipocyte differentiation in mice lacking the C/EBPbeta and/or C/EBPdelta gene.* EMBO J, 1997. **16**(24): p. 7432-43.

[35] Tontonoz, P., E. Hu, and B.M. Spiegelman, *Stimulation of adipogenesis in fibroblasts by PPAR gamma 2, a lipid-activated transcription factor.* Cell, 1994. **79**(7): p. 1147-56.

[36] Wu, Z., E.D. Rosen, R. Brun, S. Hauser, G. Adelmant, A.E. Troy, C. McKeon, G.J. Darlington, and B.M. Spiegelman, *Cross-regulation of C/EBP alpha and PPAR gamma controls the transcriptional pathway of adipogenesis and insulin sensitivity.* Mol Cell, 1999. **3**(2): p. 151-8.

[37] Kilian, K.A., B. Bugarija, B.T. Lahn, and M. Mrksich, *Geometric cues for directing the differentiation of mesenchymal stem cells.* Proc Natl Acad Sci U S A, 2010. **107**(11): p. 4872-7.

[38] Weiner, F.R., A. Shah, P.J. Smith, C.S. Rubin, and M.A. Zern, *Regulation of collagen gene expression in 3T3-L1 cells. Effects of adipocyte differentiation and*

tumor necrosis factor alpha. Biochemistry, 1989. **28**(9): p. 4094-9.

[39] Choi, S.J., P.J. Yoo, S.J. Baek, T.W. Kim, and H.H. Lee, *An ultraviolet-curable mold for sub-100-nm lithography.* Journal of the American Chemical Society, 2004. **126**(25): p. 7744-7745.

[40] Kim, P., D.H. Kim, B. Kim, S.K. Choi, S.H. Lee, A. Khademhosseini, R. Langer, and K.Y. Suh, *Fabrication of nanostructures of polyethylene glycol for applications to protein adsorption and cell adhesion.* Nanotechnology, 2005. **16**(10): p. 2420-2426.

[41] Kim, D.H., P. Kim, I. Song, J.M. Cha, S.H. Lee, B. Kim, and K.Y. Suh, *Guided three-dimensional growth of functional cardiomyocytes on polyethylene glycol nanostructures.* Langmuir, 2006. **22**(12): p. 5419-5426.

[42] Ruiz, S.A. and C.S. Chen, *Emergence of Patterned Stem Cell Differentiation Within Multicellular Structures.* Stem Cells, 2008. **26**(11): p. 2921-2927.

[43] Langer, R. and J.P. Vacanti, *Tissue Engineering.* Science, 1993. **260**(5110): p. 920-926.

[44] Lutolf, M.P. and J.A. Hubbell, *Synthetic biomaterials as instructive extracellular microenvironments for morphogenesis in tissue engineering.* Nature Biotechnology, 2005. **23**(1): p. 47-55.

[45] Kim, D.H., H. Lee, Y.K. Lee, J.M. Nam, and A. Levchenko, *Biomimetic Nanopatterns as Enabling Tools for Analysis and Control of Live Cells.* Advanced Materials, 2010. **22**(41): p. 4551-4566.

[46] Vats, A., N.S. Tolley, J.M. Polak, and J.E. Gough, *Scaffolds and biomaterials for tissue engineering: a review of clinical applications.* Clinical Otolaryngology, 2003. **28**(3): p. 165-172.

[47] Kim, H.N., A. Jiao, N.S. Hwang, M.S. Kim, D.H. Kang, D.H. Kim, and K.Y. Suh, *Nanotopography-guided tissue engineering and regenerative medicine.* Advanced Drug Delivery Reviews, 2013. **65**(4): p. 536-558.

[48] Agarwal, S., J.H. Wendorff, and A. Greiner, *Progress in the Field of Electrospinning for Tissue Engineering Applications.* Advanced Materials, 2009. **21**(32-33): p. 3343-3351.

[49] Ashammakhi, N., A. Ndreu, Y. Yang, H. Ylikauppila, L. Nikkola, and V. Hasirci,

Tissue engineering: A new take-off using nanofiber-based scaffolds. Journal of Craniofacial Surgery, 2007. **18**(1): p. 3-17.

[50] Huang, L., R.A. McMillan, R.P. Apkarian, B. Pourdeyhimi, V.P. Conticello, and E.L. Chaikof, *Generation of synthetic elastin-mimetic small diameter fibers and fiber networks.* Macromolecules, 2000. **33**(8): p. 2989-2997.

[51] Huang, Z.M., Y.Z. Zhang, M. Kotaki, and S. Ramakrishna, *A review on polymer nanofibers by electrospinning and their applications in nanocomposites.* Composites Science and Technology, 2003. **63**(15): p. 2223-2253.

[52] Bashur, C.A., R.D. Shaffer, L.A. Dahlgren, S.A. Guelcher, and A.S. Goldstein, *Effect of Fiber Diameter and Alignment of Electrospun Polyurethane Meshes on Mesenchymal Progenitor Cells.* Tissue Engineering Part A, 2009. **15**(9): p. 2435-2445.

[53] Choi, J.S., S.J. Lee, G.J. Christ, A. Atala, and J.J. Yoo, *The influence of electrospun aligned poly(epsilon-caprolactone)/collagen nanofiber meshes on the formation of self-aligned skeletal muscle myotubes.* Biomaterials, 2008. **29**(19): p. 2899-2906.

[54] Corey, J.M., D.Y. Lin, K.B. Mycek, Q. Chen, S. Samuel, E.L. Feldman, and D.C. Martin, *Aligned electrospun nanofibers specify the direction of dorsal root ganglia neurite growth.* Journal of Biomedical Materials Research Part A, 2007. **83A**(3): p. 636-645.

[55] Dang, J.M. and K.W. Leong, *Myogenic induction of aligned mesenchymal stem cell sheets by culture on thermally responsive electrospun nanofibers.* Advanced Materials, 2007. **19**(19): p. 2775-+.

[56] Huang, N.F., S. Patel, R.G. Thakar, J. Wu, B.S. Hsiao, B. Chu, R.J. Lee, and S. Li, *Myotube assembly on nanofibrous and micropatterned polymers.* Nano Letters, 2006. **6**(3): p. 537-542.

[57] Lee, C.H., H.J. Shin, I.H. Cho, Y.M. Kang, I.A. Kim, K.D. Park, and J.W. Shin, *Nanofiber alignment and direction of mechanical strain affect the ECM production of human ACL fibroblast.* Biomaterials, 2005. **26**(11): p. 1261-1270.

[58] Yang, F., R. Murugan, S. Wang, and S. Ramakrishna, *Electrospinning of nano/micro scale poly(L-lactic acid) aligned fibers and their potential in neural*

tissue engineering. Biomaterials, 2005. **26**(15): p. 2603-2610.

[59] Katta, P., M. Alessandro, R.D. Ramsier, and G.G. Chase, *Continuous electrospinning of aligned polymer nanofibers onto a wire drum collector.* Nano Letters, 2004. **4**(11): p. 2215-2218.

[60] Li, D., Y.L. Wang, and Y.N. Xia, *Electrospinning of polymeric and ceramic nanofibers as uniaxially aligned arrays.* Nano Letters, 2003. **3**(8): p. 1167-1171.

[61] Theron, A., E. Zussman, and A.L. Yarin, *Electrostatic field-assisted alignment of electrospun nanofibres.* Nanotechnology, 2001. **12**(3): p. 384-390.

[62] Bisht, G., S. Nesterenko, L. Kulinsky, and M. Madou, *A Computer-Controlled Near-Field Electrospinning Setup and Its Graphic User Interface for Precision Patterning of Functional Nanofibers on 2D and 3D Substrates.* Jala, 2012. **17**(4): p. 302-308.

[63] Yang, D.Y., B. Lu, Y. Zhao, and X.Y. Jiang, *Fabrication of aligned fibirous arrays by magnetic electrospinning.* Advanced Materials, 2007. **19**(21): p. 3702-+.

[64] Park, S.H. and D.Y. Yang, *Fabrication of Aligned Electrospun Nanofibers by Inclined Gap Method.* Journal of Applied Polymer Science, 2011. **120**(3): p. 1800-1807.

[65] Park, S.H., T.G. Kim, H.C. Kim, D.Y. Yang, and T.G. Park, *Development of dual scale scaffolds via direct polymer melt deposition and electrospinning for applications in tissue regeneration.* Acta Biomaterialia, 2008. **4**(5): p. 1198-1207.

[66] Chapleau, N., B.D. Favis, and P.J. Carreau, *Measuring the interfacial tension of polyamide/polyethylene and polycarbonate/polypropylene blends: effect of temperature.* Polymer, 2000. **41**(17): p. 6695-6698.

[67] Kressler, J., C. Wang, and H.W. Kammer, *Structure formation in thin poly(epsilon-caprolactone) films.* Langmuir, 1997. **13**(16): p. 4407-4412.

[68] Simon, D., A. Holland, and R. Shanks, *Poly(caprolactone) thin film preparation, morphology, and surface texture.* Journal of Applied Polymer Science, 2007. **103**(2): p. 1287-1294.

[69] Kim, H.N., D.H. Kang, M.S. Kim, A. Jiao, D.H. Kim, and K.Y. Suh, *Patterning Methods for Polymers in Cell and Tissue Engineering.* Annals of Biomedical Engineering, 2012. **40**(6): p. 1339-1355.

[70] Park, S.H., J.W. Hong, J.H. Shin, D.Y. Yang, and Y. Yang, *Quantitatively Controlled Fabrication of Uniaxially Aligned Nanofibrous Scaffold for Cell Adhesion.* Journal of Nanomaterials, 2011.

[71] Ahn, S., Y.H. Koh, and G. Kim, *A three-dimensional hierarchical collagen scaffold fabricated by a combined solid freeform fabrication (SFF) and electrospinning process to enhance mesenchymal stem cell (MSC) proliferation.* Journal of Micromechanics and Microengineering, 2010. **20**(6).

[72] Moroni, L., R. Schotel, D. Hamann, J.R. de Wijn, and C.A. van Blitterswijk, *3D fiber-deposited electrospun integrated scaffolds enhance cartilage tissue formation.* Advanced Functional Materials, 2008. **18**(1): p. 53-60.

[73] Mota, C., D. Puppi, D. Dinucci, C. Errico, P. Bartolo, and F. Chiellini, *Dual-Scale Polymeric Constructs as Scaffolds for Tissue Engineering.* Materials, 2011. **4**(3): p. 527-542.

[74] Blackwood, K.A., R. McKean, I. Canton, C.O. Freeman, K.L. Franklin, D. Cole, I. Brook, P. Farthing, S. Rimmer, J.W. Haycock, A.J. Ryan, and S. MacNeil, *Development of biodegradable electrospun scaffolds for dermal replacement*. Biomaterials, 2008. **29**(21): p. 3091-3104.

[75] Levenberg, S., J. Rouwkema, M. Macdonald, E.S. Garfein, D.S. Kohane, D.C. Darland, R. Marini, C.A. van Blitterswijk, R.C. Mulligan, P.A. D'Amore, and R. Langer, *Engineering vascularized skeletal muscle tissue.* Nature Biotechnology, 2005. **23**(7): p. 879-884.

[76] Cho, M.H., K.S. Kim, H.H. Ahn, M.S. Kim, S.H. Kim, G. Khang, B. Lee, and H.B. Lee, *Chitosan gel as an in situ-forming scaffold for rat bone marrow mesenchymal stem cells in vivo.* Tissue Engineering Part A, 2008. **14**(6): p. 1099-1108.

[77] Yang, J., M. Yamato, T. Shimizu, H. Sekine, K. Ohashi, M. Kanzaki, T. Ohki, K. Nishida, and T. Okano, *Reconstruction of functional tissues with cell sheet engineering.* Biomaterials, 2007. **28**(34): p. 5033-5043.

[78] Yu, Q., Y.X. Zhang, H. Chen, F. Zhou, Z.Q. Wu, H. Huang, and J.L. Brash, *Protein Adsorption and Cell Adhesion/Detachment Behavior on Dual-Responsive Silicon Surfaces Modified with Poly(N-isopropylacrylamide)-block-polystyrene*

Copolymer. Langmuir, 2010. **26**(11): p. 8582-8588.

[79] Yamato, M., M. Utsumi, A. Kushida, C. Konno, A. Kikuchi, and T. Okano, *Thermo-responsive culture dishes allow the intact harvest of multilayered keratinocyte sheets without dispase by reducing temperature.* Tissue Engineering, 2001. **7**(4): p. 473-480.

[80] Lin, J.B., B.C. Isenberg, Y.K. Shen, K. Schorsch, O.V. Sazonova, and J.Y. Wong, *Thermo-responsive poly(N-isopropylacrylamide) grafted onto microtextured poly(dimethylsiloxane) for aligned cell sheet engineering.* Colloids and Surfaces B-Biointerfaces, 2012. **99**: p. 108-115.

[81] Takahashi, H., M. Nakayama, K. Itoga, M. Yamato, and T. Okano, *Micropatterned Thermoresponsive Polymer Brush Surfaces for Fabricating Cell Sheets with Well-Controlled Orientational Structures.* Biomacromolecules, 2011. **12**(5): p. 1414-1418.

[82] Choi, J.S., K.W. Leong, and H.S. Yoo, *In vivo wound healing of diabetic ulcers using electrospun nanofibers immobilized with human epidermal growth factor (EGF).* Biomaterials, 2008. **29**(5): p. 587-596.

[83] Ghasemi-Mobarakeh, L., M.P. Prabhakaran, M. Morshed, M.H. Nasr-Esfahani, and S. Ramakrishna, *Electrical Stimulation of Nerve Cells Using Conductive Nanofibrous Scaffolds for Nerve Tissue Engineering.* Tissue Engineering Part A, 2009. **15**(11): p. 3605-3619.

[84] Ma, Z.W., W. He, T. Yong, and S. Ramakrishna, *Grafting of gelatin on electrospun poly(caprolactone) nanofibers to improve endothelial cell spreading and proliferation and to control cell orientation.* Tissue Engineering, 2005. **11**(7-8): p. 1149-1158.

[85] Wang, N., J.D. Tytell, and D.E. Ingber, *Mechanotransduction at a distance: mechanically coupling the extracellular matrix with the nucleus.* Nature Reviews Molecular Cell Biology, 2009. **10**(1): p. 75-82.

[86] Arnaoutova, I. and H.K. Kleinman, *In vitro angiogenesis: endothelial cell tube formation on gelled basement membrane extract.* Nature Protocols, 2010. **5**(4): p. 628-635.

[87] Vailhe, B., X. Ronot, P. Tracqui, Y. Usson, and L. Tranqui, *In vitro angiogenesis*

is modulated by the mechanical properties of fibrin gels and is related to alpha(v)beta(3) integrin localization. In Vitro Cellular & Developmental Biology-Animal, 1997. **33**(10): p. 763-773.

[88] Tranqui, L. and P. Tracqui, *Mechanical signalling and angiogenesis. The integration of cell-extracellular matrix couplings.* Comptes Rendus De L Academie Des Sciences Serie Iii-Sciences De La Vie-Life Sciences, 2000. **323**(1): p. 31-47.

[89] Yamamura, N., R. Sudo, M. Ikeda, and K. Tanishita, *Effects of the mechanical properties of collagen gel on the in vitro formation of microvessel networks by endothelial cells.* Tissue Engineering, 2007. **13**(7): p. 1443-1453.

[90] Asakawa, N., T. Shimizu, Y. Tsuda, S. Sekiya, T. Sasagawa, M. Yamato, F. Fukai, and T. Okano, *Pre-vascularization of in vitro three-dimensional tissues created by cell sheet engineering.* Biomaterials, 2010. **31**(14): p. 3903-3909.

국문초록

본 학위 논문은 조직공학응용을 위한 멀티스케일의 2 차원 및 3 차원 제작 기법의 개발을 목적으로 한다. 세부적으로 모세관력 리소그라피 (Capillary force lithography, CFL)을 이용해 정밀하게 제작된 멀티스케일 패턴을 분석 플랫폼으로 이용하여, 세포의 기능 발현 향상을 위한 최적의 패턴 형상을 탐색하였다. 또한 기존의 전기방사 (Electrospinning) 기법에 기반하여, 세포가 부착된 나노 섬유를 말거나, 적층하는 새로운 제작 기법을 제시하여 세포 밀도가 높은 3 차원 체외 조직의 형성을 가능하게 하였다.

세포를 둘러싼 세포외기질 (Extracellular matrix, ECM)은 친수성의 나노섬유로 이루어진 구조를 가지며, 세포 부착, 증식, 이동, 분화 등의 다양한 세포 기능의 조절에 필수적인 기계적, 생화학적 자극을 제공하는 역할을 한다. 따라서, 조직공학에의 적용을 위해서는 세포외기질 환경이 모사된 2 차원, 3 차원 담체 (Scaffold) 제작 기법의 개발이 선행되어야 한다. 이를 위하여, 자외선 경화성 재료를 이용한 모세관력 리소그라피를 바탕으로 나노 구조물에 의한 세포 기능 조절 분석을 위한 2 차원 플랫폼의 제작

기술을 개발하고, 그 응용으로 나노 구조물의 기하학적 형상이 지방세포분화에 미치는 영향을 분석하였다. 그 결과, 세포가 선형 나노 패턴 사이로 침투하여 높은 접촉 유도 경향을 경우 향상된 분화 정도를 보이는 것을 확인할 수 있었다. 이는 향상된 세포와 표면간의 상호작용이 지방세포의 분화에 있어서 중요한 역할을 한다는 것을 의미한다.

다음으로, 세포외기질 환경을 반영한 세포 밀도가 높은 3 차원 체외조직의 형성을 위하여, 경사 갭 기법 (Inclined gap method)을 이용하여 제작된 나노 섬유를 세포와 함께 말거나 (Rolling-up), 적층 (Stacking)하는 기술을 개발하였다. 먼저 롤링업 공정의 경우, 전기방사, 스핀 코팅, 미세 용융 압출의 3 가지 기법을 융합하여 나노 섬유 기반의 멀티스케일 담체를 제작하고, 근아세포 (Myoblast)가 배양된 담체를 말아서 실린더 형상의 3 차원 체외 근육 조직의 제작을 가능하게 하였다. 담체 위에 부착된 세포들은 정렬된 나노 섬유에 의하여 접촉 유도되어 높은 정렬도를 보였으며, 이동 및 마는 공정 이후에도 세포의 형상이 유지됨을 알 수 있었다. 마지막으로, 정렬된 나노 섬유로 이루어진 멤브레인을 이용하여 배양된 세포막의 손상 및 세포의 형상 변화 없이 표면으로부터 분리, 전사 및 조작을

가능케 하는 기법을 개발하였다. 이를 바탕으로 형성된 세포막의 적층을 통하여 높은 세포 밀도를 가진 3 차원 체외 조직의 형성이 가능하였고, 나아가 여러 층의 근아세포가 적층된 체외 조직의 분화를 통하여 근섬유로 이루어진 3 차원 근육 조직의 형성이 가능하였다. 또한 섬유아세포막과 혈관세포막의 교차 적층 및 공배양을 통하여 혈관망이 내부에 형성되어 있는 3 차원 피부 조직의 형성 역시 가능하였다.

주요어: 세포외기질, 마이크로/나노패터닝, 모세관력 리소그라피, 전기방사, 롤 업 공정, 세포 막 공학, 세포막 적층, 지방세포분화, 근육분화, 혈관망 형성, 3 차원 체외 조직

학번: 2010-20657